AD-A057 333 ORI INC SILVER SPRING MD F/G 8/3
MODEL RESULTS OF THE EFFECTS OF INTERNAL WAVES ON ACOUSTIC PROP--ETC(U)
AUG 78 E MOSES, W GALATI, W NICHOLAS N00014-76-C-0479
UNCLASSIFIED ORI-TR-1295 NL

| OF |
AD
A057 333

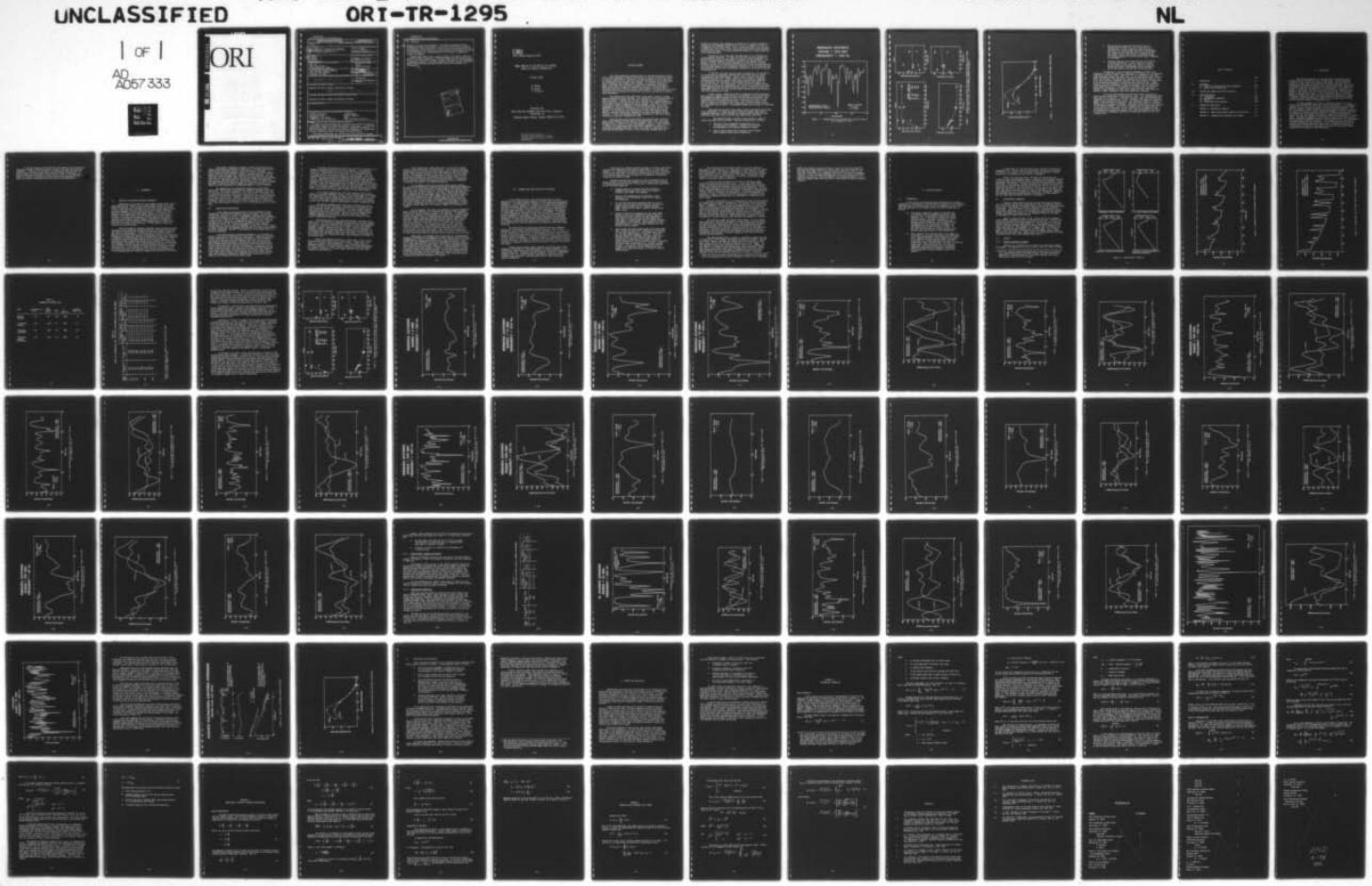

ORI

UNCLASSIFIED

SECURITY CLASSIFICATION OF THIS PAGE (When Data Entered)

REPORT DOCUMENTATION PAGE		READ INSTRUCTIONS BEFORE COMPLETING FORM
1. REPORT NUMBER TR 1295	2. GOVT ACCESSION NO.	3. RECIPIENT'S CATALOG NUMBER
4. TITLE (and Subtitle) (6) MODEL RESULTS OF THE EFFECTS OF INTERNAL WAVES ON ACOUSTIC PROPAGATION.		5. TYPE OF REPORT & PERIOD COVERED (9) Final Report.
		6. PERFORMING ORG. REPORT NUMBER
7. AUTHOR(s) (10) E. Moses, W. Galati W. Nicholas		8. CONTRACT OR GRANT NUMBER(s) (15) N000014-76-C-0479
9. PERFORMING ORGANIZATION NAME AND ADDRESS ORI, Inc. 1400 Spring Street Silver Spring, MD 20910		10. PROGRAM ELEMENT, PROJECT, TASK AREA & WORK UNIT NUMBERS 65152N R0145, NR 274-253
11. CONTROLLING OFFICE NAME AND ADDRESS Naval Analysis Program (Code 431) Office of Naval Research Arlington, VA 22217		(11) 12. REPORT DATE 3 Aug 1978 13. NUMBER OF PAGES 87 (12) 94p.
14. MONITORING AGENCY NAME & ADDRESS (if different from Controlling Office) (14) ORI-TR-1295		15. SECURITY CLASS. (of this report) UNCLASSIFIED 15a. DECLASSIFICATION/DOWNGRADING SCHEDULE

16. DISTRIBUTION STATEMENT (of this Report)

Approved for public release; distribution unlimited.

(16) R0145 / (17) R0145

17. DISTRIBUTION STATEMENT (of the abstract entered in Block 20, if different from Report)

Approved for public release; distribution unlimited.

18. SUPPLEMENTARY NOTES

19. KEY WORDS (Continue on reverse side if necessary and identify by block number)

Acoustic Propagation	Internal Waves
Transmission Loss	Acoustic Modeling
Propagation Fluctuations	Sonar
Transmission Loss Fluctuations	Sonar Performance Prediction

20. ABSTRACT (Continue on reverse side if necessary and identify by block number)

A model has been developed which simulates time variations in Acoustic transmission induced by internal wave activity in the ocean. The model produces explicit sample time series of acoustic transmission parameters. An explicit objective of the work was to provide a mechanism for investigating how such fluctuations affect low frequency sonar performance.

The model parameterizes the internal wave field according to a power spectrum proposed by Garrett and M nk, and unperturbed acoustic transmission

→ next page

DD FORM 1 JAN 73 1473 EDITION OF 1 NOV 65 IS OBSOLETE S/N 0102-014-6601

20. Continued

cont. through use of ray trace techniques. The interaction between the two considers the effect on the phase of individual ray paths, and consequent fluctuations in the multipath sum. Both the ray trace characteristics and some parameters of the internal wave field depend on environmental conditions, so that the model can investigate sensitivity of results to geographic location and season.

Sample model results show a strong increase in fluctuation rates with increasing acoustic frequency, a fluctuation magnitude (one standard deviation) of 5 to 6 dB except, perhaps, at short range, and no strong dependence on geographic location. One direct comparison of model results with experimental fluctuation data was made, and the results are considered very satisfactory.

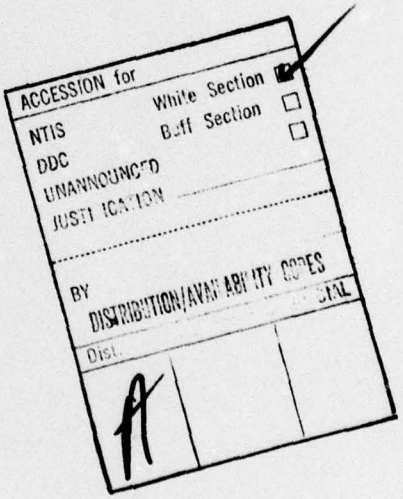

ORI
Silver Spring, Maryland 20910

MODEL RESULTS OF THE EFFECTS OF INTERNAL WAVES ON ACOUSTIC PROPAGATION

3 AUGUST 1978

E. MOSES
W. GALATI
N. NICHOLAS

PREPARED FOR:
NAVAL ANALYSIS PROGRAM, OFFICE OF NAVAL RESEARCH
ARLINGTON, VA

PREPARED UNDER CONTRACT NUMBER N00014-76-C-0479

JCP

EXECUTIVE SUMMARY

This report summarizes characteristics of, and some preliminary results from, a model developed to simulate fluctuations in acoustic transmission induced by internal wave activity in the ocean. An explicit objective of this work was to provide a mechanism for exploring transmission fluctuations which might affect the performance of low frequency sonar systems. The principal output of the model is simulated sample functions of transmission parameters (amplitude, phase) versus time, for specified frequencies and source receiver geometries. These time series can either be directly played through a particular sonar processing algorithm to provide simulated sonar behavior, or appropriate statistical descriptors can be extracted from the series, and used to analytically estimate sonar performance.

The internal wave field description in the model is based on a power spectrum proposed by Garrett and Munk. This spectrum is used to generate explicit sample functions of internal wave activity, evaluated over a selected mesh of space time points. From this set of values, internal wave induced perturbations in the speed of sound at these points may be computed. The effect of these perturbations on acoustic propagation is then estimated through a ray tracing approximation. The basic assumption is that the internal wave effects cause significant variations only in the phase of ray paths connecting source and receiver. As the internal wave field evolves in time, these phases undergo complex fluctuations whose nature depends on the particular geometry of each ray path. In turn, the coherent sum of these ray paths (e.g. the sound energy observed at a receiver) fluctuates with time.

While the basic form of the internal wave spectrum used is general, some of the parameters involved depend on characteristics of the local sound speed profile. In addition the ray path parameters used in the model depend in detail on this profile and other environmental parameters. Hence the model is suitable for investigating the sensitivity of computed fluctuations to differing environmental conditions. Also, the current implementation differs from some previous models in that it is not restricted to cases where the

direction of internal wave propagation parallels that of acoustic propagation; instead the more reasonable assumption of isotropy in propagation direction is adapted for the internal waves. Finally, as already noted, since the model simulates actual time series, rather than calculating fixed analytic parameters of such series directly, it offers considerable flexibility in applications to sonar system assessment.

Preliminary runs of the model have been made for four different sets of environmental conditions. Of these, the first two sets were designed to explore the sensitivity of model results to changes in input parameters. The first of these environments is nominally typical of the Atlantic Ocean near Bermuda in autumn, while the other represents the North Atlantic in summer. The other two sets of runs were explicitly selected to match conditions observed during two measurements of CW transmission fluctuations: one an experiment done near Eleuthera, and the other an experiment conducted over an Eleuthera Bermuda Transmission Path.

In the first two cases runs were made at frequencies of 50 and 220 Hz for source-receiver separations ranging from 5 to 200 nmi, and for several source-receiver depth combinations. Figure 1 shows a typical time series resulting from these runs. Figure 2 shows plots of statistical parameters (standard deviation and relaxation time) versus source-receiver separation for transmission loss time series in the Bermuda (autumn) environment, at 220 Hz, and at 50 Hz. The large scatter in the 50 Hz results appears to be a consequence of statistical uncertainties, but the 220 Hz results are consistent with a hypothesis that the standard deviation should increase with range to a "saturation" value of 5 to 6 dB, and then remain constant, while the relaxation time should decrease with range.

Figure 3 shows a comparison of 406 Hz propagation fluctuation measurements made near Eleuthera, with statistics derived from a model run made using environmental parameters designed to match the experimental conditions. The figure plots the rate (crossings per hour) at which the time series crosses a specified level as a function of that level. The horizontal extent of this plot is a measure of the magnitude of fluctuations, while the height reflects the fluctuation rates involved. The agreement between data and model is considered very good.

More generally the model results match typical experimental observations of CW transmission. Of these, the most striking are frequent deep fades in propagation amplitude, and the character of related phase fluctuations which take place relatively slowly, but with large (many cycles) amplitude.

The ensemble of model runs made to date indicate a number of trends which seem to be significant. These may be summarized as follows:

- The rate at which propagation fluctuations occur, for a fixed source and receiver, increases (the relaxation time decreases) as the acoustic frequency increases
- There is some evidence that fluctuation rates increase with increasing source-receiver separation

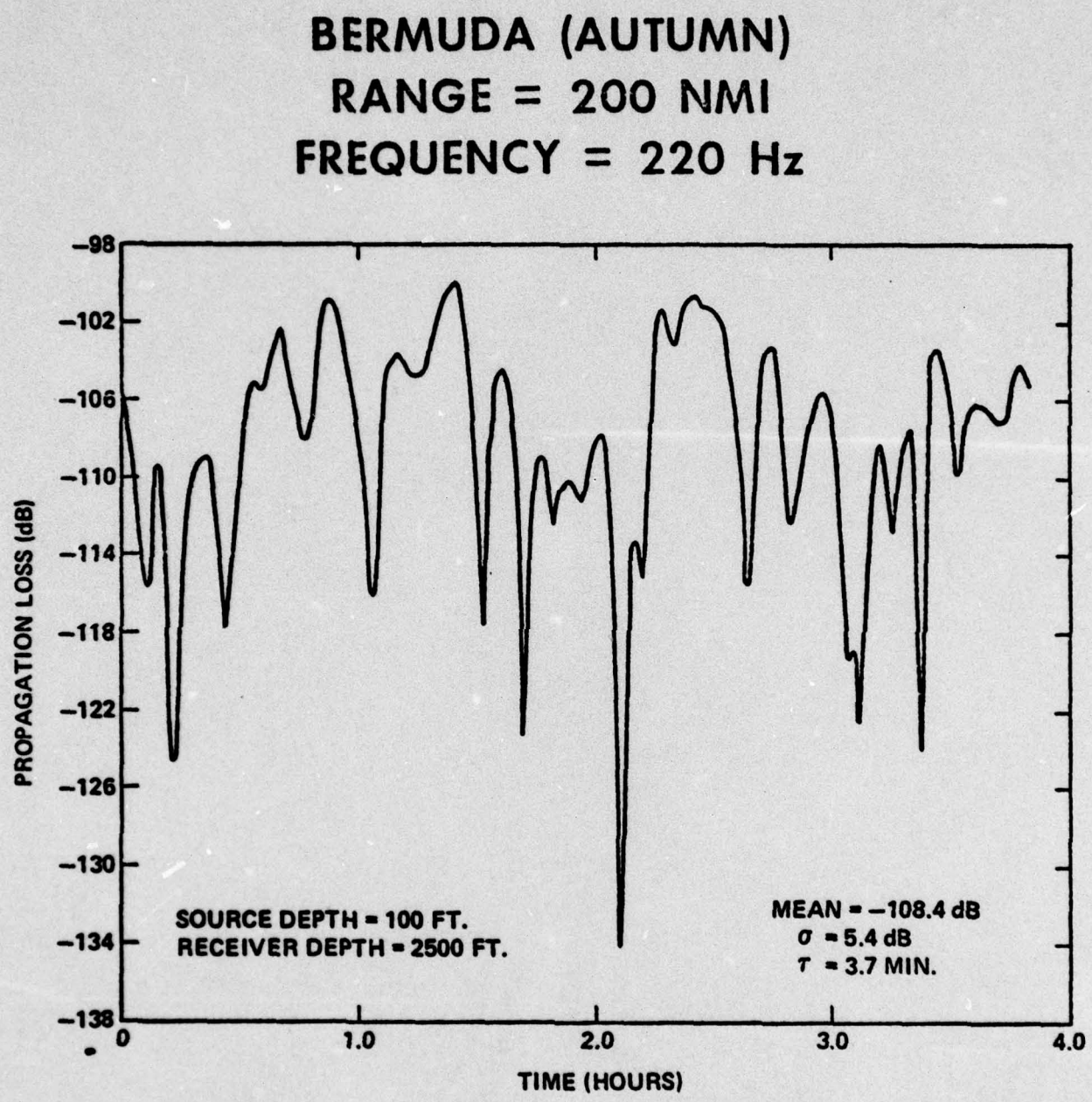

FIGURE 1 PROPAGATION LOSS TIME SERIES FOR A RANGE OF 200 NMI AND A FREQUENCY OF 200 HZ

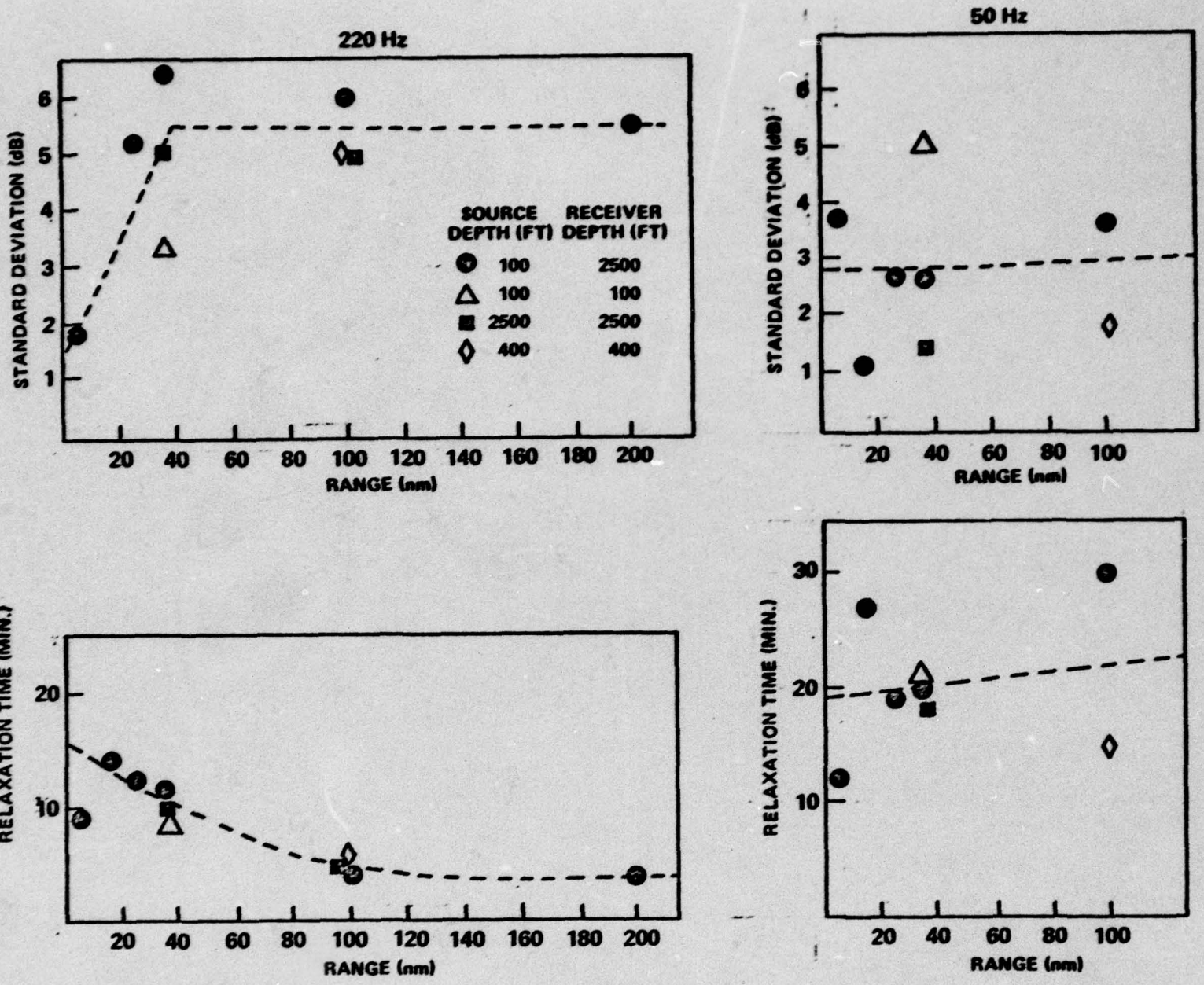

FIGURE 2 STANDARD DEVIATION AND RELAXATION TIME OF PROPAGATION LOSS VERSUS RANGE, AT 220 Hz AND AT 50 Hz, FOR THE BERMUDA (AUTUMN) ENVIRONMENT

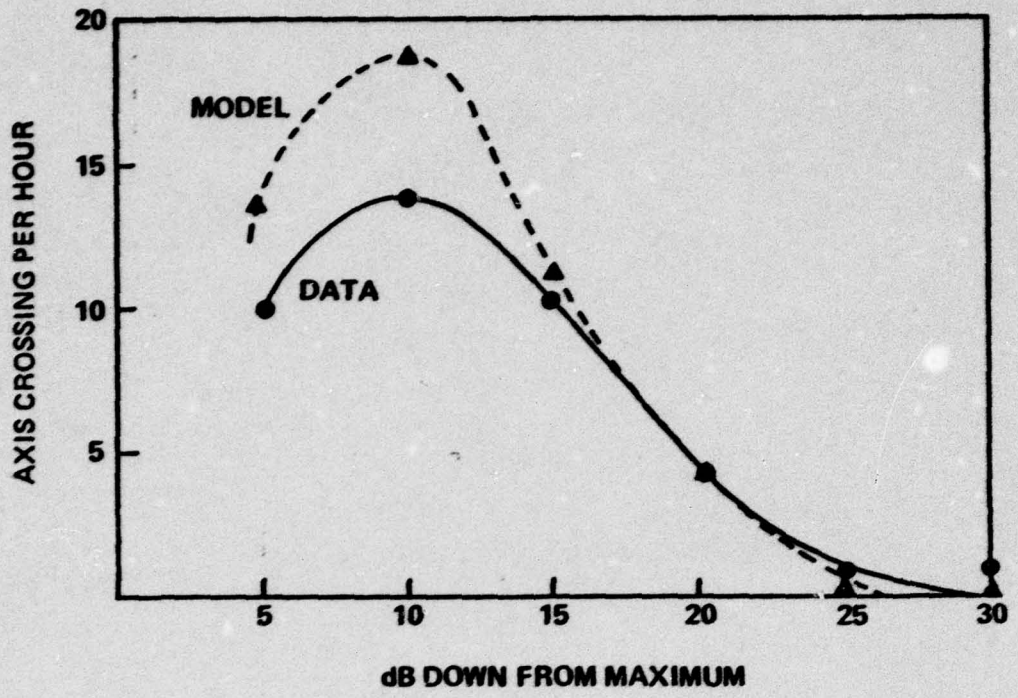

FIGURE 3 AXIS CROSSING RATE FOR ELEUTHERA DATA AND MODEL PREDICTIONS

- Both predicted and observed fluctuations tend to a maximum value of about 5 to 6 dB, a value which is characteristic of phase random multi-path propagation. One set of runs shows evidence that this value decreases with range at short (less than 40 nmi) separations but the current runs are insufficient to determine whether this feature changes with source-receiver depth, frequency, or environment

- Computed relaxation times range from one to two minutes up to about 30 minutes. Values at 220 Hz, at ranges of 100 to 200 nmi, are about five minutes in both the Bermuda and Atlantic environments, and on the order of one to two minutes in the two 400 Hz cases examined.

Conventionally, sonar fluctuation parameters are taken to be independent of range and essentially independent of frequency over the operating range of any particular sonar. Empirical fits to low frequency, long range, sonar performance suggest relaxation times, for the detecting process, of hours rather than minutes. The possibility, suggested by the results cited in this study, that fluctuation parameters may vary with both frequency and range could be of considerable importance in optimizing sonar design and use. Crudely speaking, the cited propagation fluctuation characteristics imply relatively better performance with increasing range and frequency, than is predicted by conventional calculations. For example, to the extent that such effects dominate, sonars designed to reach a given range could have lower gains, and operate at higher frequencies, then would otherwise be necessary.

Of course, many phenomena besides those treated can produce or modify observed fluctuations on any particular sonar. In a complete description these must be included also. In addition the sonar system itself modifies the properties of an incoming signal so that, ultimately, the observed fluctuations depend on the properties of the system. Long integration times will remove, or smooth, relatively rapid fluctuations. High resolution systems can introduce fluctuations by responding to changes in parameters which would not be resolvable on less powerful systems. This is not to suggest that the trends observed in this study are not of interest, but only that realistic assessment of sonar performance must integrate such results into a more comprehensive sonar model. As such models are developed, estimates of transmission statistics will play a central role.

TABLE OF CONTENTS

I. INTRODUCTION

Modeling and assessment of the performance of narrowband sonar systems requires information on both the mean value, and the variability, of acoustic inputs (signal and noise) to the system. While substantial attention has been given to the problem of estimating the mean values from environmental and system parameters, the problem of predicting corresponding statistical properties has been given far less emphasis. This report considers, in particular, the question of time variations in transmission loss between a fixed source, and a fixed receiver in the ocean. There are two bases for this choice of topics. First, transmission loss is a critical element in determing both received signal levels and received noise levels. In addition, there now exists a considerable body of information on details of acoustic transmission phenomena, some of which provide a basis for predicting stochastic elements of propagation loss.

Of these phenomena, this report concentrates especially on transmission loss perturbations induced by internal wave activity. It is generally conceded that this is one of the most significant mechanisms affecting propagation at acoustic frequencies between a few Hz and a few hundred Hz. The bulk of the material which follows concerns development, and initial application of a model for simulating acoustic propagation through an internal wave field. The internal wave description used rests on a power spectrum proposed by Garrett and Munk, and assumes a horizontally isotropic distribution of internal waves. The acoustic propagation calculations use ray tracing techniques, and require propagation parameters (velocity profile, bottom class, etc.) appropriate to the particular problem of interest. The principal output of the model is estimated transmission loss versus time. Such simulated time series may be used directly (through additional simulations), or indirectly (through calculated values of statistical parameters), to evaluate the expected impact of predicted fluctuations on sonar performance.

In the next section, we review briefly the elements of the transmission fluctuation program, including discussion of some of the important perturbing mechanisms. In Section III, we discuss, in qualitative terms, the nature of internal waves, and how we model their effect on acoustic transmission. (A detailed quantitative discussion of these issues is given in the Appendices.) Section IV displays and discusses results from the model developed in this study, and Section V summarizes study conclusions and recommendations.

II. BACKGROUND

2.1 ACOUSTIC FLUCTUATIONS AND SONAR PERFORMANCE

Observation of the outputs of low frequency passive sonars readily establishes that the signals in such systems normally exhibit very large random fluctuations. Such fluctuations arise partly because the output levels of sound sources in the ocean vary with time, partly because of the way sound propagates from the sources to the sonar receiver, and partly because of attributes of the sonar system itself. In particular, the propagation characteristics of the medium contribute to fluctuations in two ways: first, when either source or receiver are in motion, spatial variations in transmission properties will cause temporal variations in received acoustic energy; second, temporal variations in transmission properties will cause fluctuations in the observed acoustic fields, even when source and receiver are stationary. In this report, we focus particularly on this last effect.

While the problem of estimating the mean values of acoustic signals received by sonar systems has received continuing and aggressive attention, the problem of predicting the statistical properties of these signals has been given far less emphasis. In 1975 Code 431 of the Office of Naval Research and the Naval Ship Research and Development Center jointly sponsored a symposium on fluctuations and sonar performance which explicitly addressed how temporal fluctuations affect passive sonar system performance.[1] This symposium reviewed a considerable range of topics dealing with signal and noise temporal fluctuations, and the formalisms available for incorporating such phenomena into passive sonar system performance predictions. The principal conclusion of the symposium was that, although fluctuation phenomena are frequently a critical element in determining sonar performance, descriptions of the significant phenomena, and related sonar performance prediction methodologies,are frequently inadequate and occasionally nonexistent.

The potential importance of properly treating fluctuations may be readily appreciated by considering a simple case: a narrowband passive sonar presented with fixed mean values of signal and noise at its inputs. In such a system the signal detection criterion is usually equivalent to asking whether the signal to noise ratio exceeds a specified threshold. For any given mean value the probability of this occurring, the time over which the condition will last (holding time), and the time between occurrences (recontact time), are all determined solely by fluctuations in the input quantities. When deterministic variations (e.g., due to target motion or diurnal changes) are added the effect of random fluctuations cannot be separated out so readily, but the contribution to system performance is no less important.

The complexity of the fluctuation problem may also be readily appreciated. Sonar inputs are affected by a number of processes, each with its own set of stochastic parameters. The resulting composite fluctuations are superpositions of many distributions and time scales. Furthermore, the character of the observed fluctuation is affected not least by the properties of the sonar system itself: bandwidth, integration time, processing methodology and sensor directivity all help shape how the observed signals vary. Ultimately, therefore, the character of sonar fluctuations is a function as much of the sonar system of interest as it is of the external acoustic environment.

2.2 SOUND SPEED MICROSTRUCTURE

In this report we deal particularly with the assessment of time dependence of low frequency propagation loss in the ocean. The interest in this topic reflects, of course, the fundamental importance which proper treatment of transmission loss has in determining sonar detection performance. In the familiar context of the sonar equation, transmission loss enters in a number of ways: explicitly in assessing the loss from target to receiver, and implicitly in estimating such factors as ambient noise, array gain, reverberation levels, etc. Standard treatments of the sonar detection problem treat all these factors as independent, but they are, in fact, linked by common transmission loss phenomena, and the ability to model sonar detection should be considerably improved if the statistics of this common factor can be better understood.

In discussing acoustic transmission phenomena, it is necessary to decide in what terms the discussion will take place. Although, in principle, acoustic transmission in the ocean must be treated as a wave phenomenon, it is well known that open ocean conditions are very often such as to allow approximating transmission effects through various ray trace techniques. Such techniques permit estimates of the two most important characteristics of open ocean transmission: refraction effects due to a spatially varying index of refraction (sound velocity), and reflection and absorption at the ocean surface and bottom. Such calculations properly deal with properties of the medium whose spatial variation occurs on a scale at least several times larger than an acoustic wave length and lead to the familiar picture that sound transmission between two specified points takes place along a number of well defined, but distinct paths (rays).

Of course, the paths which result from ray tracing do actually correspond to approximate solutions of the wave equation. The wavefronts (regions of constant phase) for each ray are the surfaces perpendicular to the ray. Phase shifts along a given path, for any frequency, can be calculated from the sound speed at each point along the path. With this interpretation many nominally wave effects can be estimated from ray trace results. Interference effects are obtained by adding multipaths coherently using the intensities and phases derived from ray tracing. Responses of extended sets of transducers (arrays) may be computed using phases similarly obtained. Under many circumstances certain diffraction effects can be treated as a straightforward perturbation of the ray trace solutions. In a similar manner, it is often possible to interpret and evaluate those mechanisms which cause transmission loss fluctuations in terms of a ray trace picture.

It is readily apparent that, from this viewpoint, there are two classes of fluctuation phenomena: those in which the amplitudes of the component multipaths vary with time, and those in which their phases vary. While the latter effect does not change the intensities of individual ray paths, it can by altering their relative phases, cause variations in the intensity of their sum, and hence generate fluctuations in overall transmission loss.

The physical phenomena which cause these variations can also be divided into two principal catagories: interactions of ray paths with the time varying sea surface, and propagation of ray paths through structure within the ocean which changes with time. The first of these involves fluctuations which arise as ray paths reflect from the corrugated moving boundary presented by surface waves. The second involves a number of different phenomena each of which contribute to time variations in the ocean's transmission properties.

The starting point for ray trace calculations is the ocean sound speed profile: the functional dependence of sound speed in the sea on depth and position. Typically these profiles characterize sound speed dependence with spatial resolutions of several tens of meters in depth and several hundreds to several thousands of meters in range. Careful observations establish, however, that the sound speed at any point is not constant, and fluctuations occur on spatial scales which range from much finer than, to much grosser than, the nominal resolutions cited above. These fluctuations act to perturb acoustic transmission paths, causing temporal variations in transmission loss.

Much of the observed fluctuation in sound speed, in turn, arises from mechanisms which cause mixing of ocean waters. Sound speed in the ocean is a function of water temperature. In regions where there is a temperature gradient, such mechanisms mix waters of different temperatures. This local intrusion of slightly different temperatures manifests itself as stochastic variations in the sound speed structure, which can affect propagation characteristics.

At the largest scale, ocean water flow is in the form of global currents, large scale eddies, and tidal effects. Such motion can generate large turbulent vortices which dissipate their energy by generating somewhat smaller scale vortices, starting a chain which ends with very small scale motions. The expected distribution over spatial scales in such situations was derived by Kolmogorov[2], who predicted that the energy density in turbulent flow varies as wavelength to the five-thirds power. This spectrum of fluid movement induces a corresponding spatial continuum of temperature fluctuations, and hence of sound speed fluctuations.

In a homogeneous medium this turbulent spectrum would dominate. The real ocean is stratified, exhibiting variations in density and temperature with depth. This stratification allows other types of fluid mixing, which modify the purely turbulent spectrum. The most notable of these are internal waves, which are the major subject of this study. Internal wave effects tend to dominate the low wave number region of the fluid velocity spectrum. More generally Mosely and Del Balzo[3] suggest that the spectrum of fluid velocity can be divided into seven regions: beyond the very large scale currents which derive their energy from geophysical processes, there are large stable eddies, the internal wave region, a buoyancy region, a region of inertial turbulance, and finally, at very large wavenumbers, a viscous dissipation region, where the fluid motion is damped, and its energy dissipated.

For low frequency (less than a few hundred Hz) acoustic propagation there is especial interest in the internal wave portion of this spectrum. First this is the most energetic region of the spectrum. In addition, the acoustic wave lengths at low frequencies are on the order of several meters or more in length. Much of the inhomogeneity spectrum (and especially the upper region where turbulence dominates) has much shorter spatial scales than this. Under these conditions the structure tends to act as weak isotropic scatterers, whose major effect is to remove small amounts of energy from a ray path. The internal wave region, on the other hand, presents inhomogeneities large compared with the acoustic wavelength. These tend to act as very forward scatterers whose net effect is to preserve ray paths, but alter their phase. This random phase perturbation, by generating time varying interference effects, can have a strong effect on total transmitted intensity, when more than one acoustic path contributes.

There exists a considerable body of work (much of it developed for atmospheric propagation) on propagation of energy through media with random inhomogenieties. Much of this material (e.g., the classic work by Tatarskii[4]) assumes that the inhomogenieties follow the Kolmogrorov spectrum. Much of it, also, seeks analytic solutions for particular statistical parameters under conditions (very large wave number, short ranges, homogeneous ocean) which severely limit application of results. In the chapter which follows we outline a model which assesses the effect of internal waves on acoustic propagation through a simulation approach. This has the decided advantage of not tying the model to particular measures of acoustic variability. Instead, the model generates explicit sample time series, which can be used to obtain any statistical parameters of interest.

III. INTERNAL WAVE MODEL-QUALITATIVE DISCUSSION

In this chapter we give a qualitative description of a model developed to allow simulating the effects of internal wave fields on acoustic propagation. (A roughly parallel treatment of the corresponding mathematical formalism is given in Appendix A.) Essentially the model uses estimates of the space-time power spectrum of internal waves to build up simulated sample functions of the internal wave field which can be explicitly evaluated at any given space-time point. From this function, estimates of the variation in sound speed, due to internal wave activity, can be formed. A standard ray trace transmission loss model is then used to establish expected transmission parameters in the absence of internal waves, and also to estimate how the internal wave field induced sound speed fluctuations perturb these parameters. For any one sample function the perturbations can be evaluated as a function of both time, and source-receiver position. The calculation can be replicated, to build up statistics, by constructing additional sample functions.

The construction of internal wave functions rests on a canonical description of the ocean's density-temperature structure. There is some expectation that the form of internal wavefield spectrum is not very sensitive to local conditions so that use of a single general description may be satisfactory. On the other hand, the ray trace calculations and evaluation of certain internal wavefield parameters are based on estimates of the mean sound speed at the site and for the conditions of interest, making the model results particular to those conditions. This makes it possible to use the model to explore whether some sets of propagation conditions are more sensitive to internal wave effects than others.

Internal waves are wave motions (somewhat like surface waves) which propagate in the body of a fluid, where there is a density gradient. Like surface waves, they involve vertical motions of the fluid, which induce local mixing of the fluid. As noted in the last chapter, if there is a temperature gradient as well as a density gradient, the effect of such mixing is to introduce local anomalies in the sound speed profile, which can perturb acoustic propagation.

Recent work by a number of workers has begun to provide a quantitative foundation for understanding and modeling these effects. In outlining this progress, it is convenient to divide the problem into three parts: the nature of the internal wave field, the effect of internal waves on the velocity profile (index of refraction), and the modeling of transmission fluctuations induced by the velocity changes.

Characterizations of the internal wave field are based on work by Garret and Munk[5], which combines mathematical forms derived from solutions of the wave equation with empirical fits to data. Briefly their description has the following properties:

- Internal waves are a superposition of horizontally propagating plane waves with a specified propagation direction, wave number, and frequency.

- Internal wave propagation can be sustained, in two dimensions, for a considerable range of wave numbers and frequencies.

- For any particular density gradient there is a set of internal wave solutions (normal modes) at discrete (but densely spaced) combinations of frequency and wave number which span the range of possible frequency-wave number values.

- Garrett and Munk derive equations for the normal modes assuming a particular (exponential) density function. They note that while the form (vertical dependence) of these modes is highly detailed, an RMS average over a large number of adjacent modes (nearly constant frequency-wave number) is quite smooth. They postulate that the averaged function is also relatively insensitive to the choice of density gradient.

- Coupling among the modes causes energy to be shared among them. Garret and Munk derive a semi-empirical expression for the power spectrum (e.g., the average energy density per unit wave number-frequency interval). Since the physical process is stochastic, the actual amplitude of any mode at any time is a random variable whose mean square value is determined by the power spectrum. A natural assumption is that the amplitude itself is Rayleigh distributed with random phase (e.g., a Gaussian Random process). (The sum over closely spaced modes referred to above has essentially the same frequency and wave number as the constituent modes, and is again a Gaussian Random process.)

The vertical mixing of the water column at any given location is thus given by a superposition of a large number of traveling waves with random amplitude and phase. The change in temperature at that location is assumed to be proportional to the vertical displacement and the mean thermal gradient, and is therefore itself a random process. The change in temperature causes a change in the local speed of sound which in turn is equivalent to a local change in the acoustic index of refraction.

In principle such variations in the index of refraction extend vertically through the entire water column. In fact, the Garret and Munk vertical distributions indicate that the bulk of the effect takes place over a relatively narrow range of depths at the base of the thermocline. Porter, et al[6], take advantage of this by introducing an approximation where the total change in index of refraction (over all depths) is imagined to be concentrated in a thin layer at the base of the thermocline. In this approximation the variations in index of refraction are still expressed as a superposition of horizontally propagating random waves, but the effect is confined to a thin slab in depth.

With this approximation it is straightforward to deal with the effects of internal waves on acoustic propagation, in the context of ray trace treatments of propagation effects. Any ray which does not cross the internal wave layer is unaffected; a ray which does cross behaves like any ray traversing a thin slab with index of refraction different from its surroundings. Its direction and amplitude* are essentially unaffected, but its phase is perturbed. Thus, in this picture, the main effect of internal waves is to perturb the phase of those acoustic paths which spend significant time at the depths of principal internal wave activity. These perturbations in phase will cause fluctuations in acoustic intensity when ray paths are combined at a receiver.

The technique adopted for modeling these effects is to use a Monte Carlo technique in which each replication involves constructing a particular realization of the internal wave field (e.g., picking amplitudes and phase for each constituent traveling wave), and then evaluating the resultant acoustic fluctuations as a function of position and time for that particular realization. Data from several such replications can be used to provide distribution functions, and spatial and temporal correlation functions,which characterize the variations in acoustic propagation which result from the internal wave perturbations.

The model developed here is similar in conception to models reported on by DeFarrari[7] Porter Spindel and Jaffee[6], and Flatte and Tappert[8]. The work by DeFarrari however, describes the internal wavefield using only a single mode, rather than the full spectrum incorporated in the other models. The work reported on here closely parallels that of Porter et al. However, we have adapted a considerably more sophisticated acoustic propagation module than theirs, and we have removed the simplifying restriction that internal waves propagate parallel to the acoustic propagation direction only and replaced it with the more reasonable condition of isotropy. Flatte and

---

* There will also be a change in amplitude due to reflections from the layer, but if the perturbation in index of refraction is small, this is negligible.

Tappert use parabolic equation techniques to deal with acoustic propagation and treat the internal wavefield in three, rather than two, dimensions. However their model deals with a canonical velocity profile only, and is also restricted to internal waves propagating parallel to the acoustic propagation direction. Finally the model developed here is the only one which explicitly simulates time series of acoustic propagation and related parameters. This offers considerable power and flexibility in applications to sonar performance problems.

IV. SIMULATION RESULTS

4.1 INTRODUCTION

In this section we investigate predicted properties of acoustic propagation in the presence of internal waves, through use of the simulation model described in the last section, and in the appendices to this report. Runs have been made with this model towards two distinct objectives as follows:

a) The acoustic propagation elements of the model deal with specific sets of propagation parameters (sound speed profiles, source/receiver depths, water depth, frequency, etc.). This makes it possible to investigate how sensitive predicted fluctuations are to changes in these parameters. This has been done for two seperate sets of environmental parameters, one representative of the Bermuda area in Autumn, and one representing the North Atlantic in Summer. In each case runs were made for several frequency-source receiver depth-source/receiver range combinations.

b) Again, because of the specific nature of the model, it is possible to run direct comparisions with experimental data. Detailed agreement in such comparisons is hardly to be expected, but gross features should correspond. In any case, it is such comparisons which can most effectively identify deficiencies in the model's predictive capabilities. Below we deal briefly with two such comparisons, one involving data from a propagation experiment conducted off of Eleuthera[9], and another from an experiment conducted between Eleuthera and Bermuda.[10]

In each model run, the basic result was a four hour time series of propagation loss. Plots of these allow qualitative inspection of predicted fluctuations. For several runs, estimates of the time variation of phase along one or two selected ray paths were also generated.*

Finally, for each time series, the mean, the variance and the relaxation time of the propagation loss, in decibels, were estimated. (Decibel values were used since these are normally the quantities of interest in sonar performance calculations.) The mean and variance were computed using standard definitions. The relaxation time was defined as the interval over which the autocorrelation function for the time series drops to 1/e of its initial value. (Note that the mean of a set of dB values is not the same as the mean of the equivilent power values, even when the latter is expressed in dB. Hence the means quoted below will not converge to conventional "incoherent" propagation loss estimates even when predicted phase fluctuations are large enough to make the constituent multipaths essentially incoherent.)

4.2 ENVIRONMENTAL PARAMETERS

Figure 4.1 shows velocity profiles for the four sites of interest. The first two are from the Naval Oceanographic Office "Oceanographic Atlas,"[11] which cites class averages for measured velocity profiles over selected regions of the ocean. The last two are profiles reported in the two experiments cited above. Figures 4.2 and 4.3 show conventional (incoherent sum) propagation loss versus range curves for the Bermuda (autumn) and North Atlantic (summer) environment as predicted by the propagation module of the model, in the absence of internal wave activity.

Table 4.1 shows, for each run set, values used for the parameters which determine space/time scales for internal wave activity. The first two columns are derived from the sound speed profile, while the last three are obtained from the first two (see Appendix B). The parameter n_o is the peak value of the Brünt Väisälä frequency and defines the peak frequency for internal wave activity. The parameter b is a length scale which defines how rapidly the Brünt Väisälä frequency falls off with depth. The "In Layer Depth" in the last column is the depth at which the model assumes internal wave activity to be localized. Bottom class 3 was assumed for all runs except the North Atlantic runs, which assumed bottom class 4.

4.3 RESULTS

4.3.1 Bermuda (Autumn) Environment

Table 4.2 is a compilation of all results for the Bermuda (autumn) environment. The emphasis was on runs at 220 Hz, and 50 Hz, with a 100 foot

---

* Typically, the most intense representatives of two distinct ray families (e.g., the loudest RSR and the loudest RR path) have been selected for presentation. Those displayed are illustrative examples only; actual model calculations allow up to 30 paths.

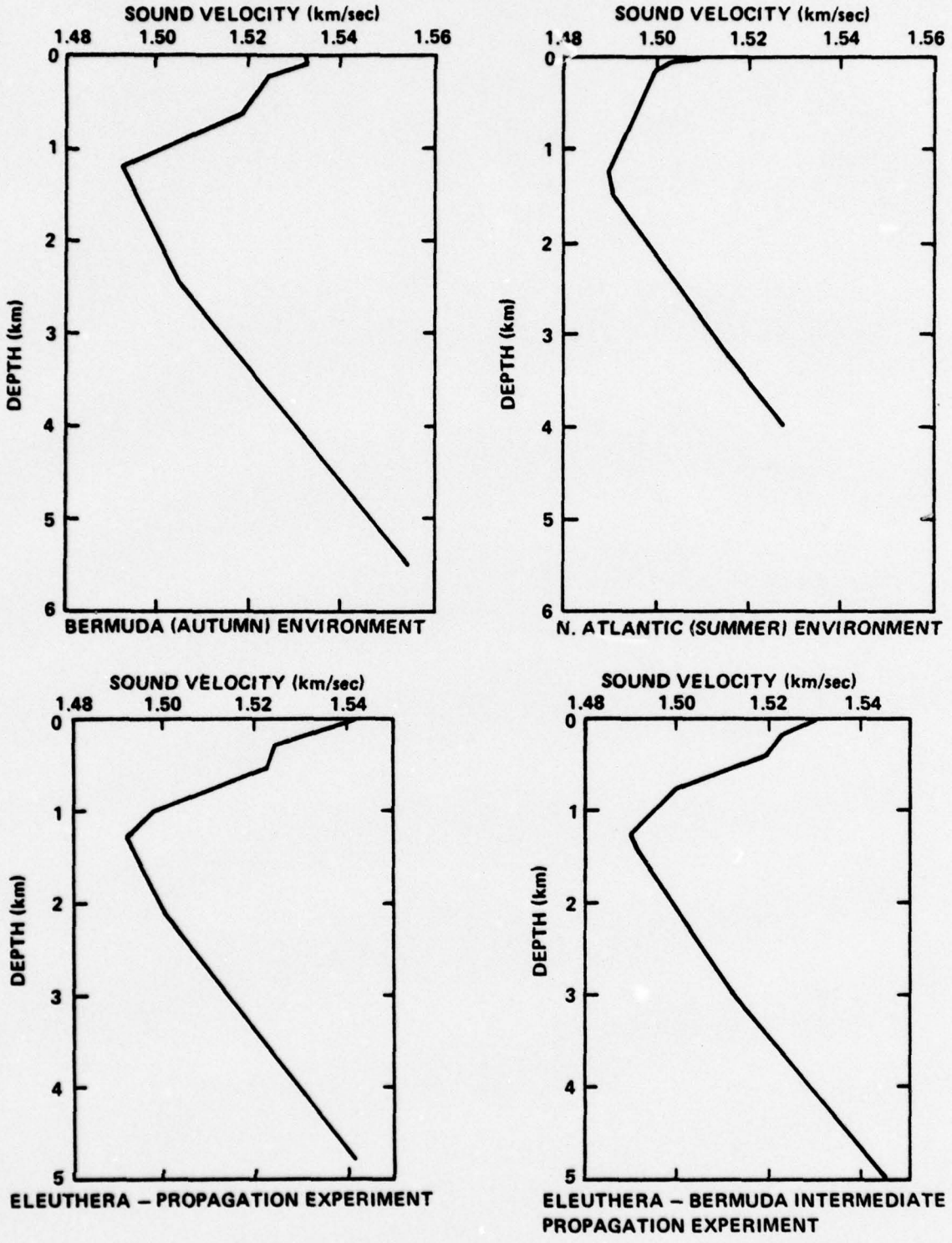

FIGURE 4.1 SOUND VELOCITY PROFILES

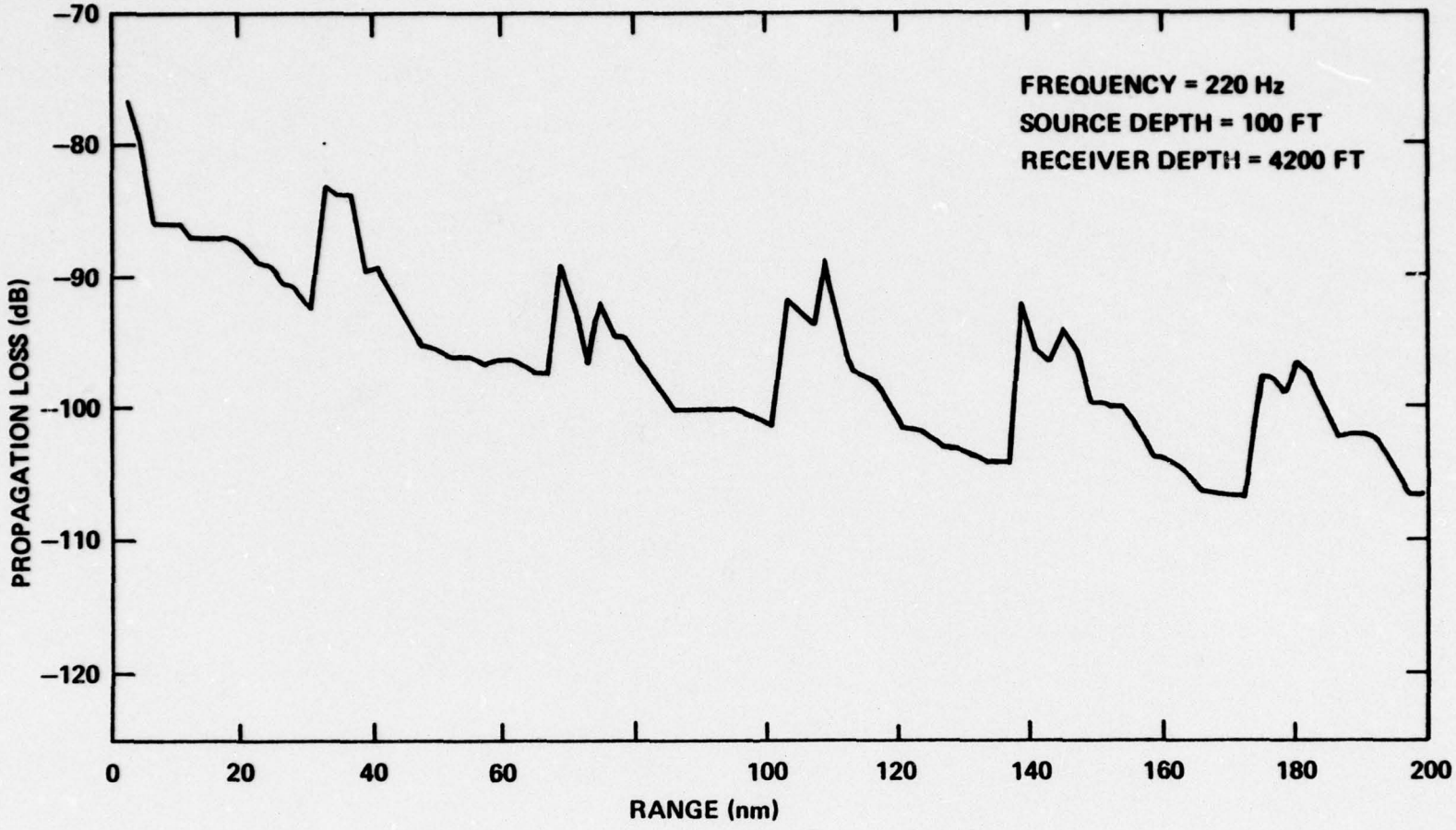

FIGURE 4.2 PROPAGATION LOSS FOR BERMUDA (AUTUMN) ENVIRONMENT

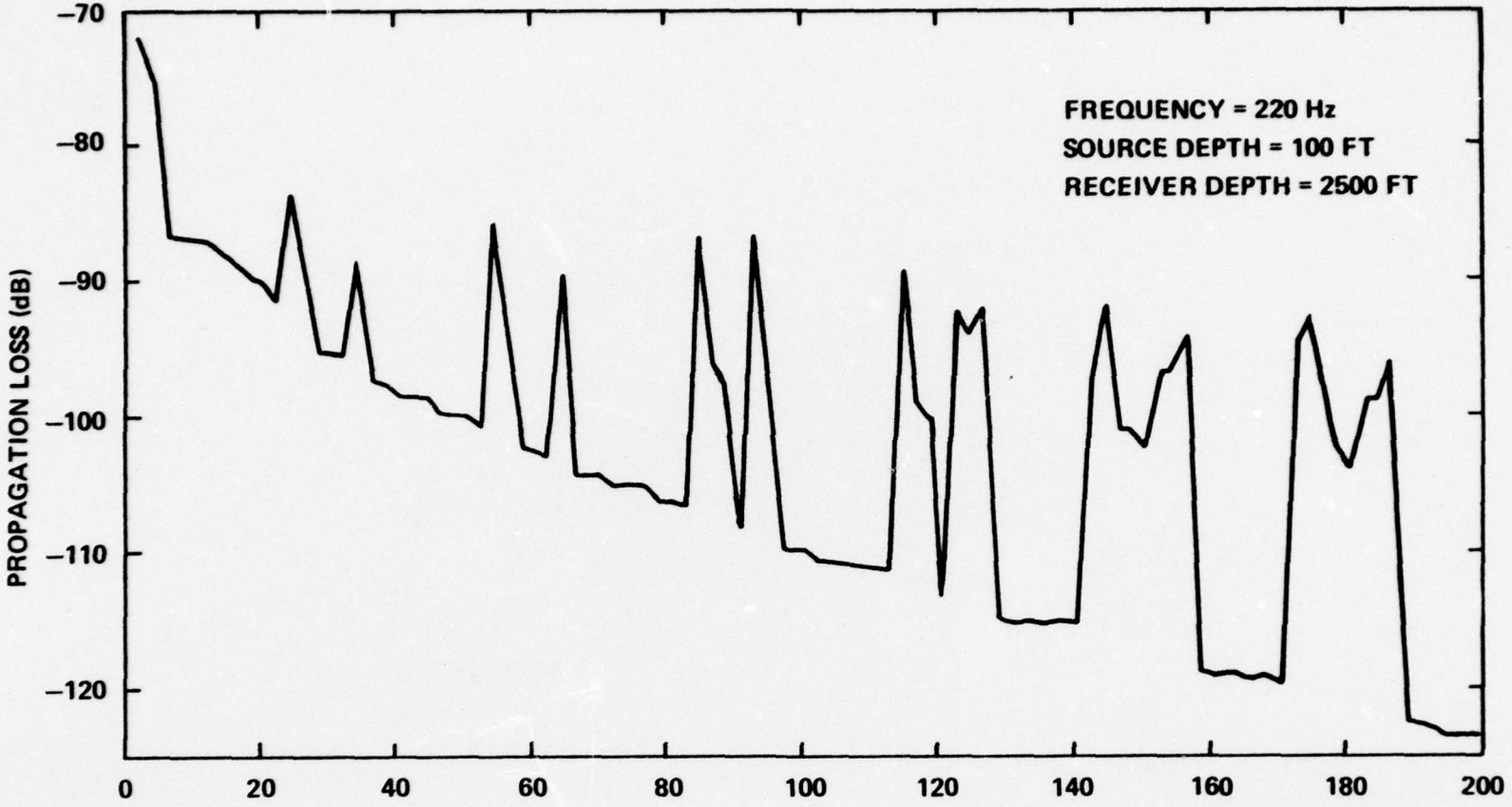

FIGURE 4.3 PROPAGATION LOSS FOR NORTH ATLANTIC (SUMMER) ENVIRONMENT

TABLE 4.1

PARAMETERS FOR MODEL RUNS

CASE	AXIS DEPTH (h) (km)	$\frac{1}{c}\frac{dc}{dz}\Big\|_o$ (Km^{-1})	b (Km)	n_o (Rad/Sec)	IW LAYER DEPTH (Km)
Bermuda (Autumn)	1.22	-.05	1.45	.0058	.72
N. Atlantic (Summer)	1.25	-.043	2.0	.0054	1.0
"Eleuthera Experiment"	1.30	-.039	1.27	.0052	.63
"Eleuthera-Bermuda Experiment"	1.25	-.029	1.33	.0047	.66

TABLE 4.2

RESULTS OF PROPAGATION LOSS TIME SERIES FOR BERMUDA (AUTUMN) ENVIRONMENT

Range (nm)	Source Depth (Ft)	Receiver Depth (Ft)	Frequency = 220 Hz			Frequency = 50 Hz		
			Mean Loss (dB)	σ (dB)	τ (min)	Mean Loss (dB)	σ (dB)	τ (min)
5*	100	2500	-77.9 ± 0.4	1.8	9	-93.6 ± 0.9	3.7	12
15*	100	2500	-88.2 ± 0.8	2.9	14	-85.7 ± 0.4	1.1	27
25*	100	2500	-92.4 ± 1.4	5.3	12	-90.2 ± 0.8	2.6	19
35*	100	2500	-96.1 ± 1.6	6.4	11	-96.5 ± 0.8	2.6	20
	100	100	-73.5 ± 0.9	3.3	8.5	-74.4 ± 1.1	5.0	21
	2500	2500	-82.7 ± 1.5	5.0	10	-76.9 ± 0.5	1.4	18
100	100	2500	-103.4 ± 1.2	5.9	4.4	-94.5 ± 1.8	3.6	29.7
	400	400	-103.3 ± 1.1	5.0	5.2	-95.8 ± 0.6	1.8	15
	2500	2500	-96.9 ± 1.0	4.9	4.5			
200	100	2500	-108.4 ± 1.0	5.4	3.7			

* Results at these ranges are a composite of more than one time series simulation computer runs.

source, and a 2500 foot receiver. There is a surface duct, and this choice of depths forced propagation paths to go through both the surface layer and the internal wave layer. The runs with source and receiver at 100 feet place both in the surface duct, while those runs with both at 2500 feet define a case where both are well below the surface layer and the internal wave layer. Figure 4.4 plots the statistical parameters in Table 4.2 against range. Figures 4.5 through 4.20 show the time series for the 220 Hz runs, and Figures 4.21 through 4.32 show the time series for the 50 Hz runs.

Qualitatively, the time series show features which also characterize typical experimental results: frequent fluctuations of several dB or more, with occasional deep fades, where the signal disappears entirely. It is evident that the 220 Hz results fluctuate rather more rapidly than the 50 Hz results, a conclusion which might have been anticipated since the size of the underlying phase fluctuations is inversely proportional to acoustic wavelength (Equation A20).

Examination of Figure 4.4 suggests that the statistical descriptions of the 220 Hz results, at least, show fairly clear range trends. It appears that the standard deviation increases with range until it reaches about five to six dB, after which it holds constant. (This would accord well with predictions that propagation fluctuations should have a standard deviation of 5.5 dB for long range multipath propagation.[12]) The relaxation time drops off smoothly with range, confirming the qualitative impression, suggested by the time series plots, that the fluctuations are more rapid at longer ranges. It is not clear whether the spread among the three standard deviation values (for different source-receiver depth combinations) at 35 miles is statistically significant; if so it would suggest that the fluctuations for a shallow source and receiver rise in amplitude more slowly, with range, than do those in cases where either source or receiver is deep. Finally, it is worth noting that while a source at 35 miles distance is clearly within a convergence zone according to Figure 4.2, there is no significant structure at this point in the 200 Hz relaxation time vs. range curve, and probably no significant departure from general trends in the standard deviation curve.

In contrast to the 220 Hz curves, the 50 Hz plots in Figure 4.4 show no discernable trends whatsoever. One possible explanation is that the values plotted are dominated by random variations--that is, the time series from which these parameters were estimated were not long enough to provide statistically reliable results. Figure 4.4 itself provides some internal evidence for this possibility; the mean value of the relaxation times shown at 50 Hz appears to be three to four times that of the values for 220 Hz, so that time series of a given length at 50 Hz would have fewer degrees of freedom, and less statistical reliability, than similar series at 220 Hz. Direct examination of the time series themselves suggests the same conclusion qualitatively; major fluctuations rarely occur more than once in a four hour period, and each plot shows relatively few fluctuation maxima of any kind, indicating that the duration of the series is too short to sample the full range of fluctuations.

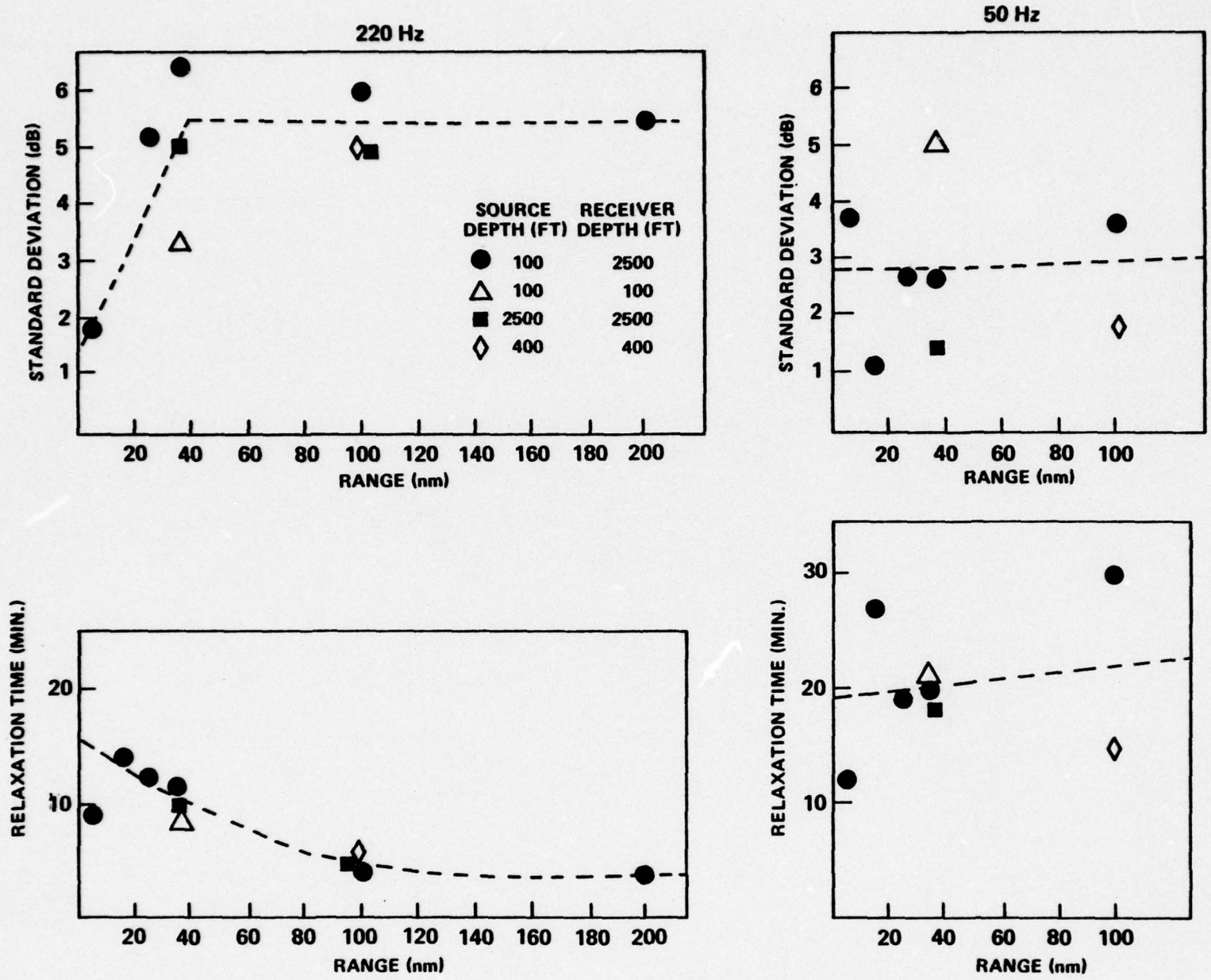

FIGURE 4.4 STANDARD DEVIATION AND RELAXATION TIME OF PROPAGATION LOSS VERSUS RANGE, AT 220 Hz AND AT 50 Hz, FOR THE BERMUDA (AUTUMN) ENVIRONMENT

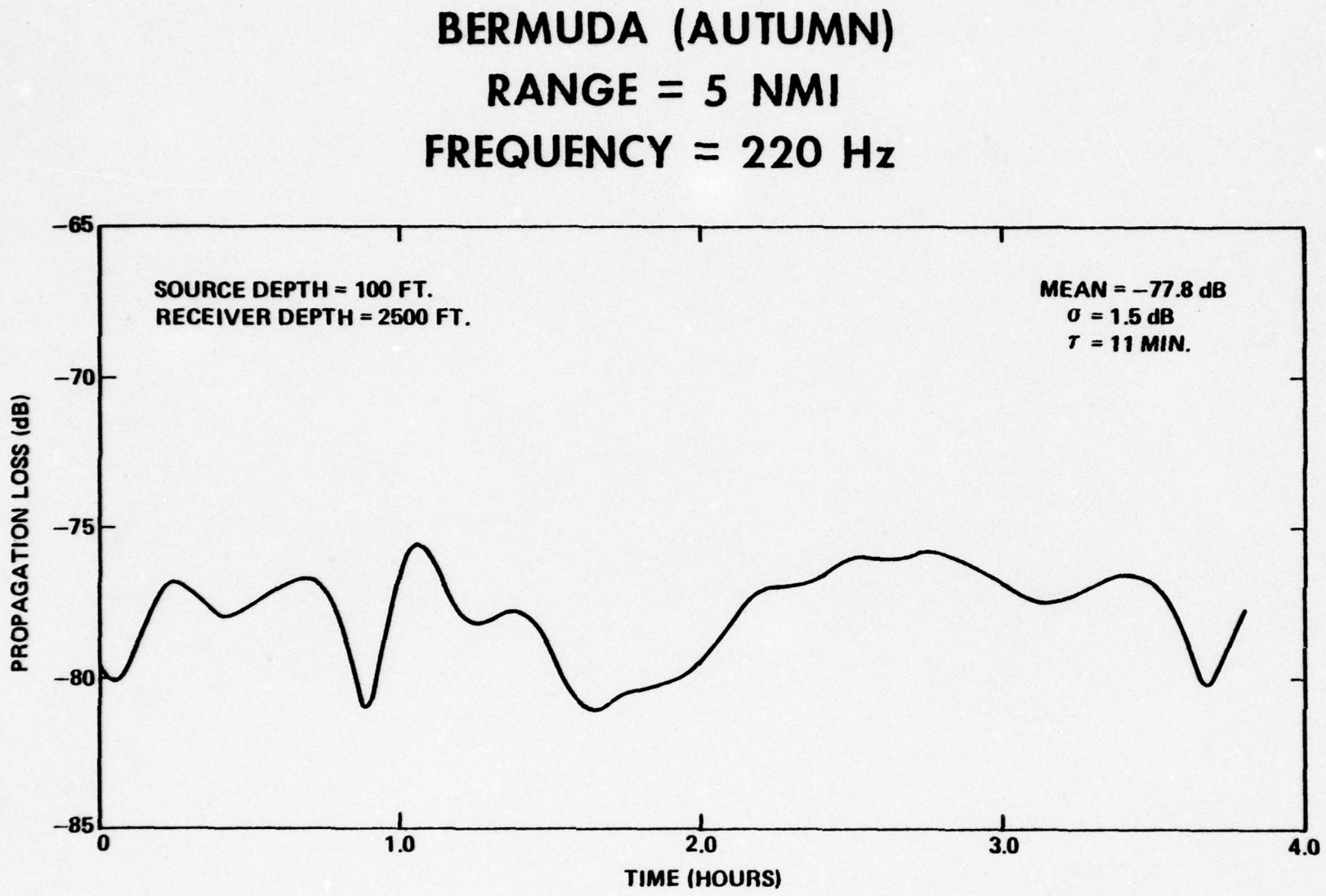

FIGURE 4.5 PROPAGATION LOSS TIME SERIES FOR A RANGE OF 5 NMI AND A FREQUENCY OF 220 Hz

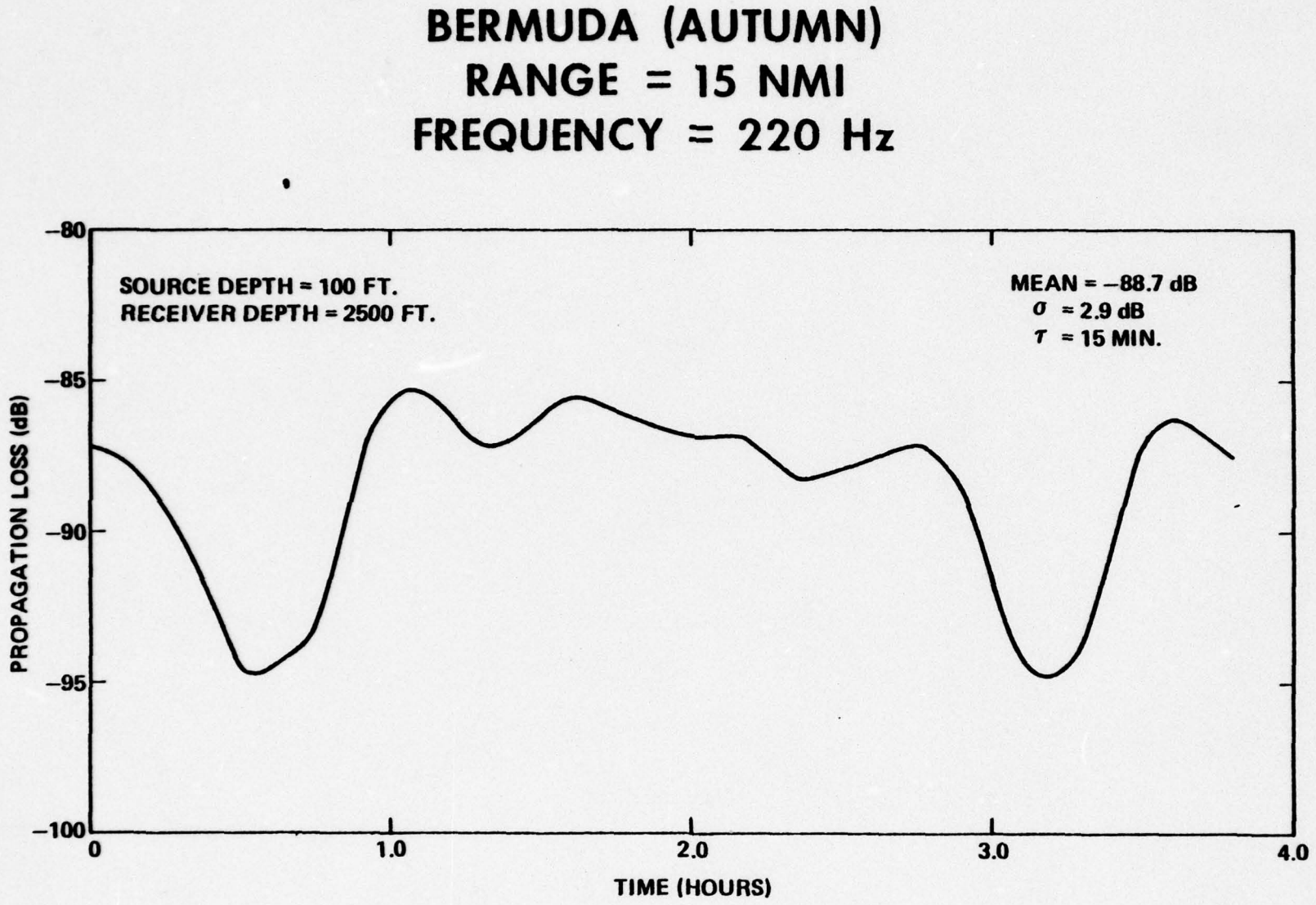

FIGURE 4.6 PROPAGATION LOSS TIME SERIES FOR A RANGE OF 15 NMI AND A FREQUENCY OF 220 HZ

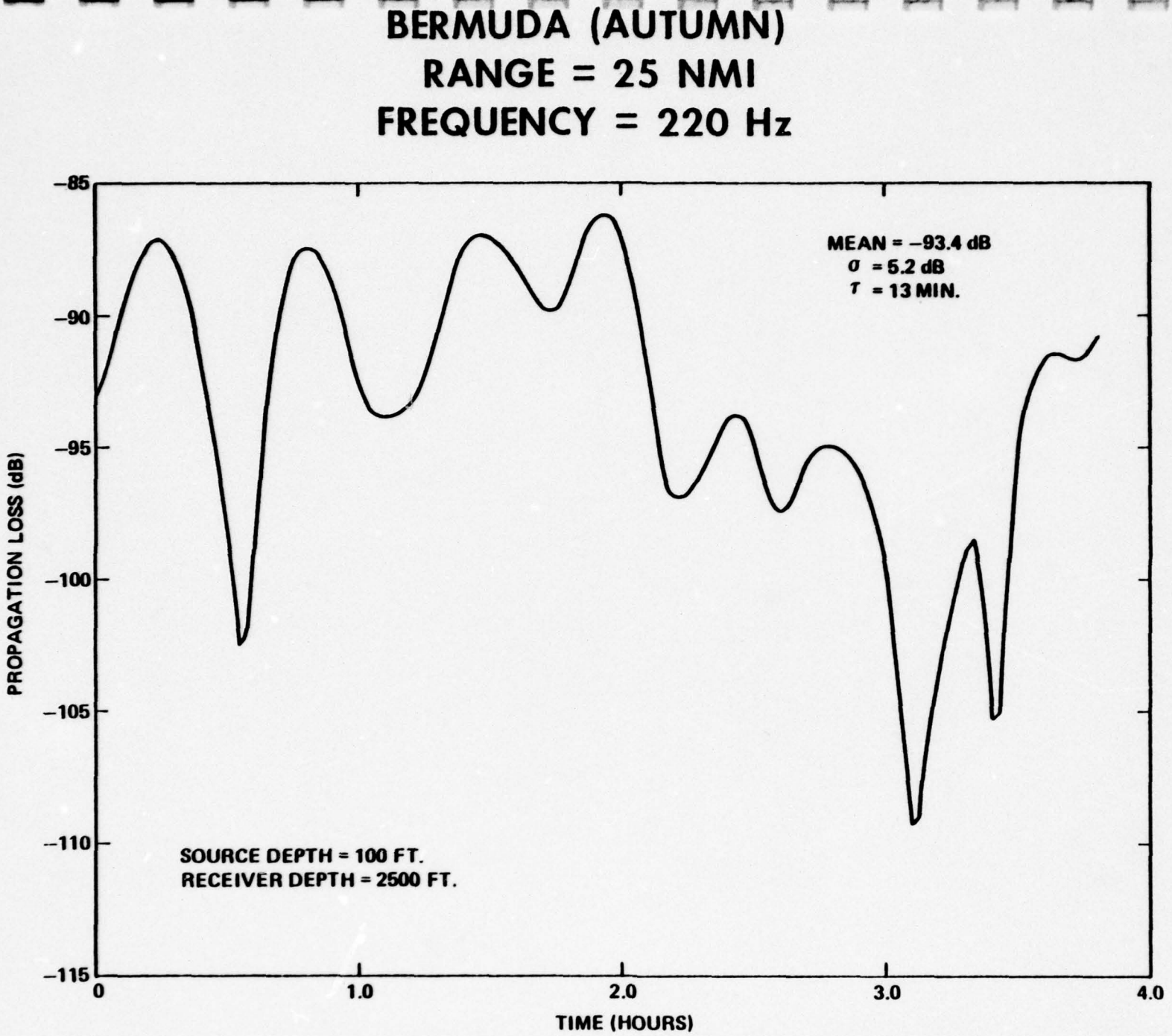

FIGURE 4.7 PROPAGATION LOSS TIME SERIES FOR A RANGE OF 25 NMI AND A FREQUENCY OF 220 HZ

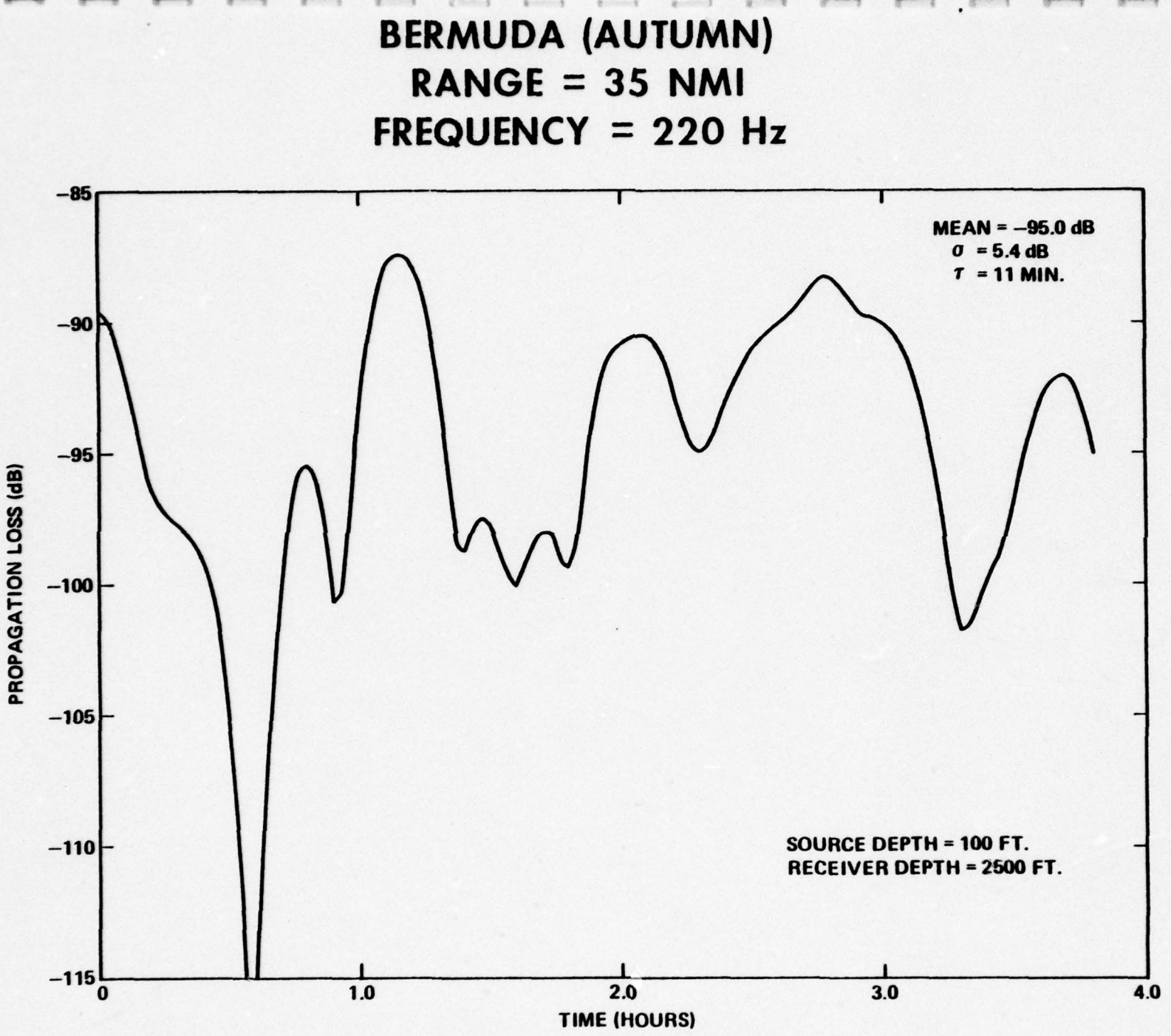

FIGURE 4.8 PROPAGATION LOSS TIME SERIES FOR A RANGE OF 35 NMI AND A FREQUENCY OF 220 Hz

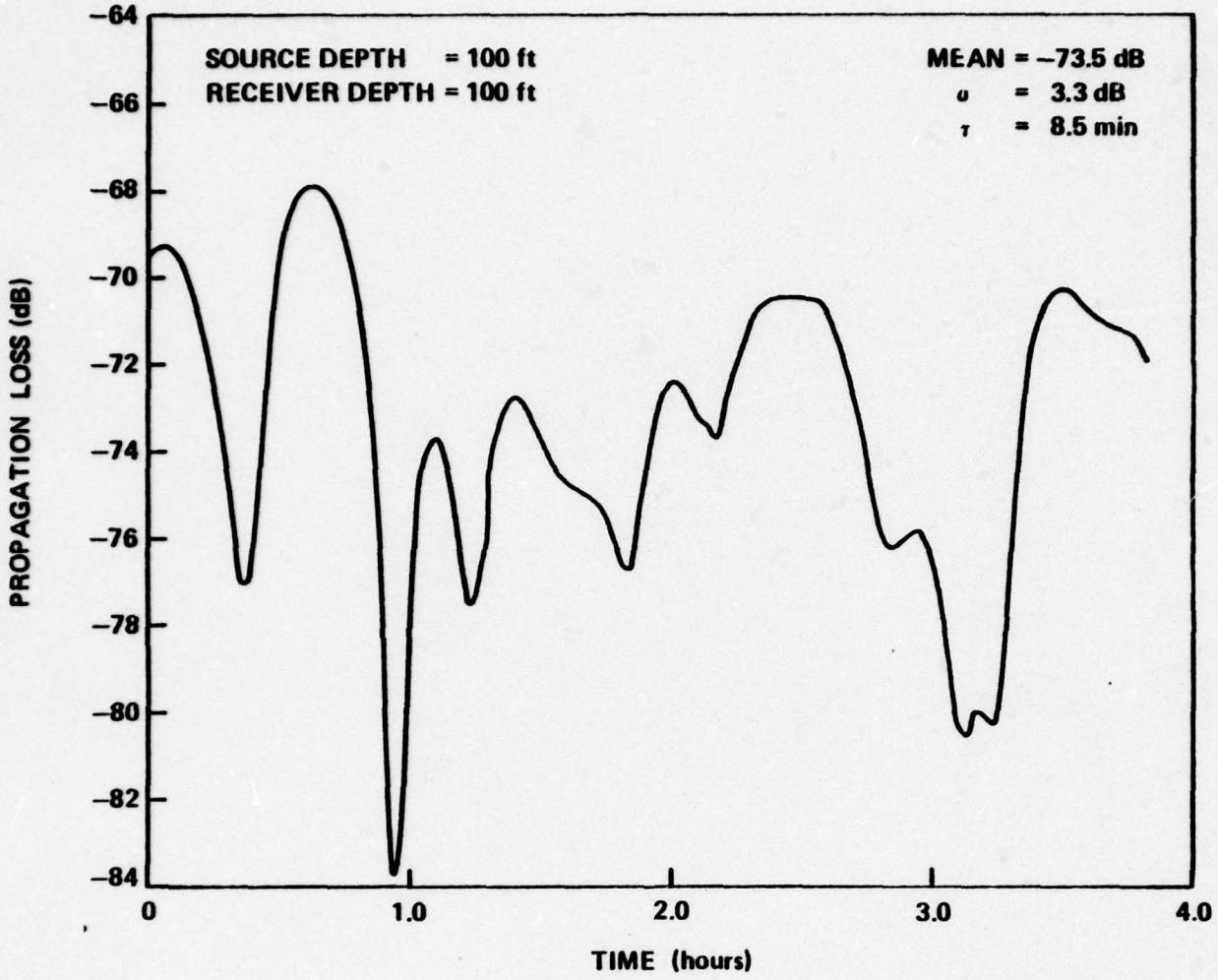

FIGURE 4.9 PROPAGATION LOSS TIME SERIES FOR A RANGE OF 35 NMI AND A FREQUENCY OF 220 HZ

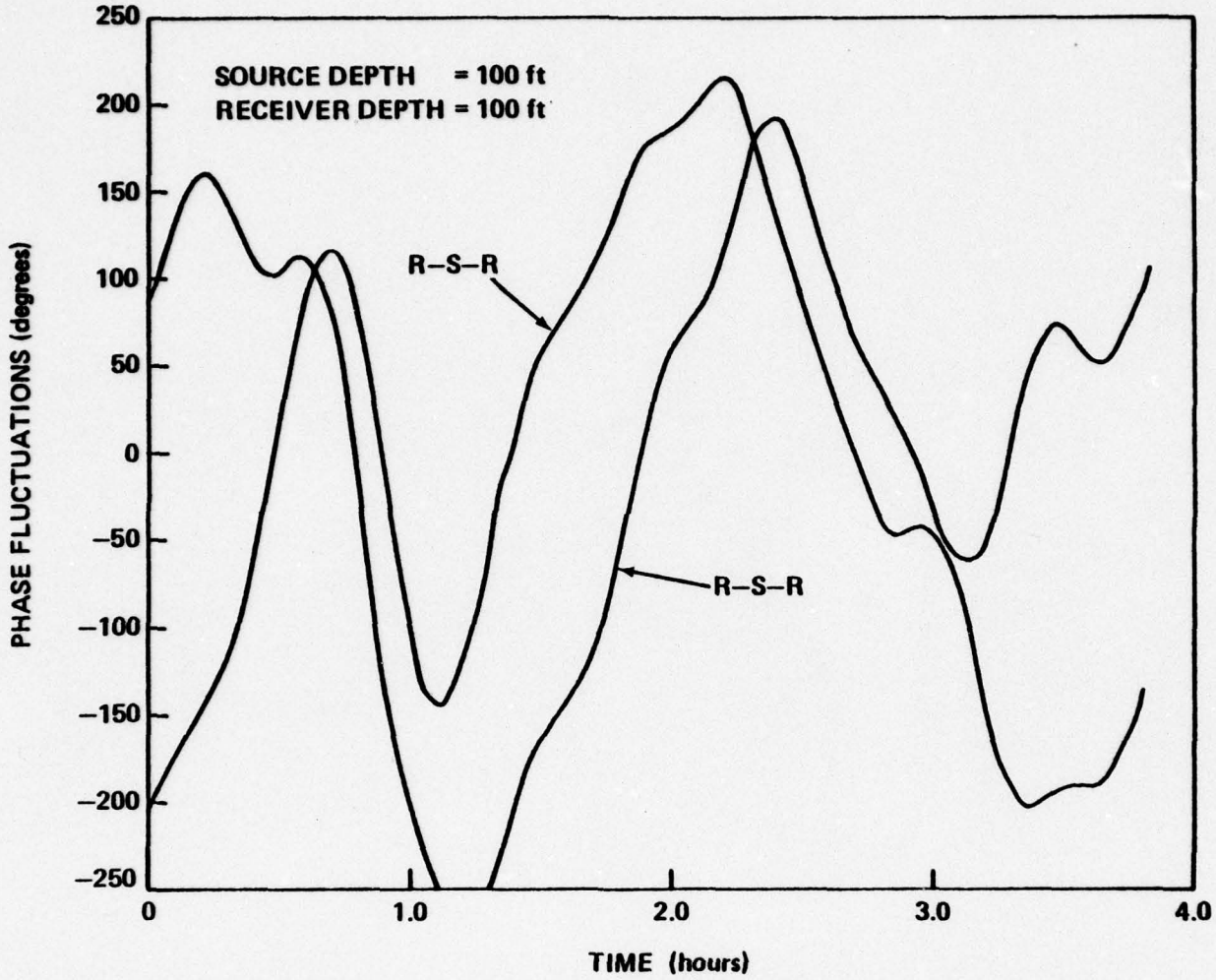

FIGURE 4.10 PHASE FLUCTUATIONS FOR DOMINANT EIGENRAY AT A RANGE OF 35 NMI AND A FREQUENCY OF 220 HZ

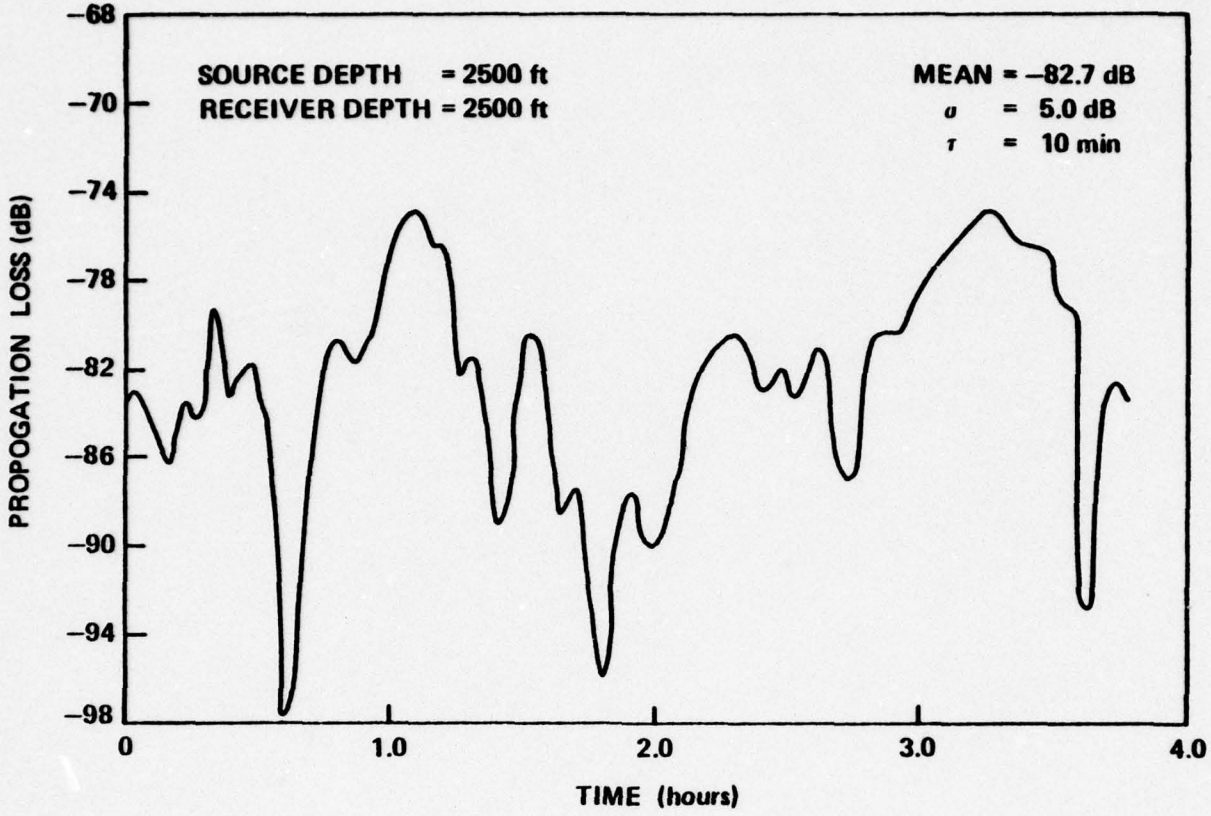

FIGURE 4.11 PROPAGATION LOSS TIME SERIES FOR A RANGE OF 35 NMI AND A FREQUENCY OF 220 HZ

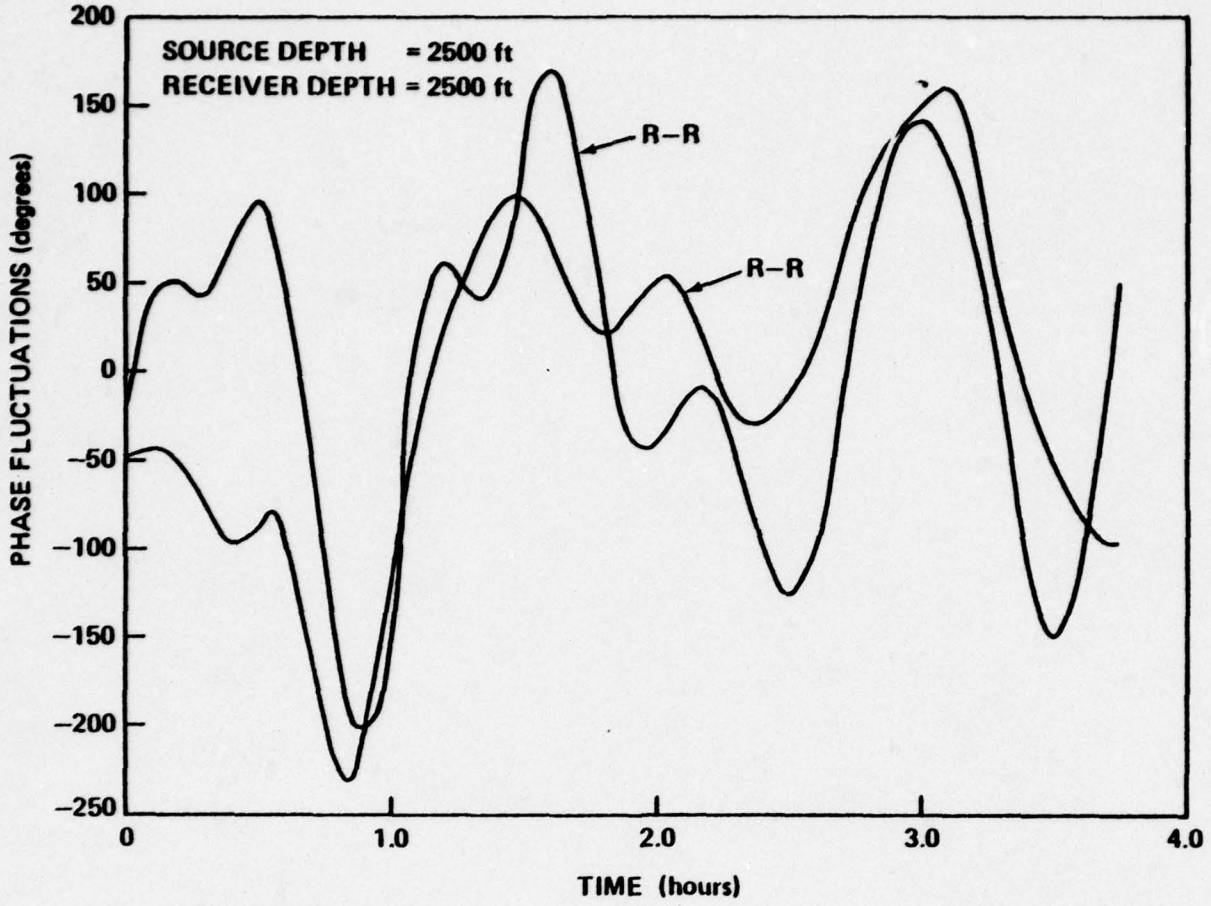

FIGURE 4.12 PHASE FLUCTUATIONS FOR DOMINANT EIGENRAYS AT A RANGE OF 35 NMI AND A FREQUENCY OF 220 HZ

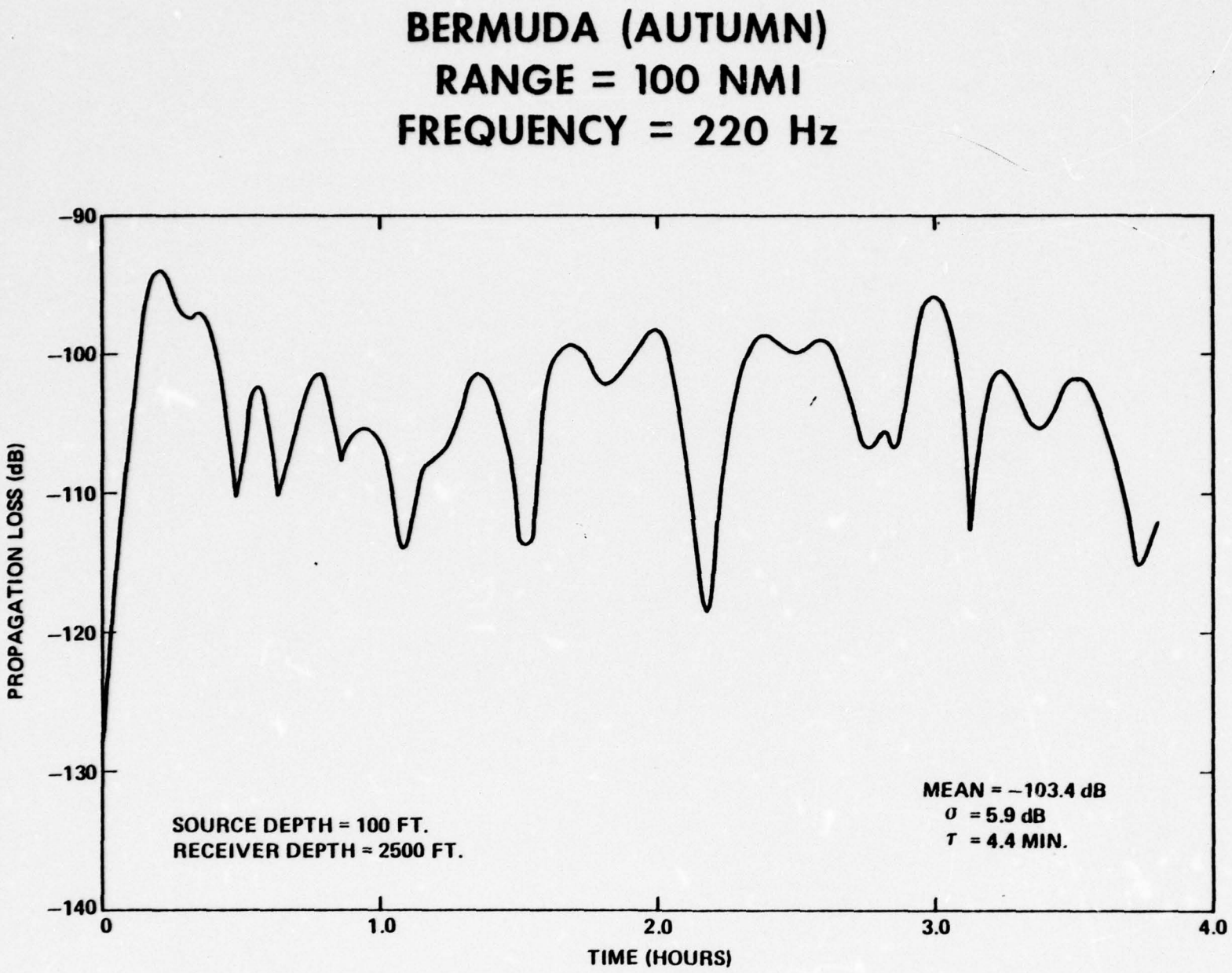

FIGURE 4.13 PROPAGATION LOSS TIME SERIES FOR A RANGE OF 100 NMI AND A FREQUENCY OF 220 HZ

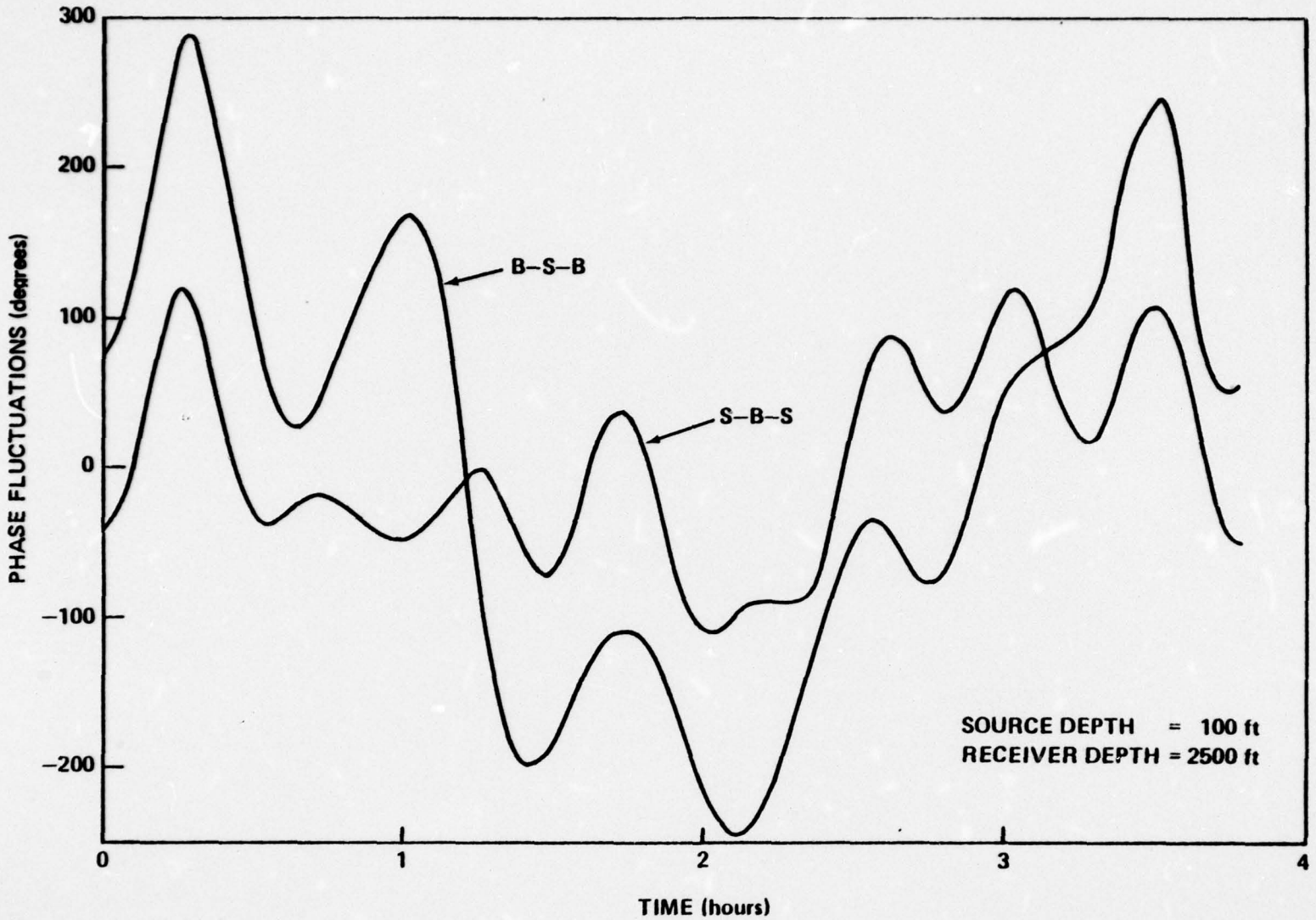

FIGURE 4.14 PHASE FLUCTUATIONS DOMINANT EIGENRAYS AT A RANGE OF 100 NMI AND A FREQUENCY OF 220 HZ

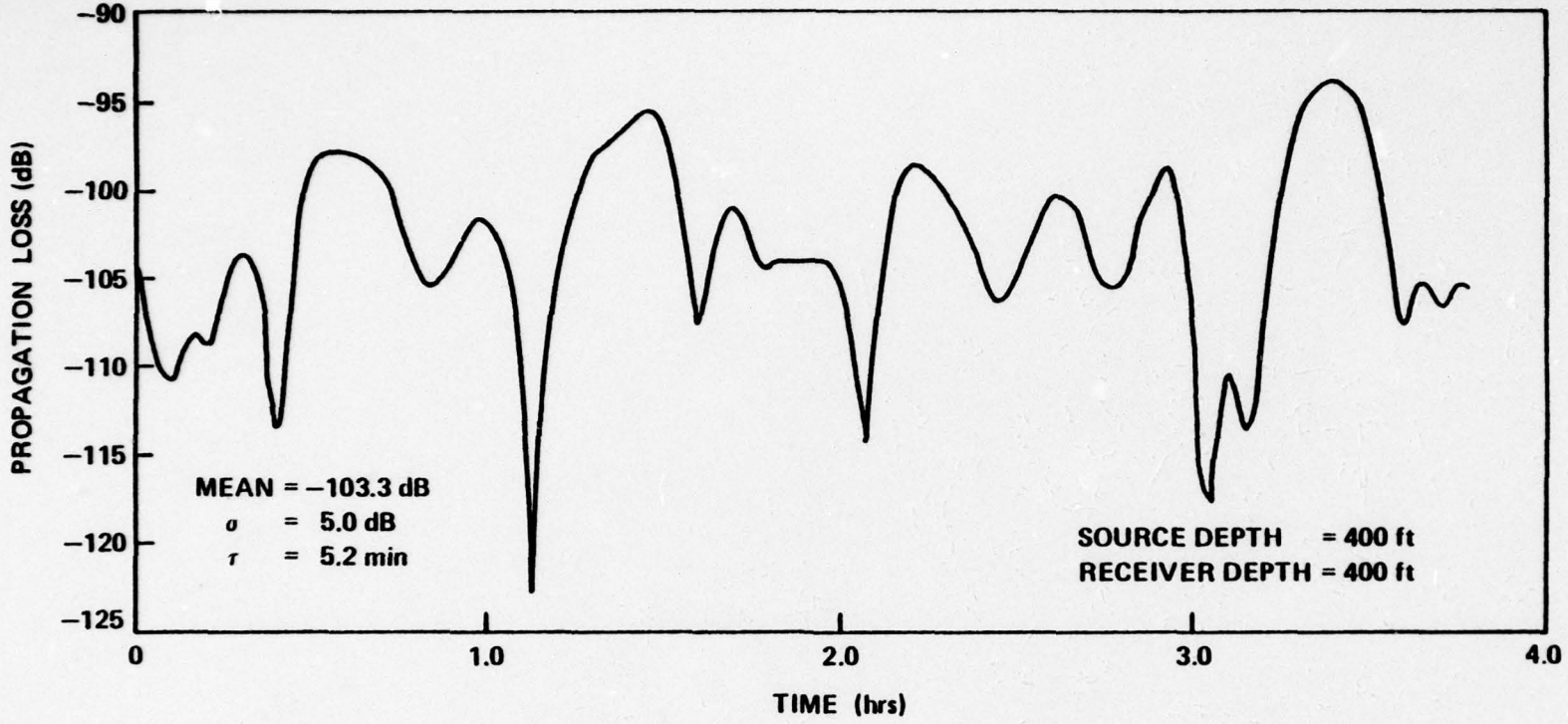

FIGURE 4.15 PROPAGATION LOSS TIME SERIES FOR A RANGE OF 100 NMI AND A FREQUENCY OF 220 HZ

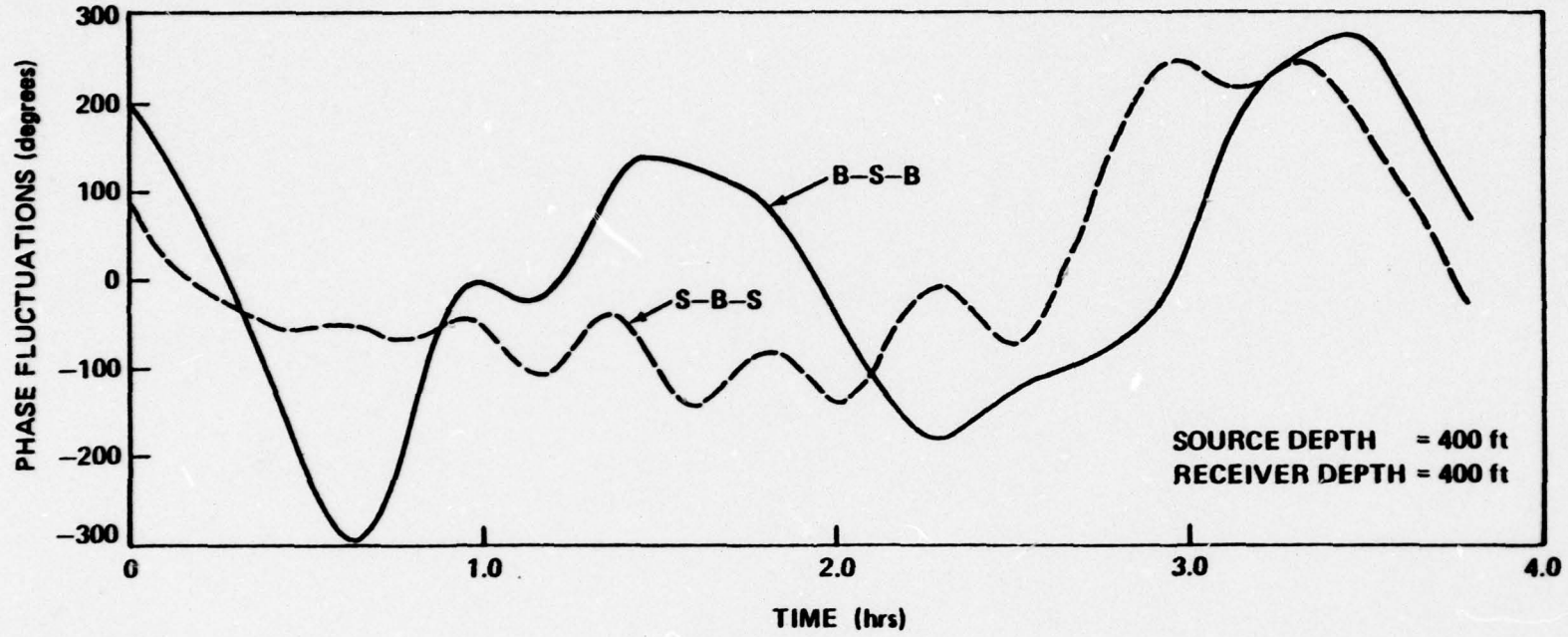

FIGURE 4.16 PHASE FLUCTUATIONS FOR DOMINANT EIGENRAYS AT A RANGE OF 100 NMI AND A FREQUENCY OF 220 HZ

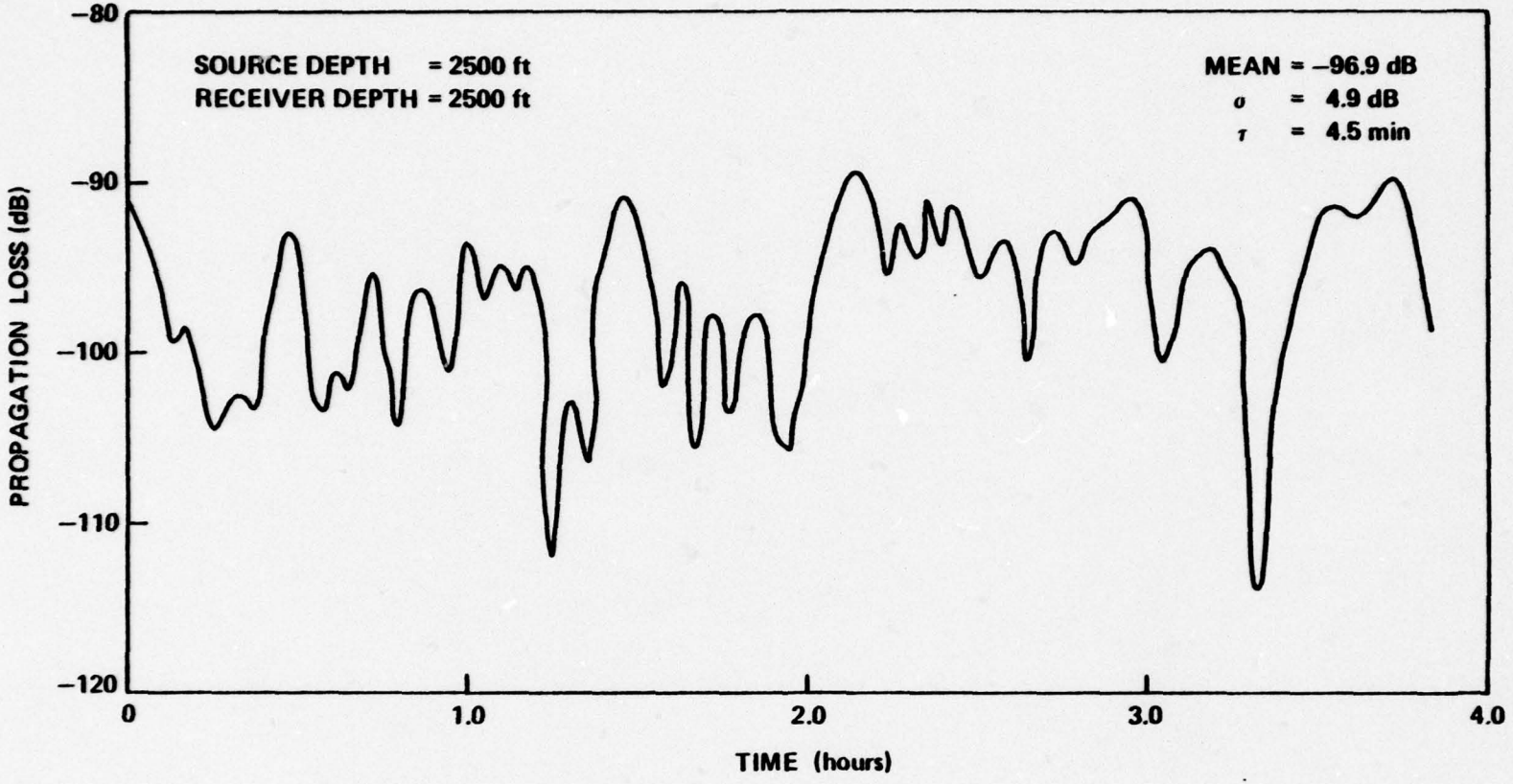

FIGURE 4.17 PROPAGATION LOSS TIME SERIES FOR A RANGE OF 100 NMI AND A FREQUENCY OF 220 HZ

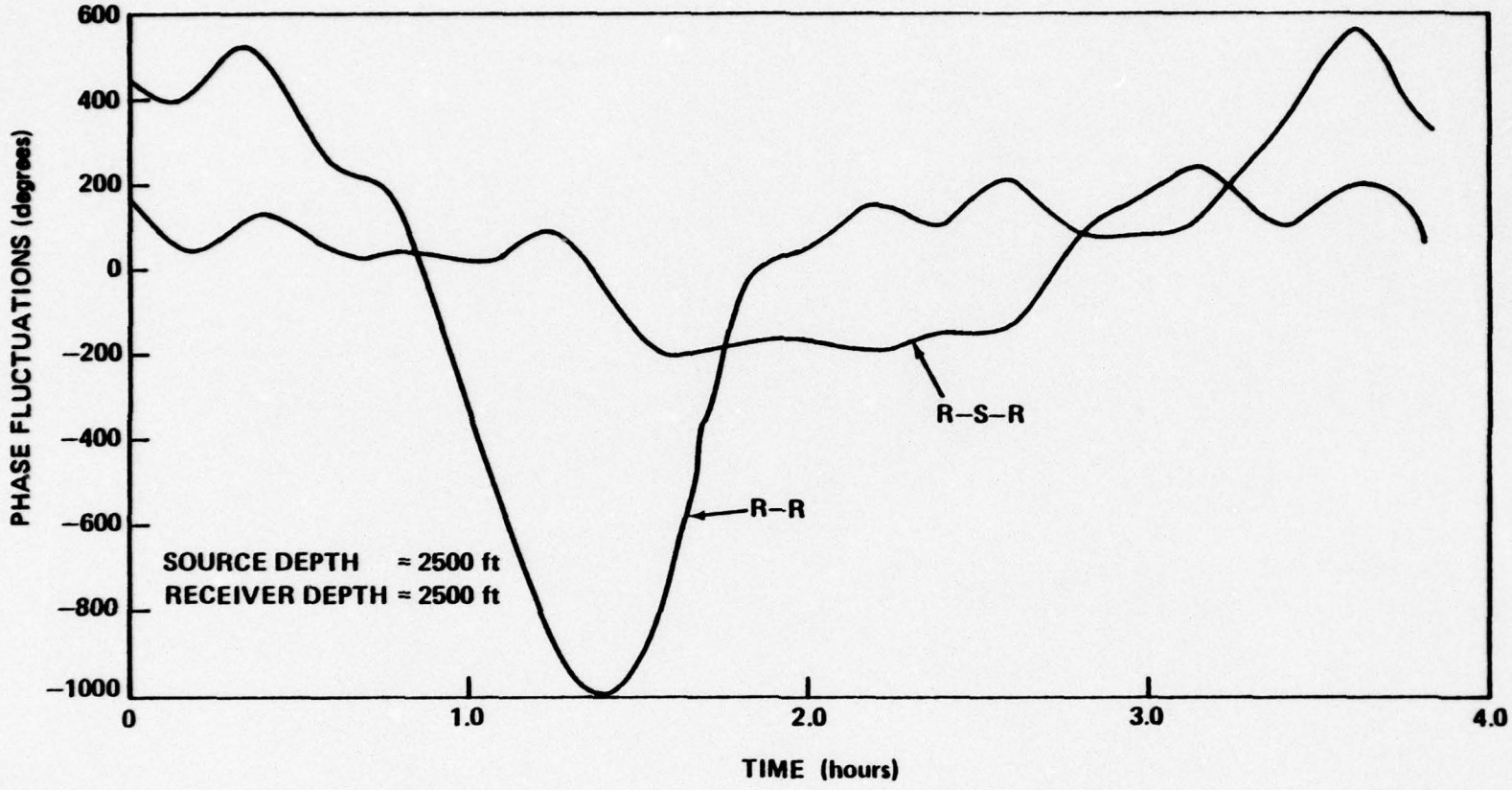

FIGURE 4.18 PHASE FLUCTUATIONS FOR DOMINANT EIGENRAYS AT A RANGE OF 100 NMI AND A FREQUENCY OF 220 HZ

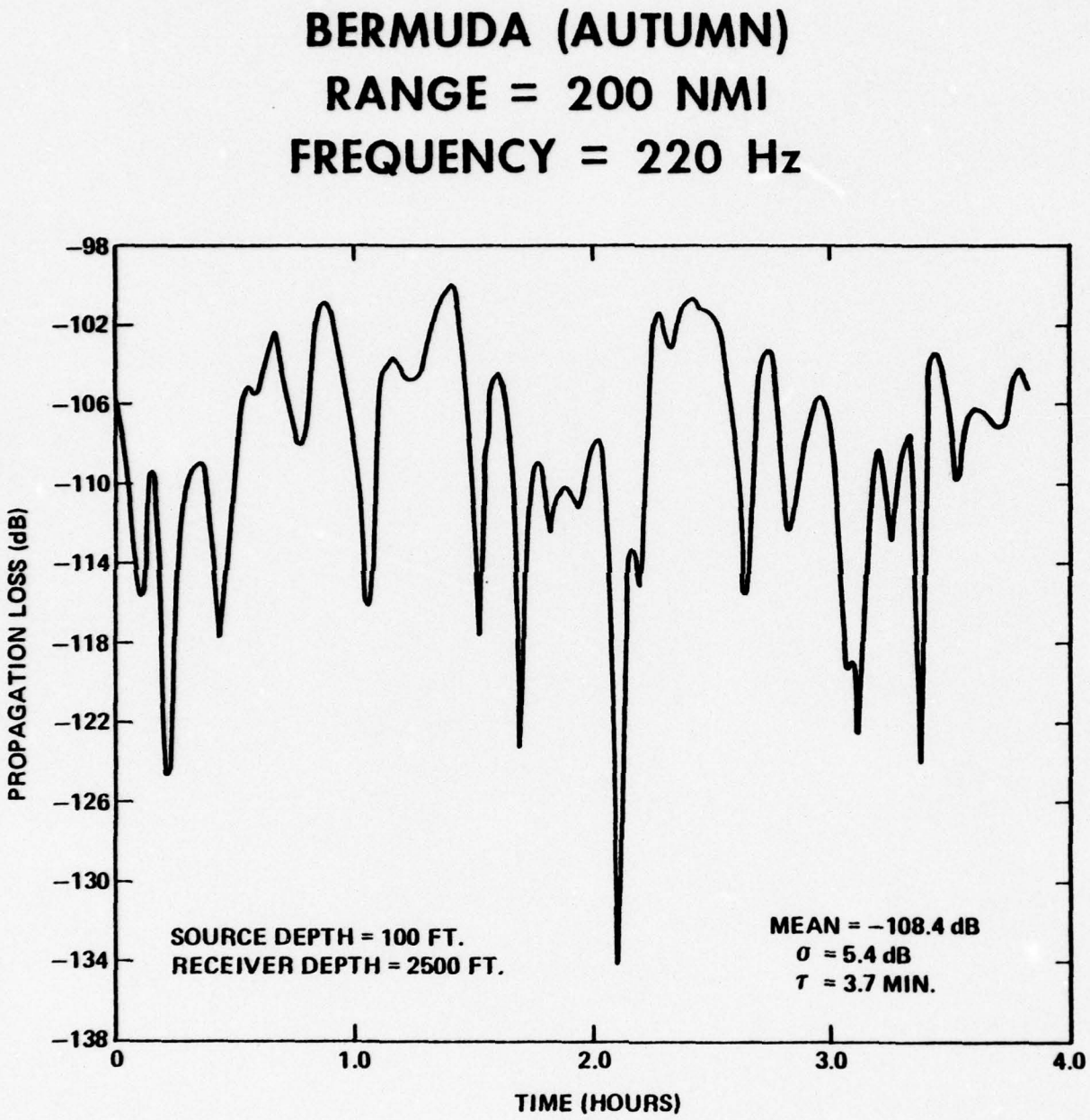

FIGURE 4.19 PROPAGATION LOSS TIME SERIES FOR A RANGE OF 200 NMI AND A FREQUENCY OF 200 HZ

BERMUDA (AUTUMN)
RANGE = 200 NMI
FREQUENCY = 220 Hz

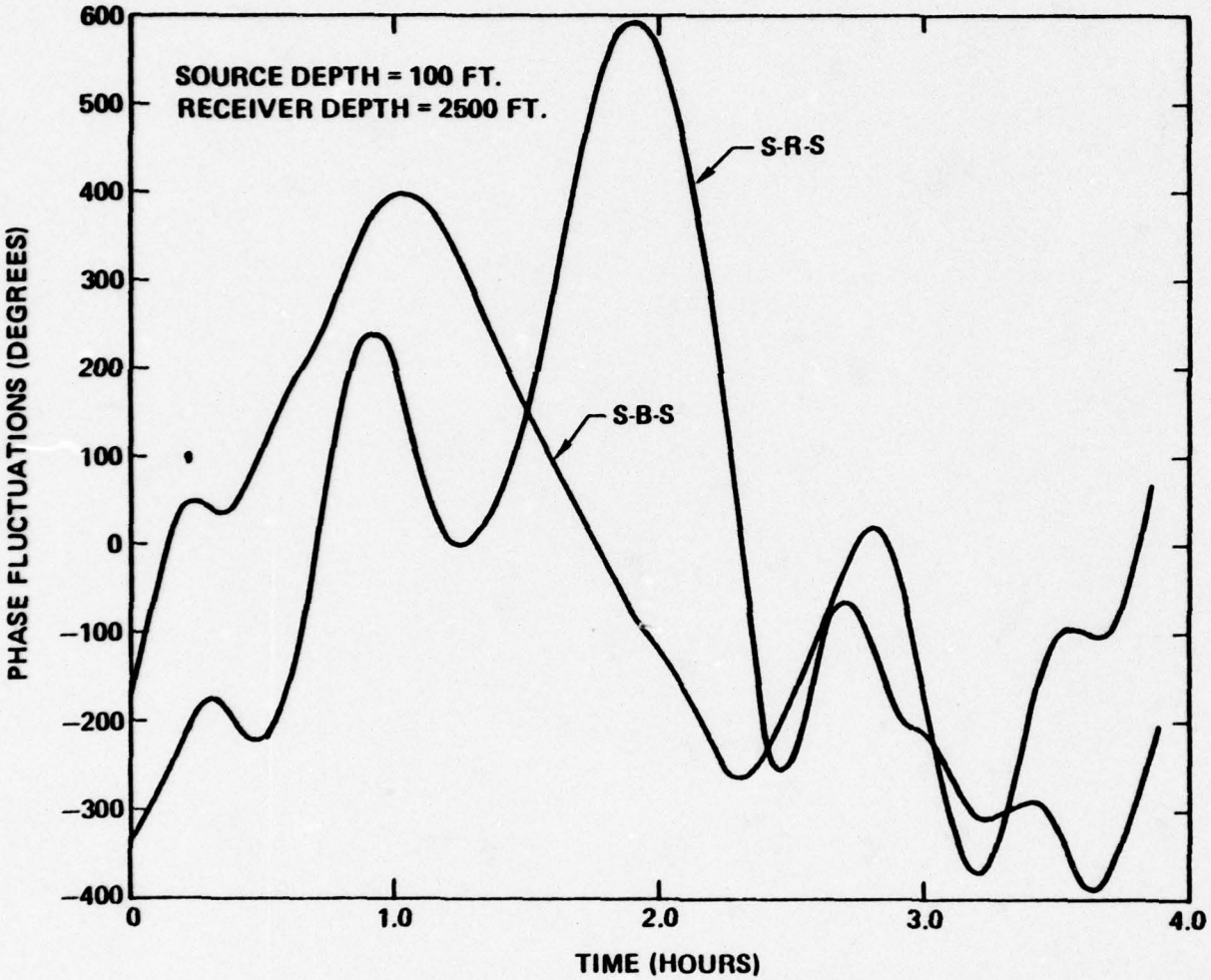

FIGURE 4.20 PROPAGATION LOSS TIME SERIES FOR A RANGE OF 200 NMI AND A FREQUENCY OF 200 HZ

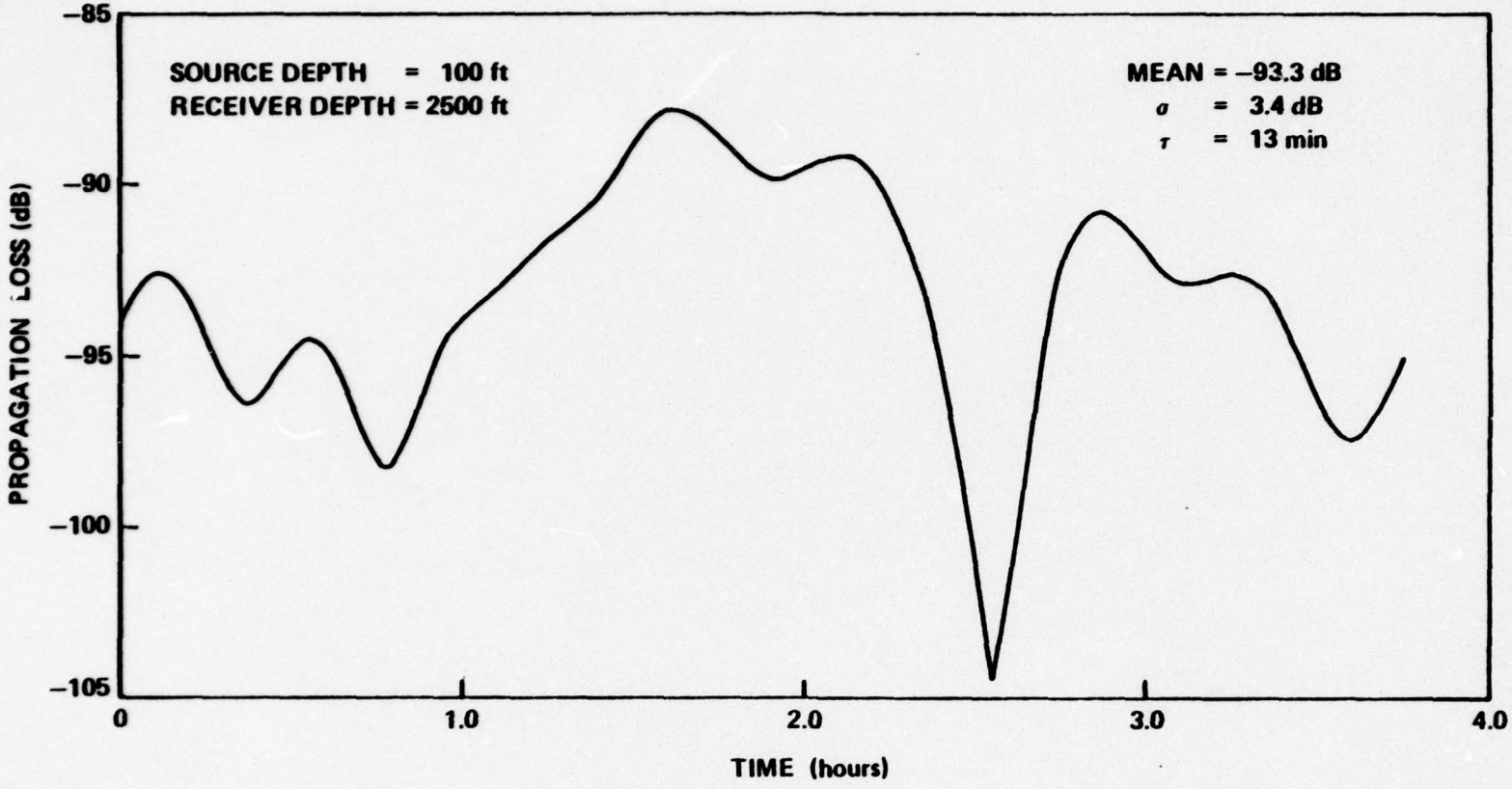

FIGURE 4.21 PROPAGATION LOSS TIME SERIES FOR A RANGE OF 5 NMI AND A FREQUENCY OF 50 HZ

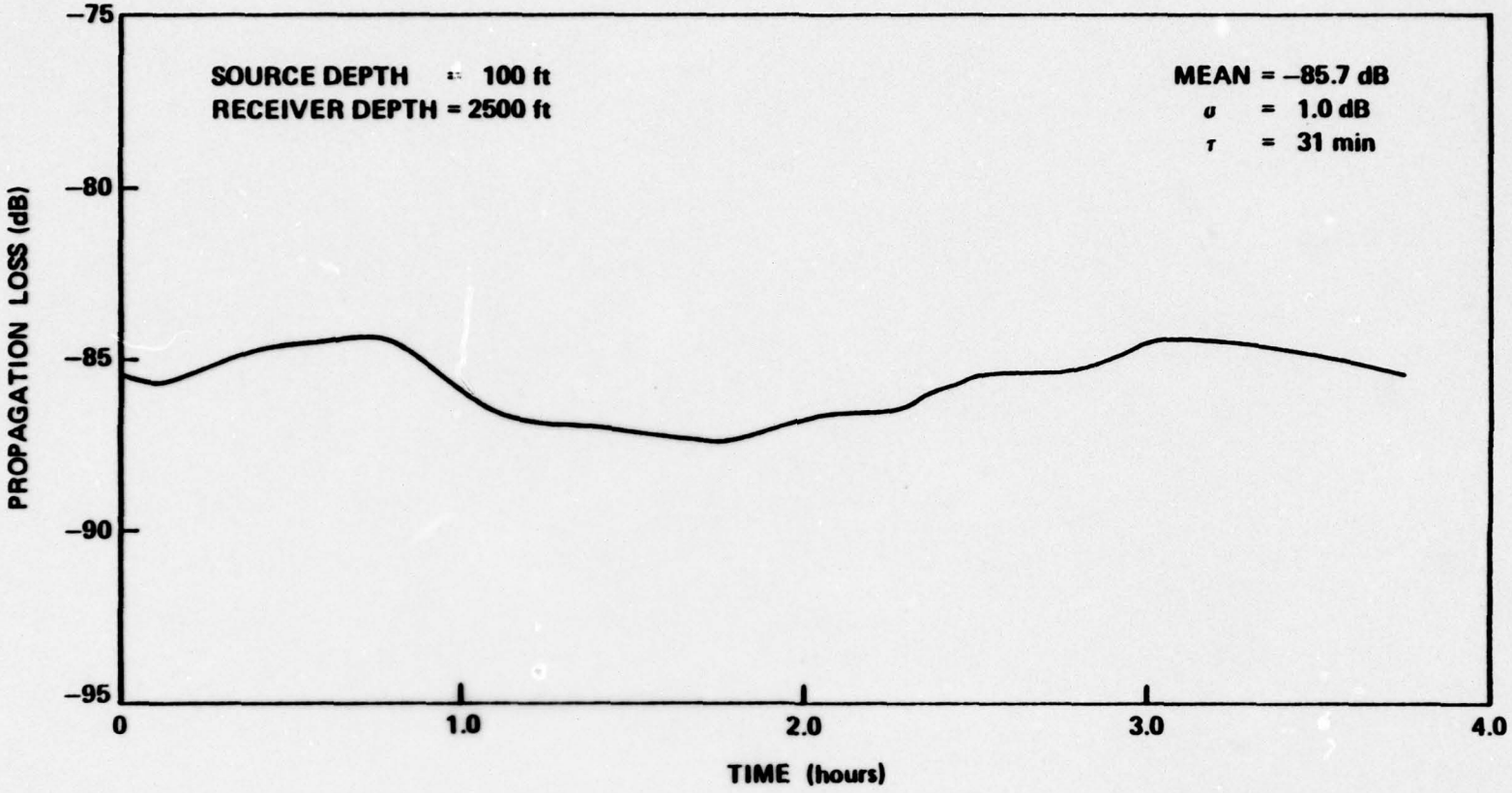

FIGURE 4.22 PROPAGATION LOSS TIME SERIES FOR A RANGE OF 15 NMI AND A FREQUENCY OF 50 HZ

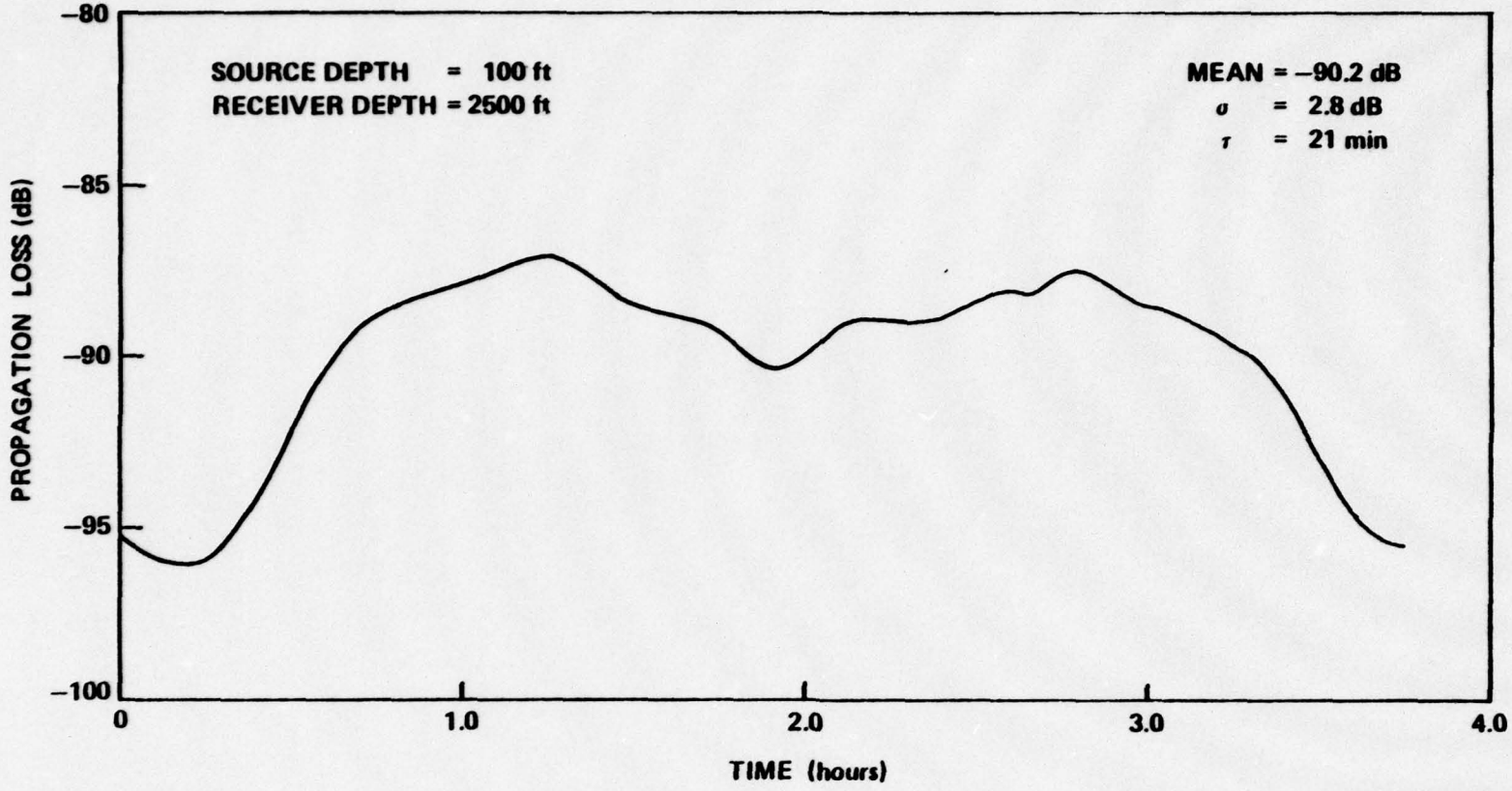

FIGURE 4.23 PROPAGATION LOSS TIME SERIES FOR A RANGE OF 25 NMI AND A FREQUENCY OF 50 HZ

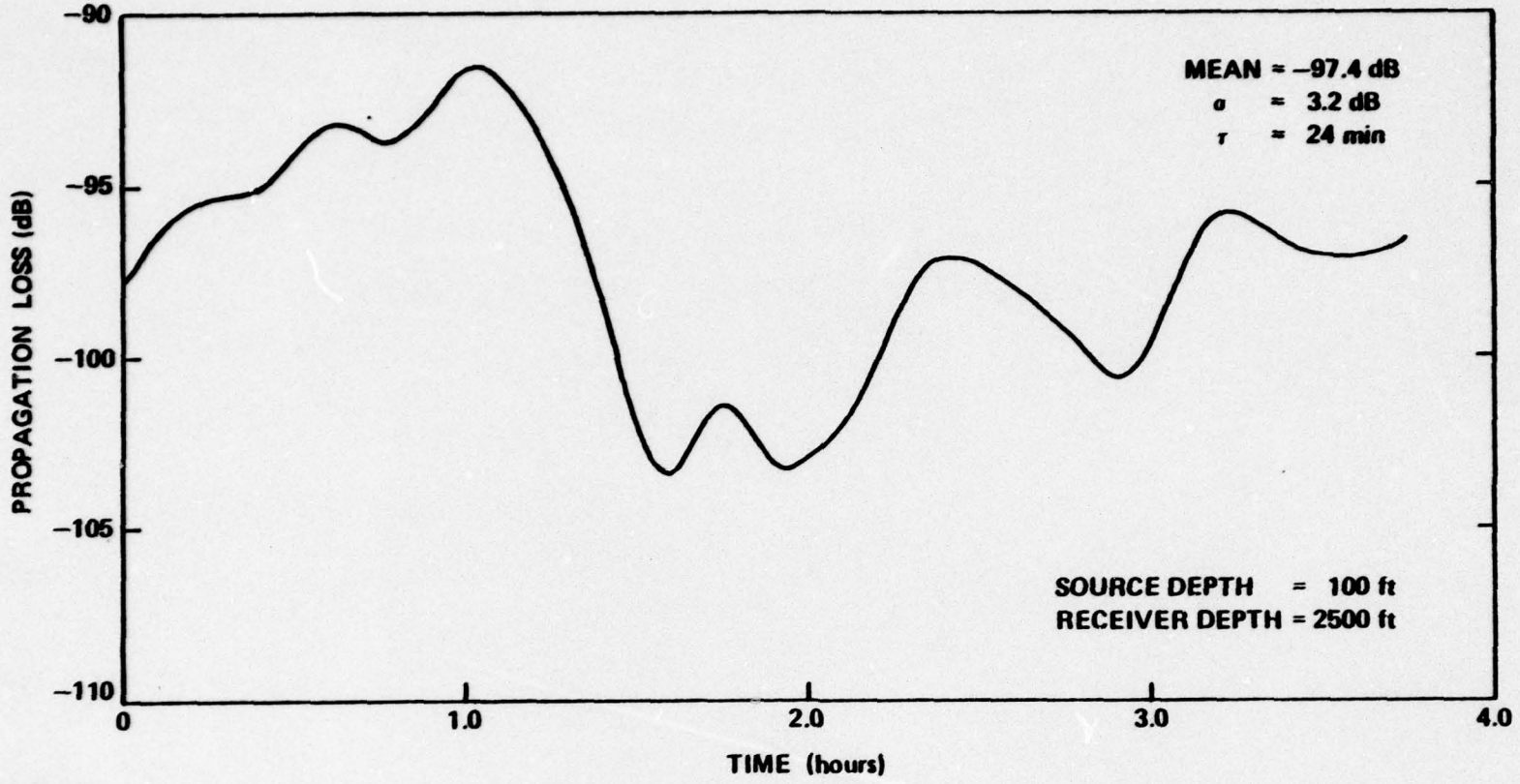

FIGURE 4.24 PROPAGATION LOSS TIME SERIES FOR A RANGE OF 35 NMI AND A FREQUENCY OF 50 HZ

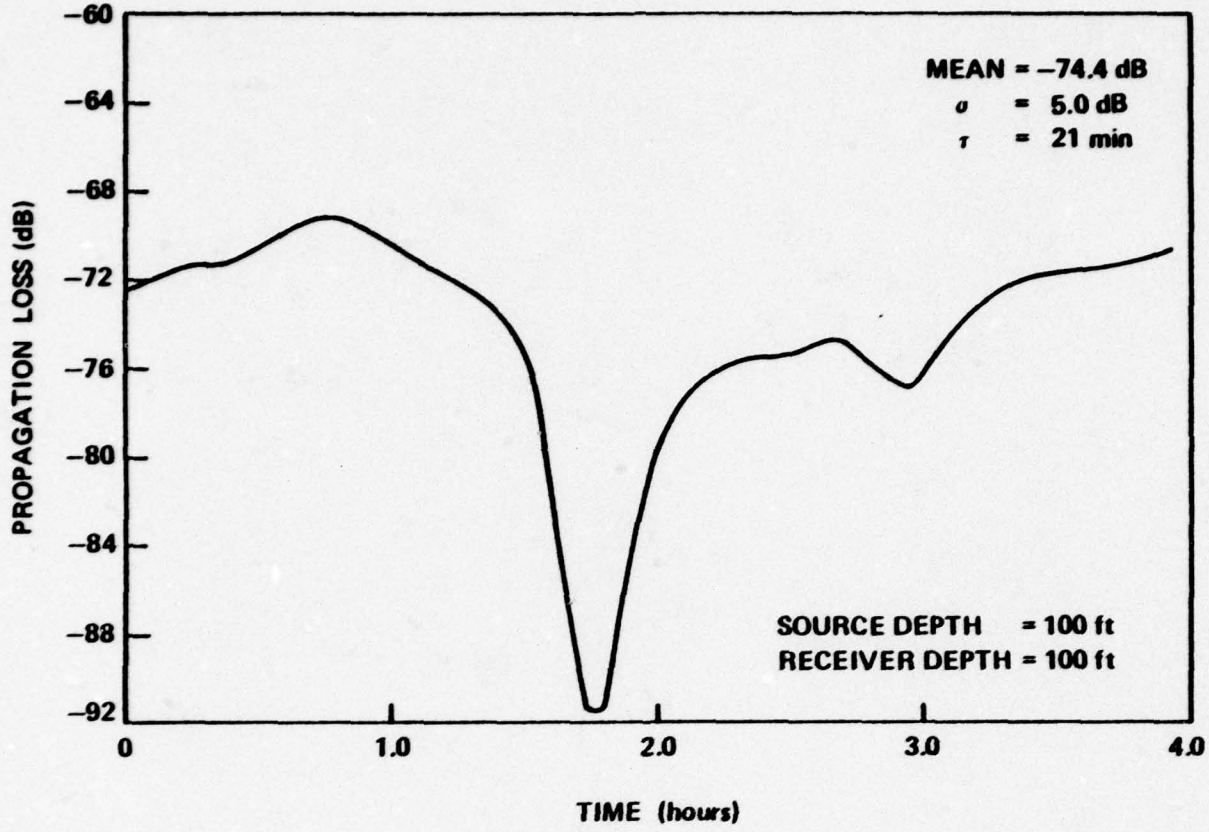

FIGURE 4.25 PROPAGATION LOSS TIME SERIES FOR A RANGE OF 35 NMI AND A FREQUENCY OF 50 HZ

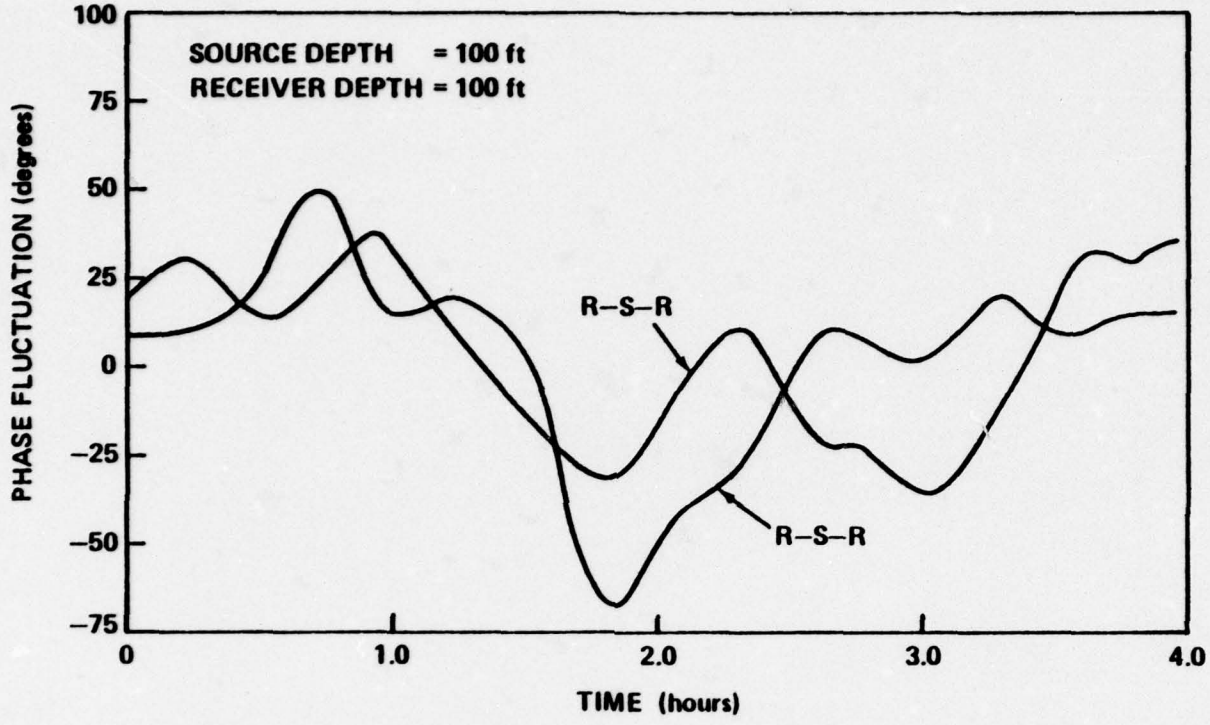

FIGURE 4.26 PHASE FLUCTUATIONS FOR DOMINANT EIGENRAYS AT A RANGE OF 35 NMI AND A FREQUENCY OF 50 HZ

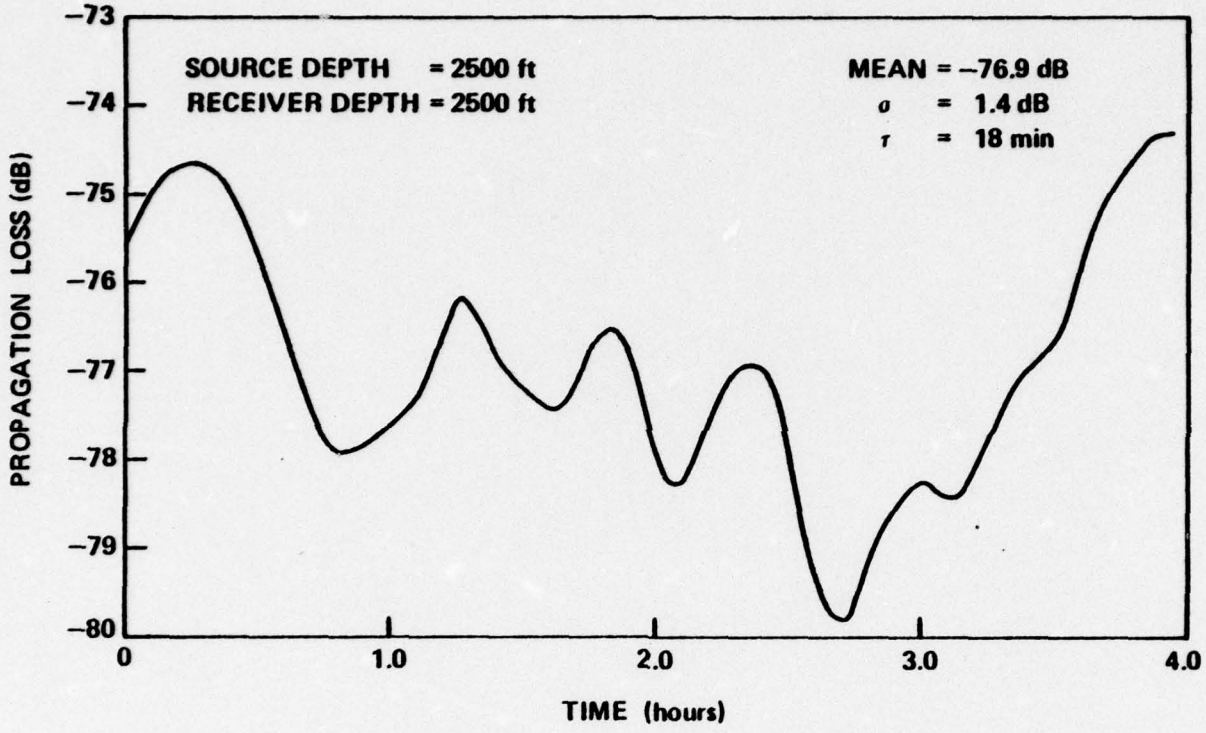

FIGURE 4.27 PROPAGATION LOSS TIME SERIES FOR A RANGE OF 35 NMI AND A FREQUENCY OF 50 HZ

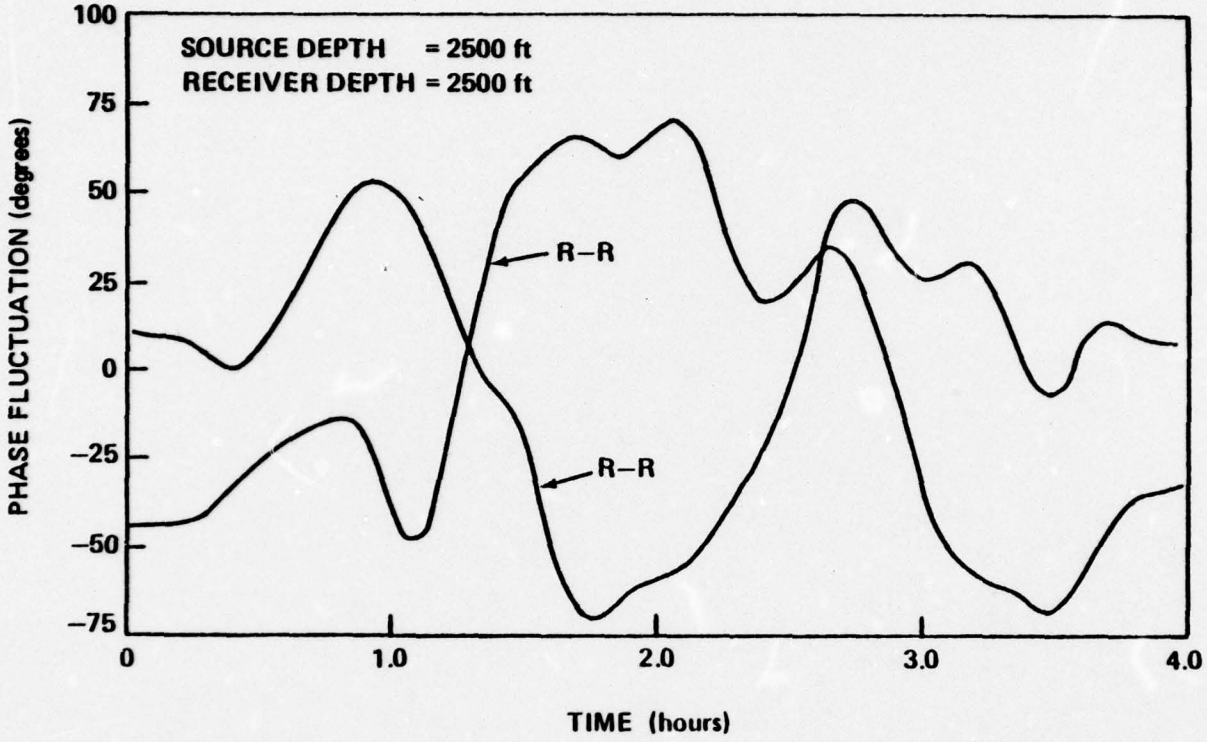

FIGURE 4.28 PHASE FLUCTUATIONS FOR DOMINANT EIGENRAYS AT A RANGE OF 35 NMI AND A FREQUENCY OF 50 HZ

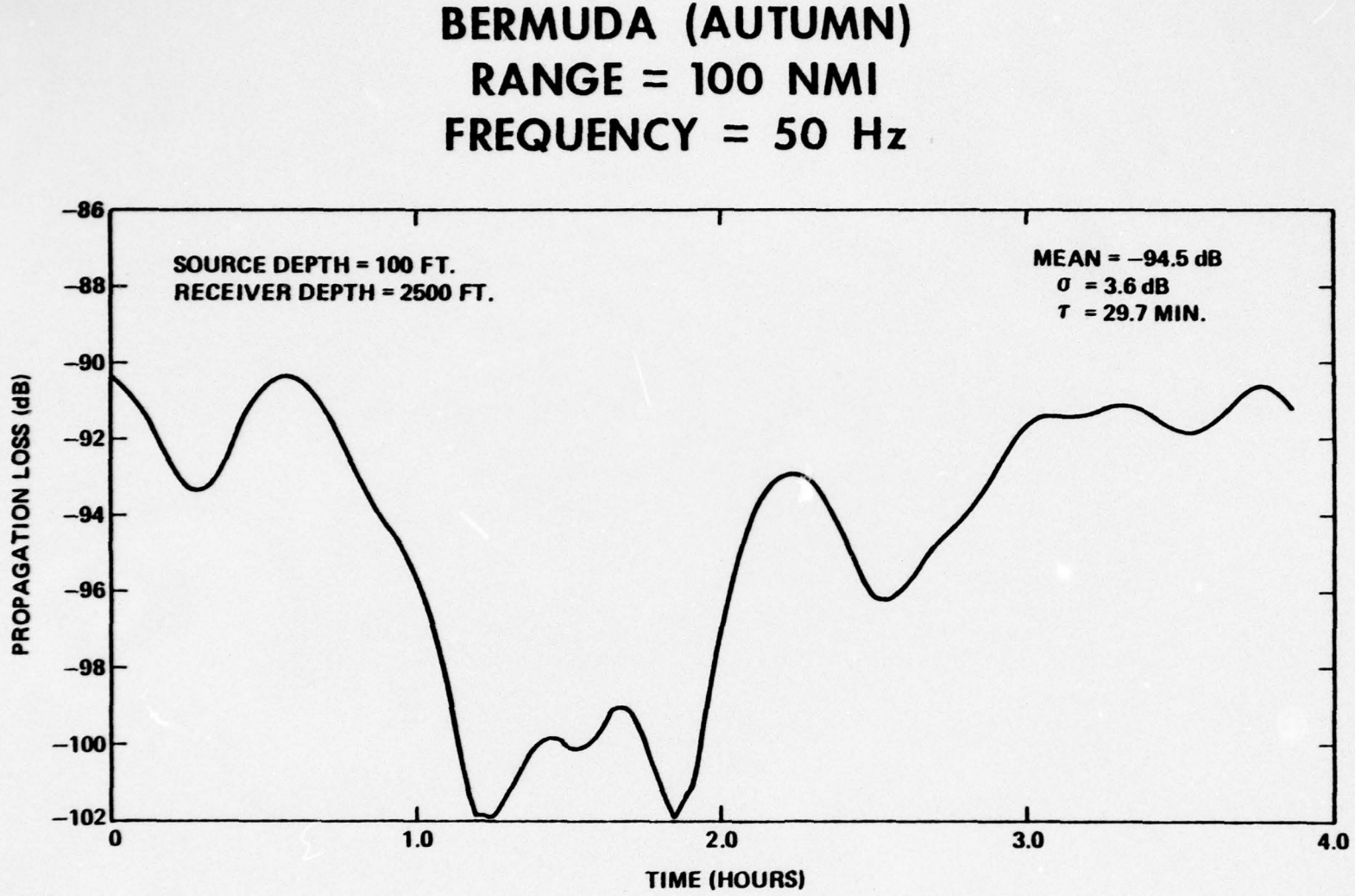

FIGURE 4.29 PROPAGATION LOSS TIME SERIES FOR A RANGE OF 100 NMI AND A FREQUENCY OF 50 HZ

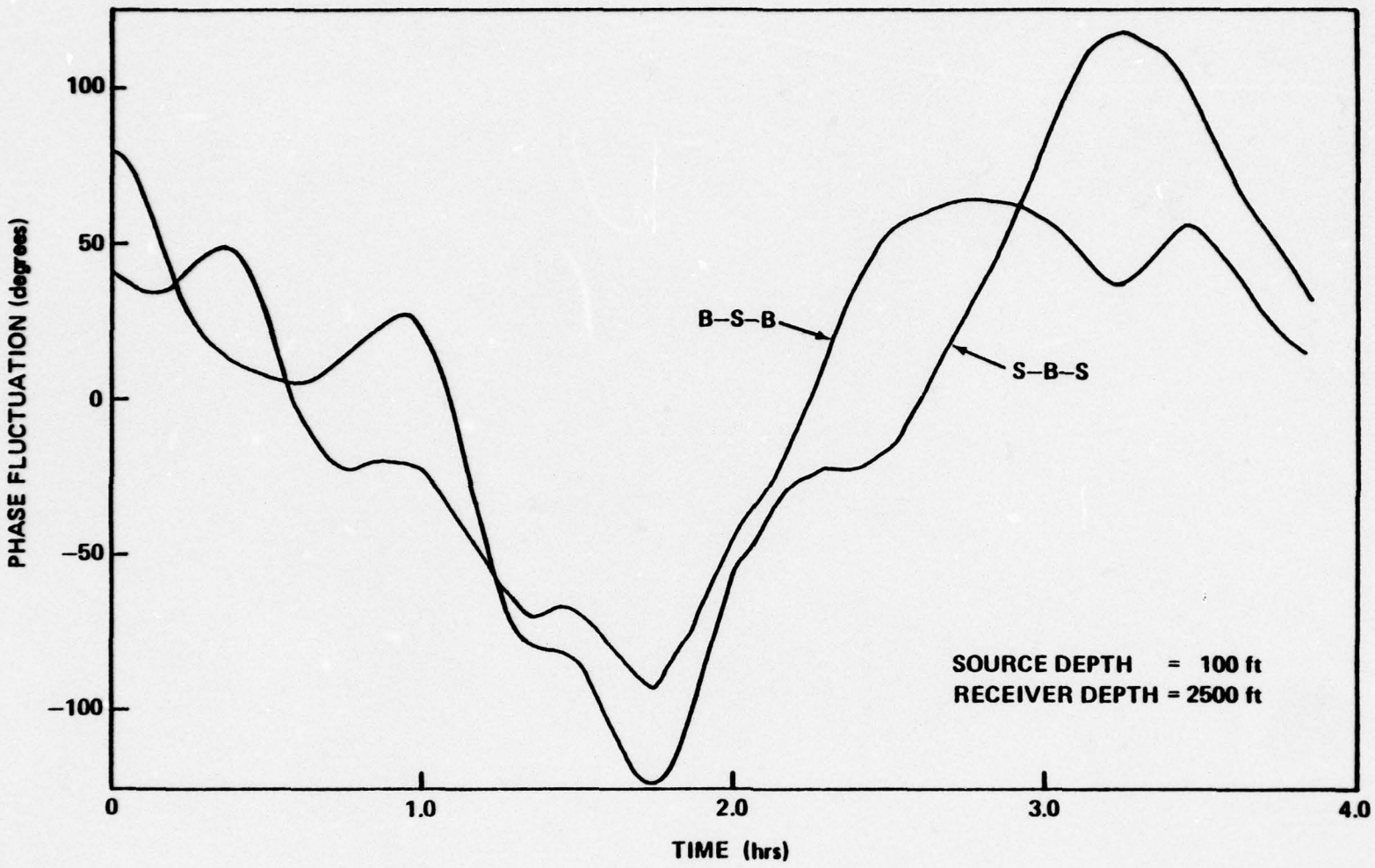

FIGURE 4.30 PHASE FLUCTUATIONS FOR DOMINANT EIGENRAYS AT A RANGE OF 100 NMI AND A FREQUENCY OF 50 HZ

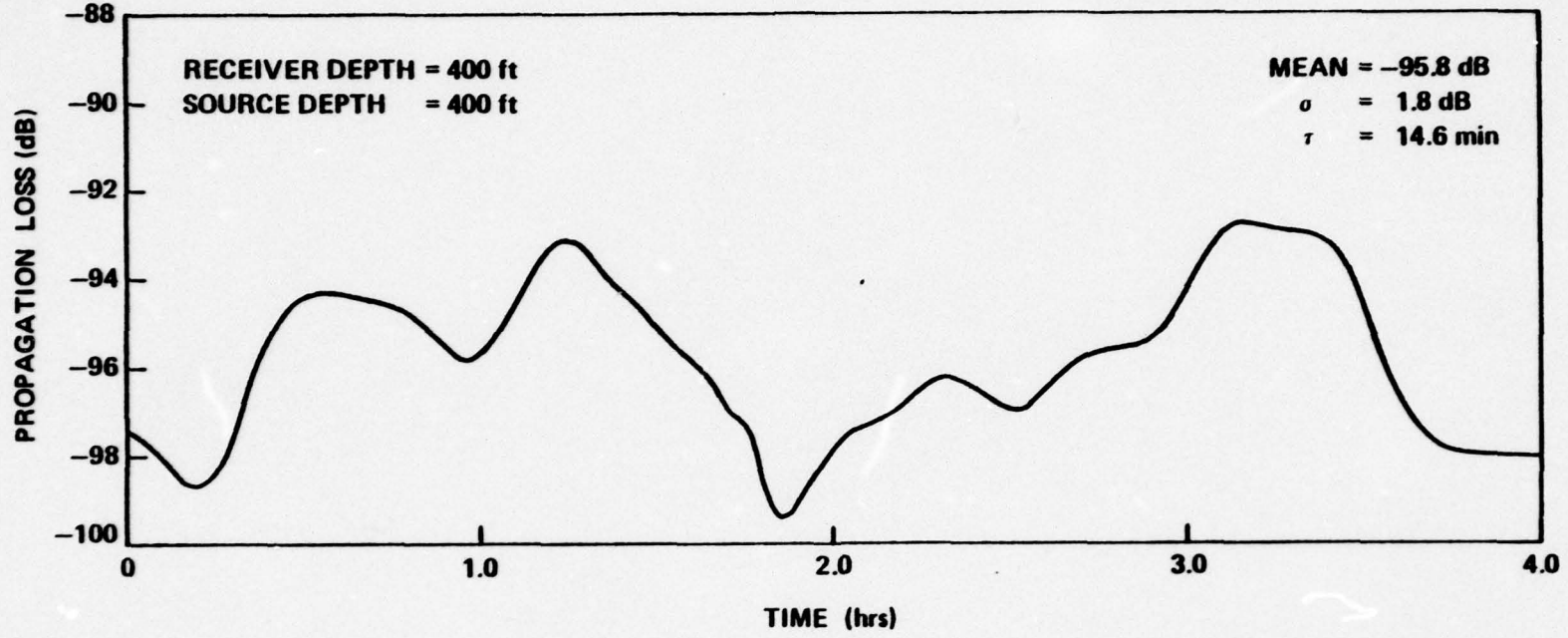

FIGURE 4.31 PROPAGATION LOSS TIME SERIES FOR A RANGE OF 100 NMI AND A FREQUENCY OF 50 HZ

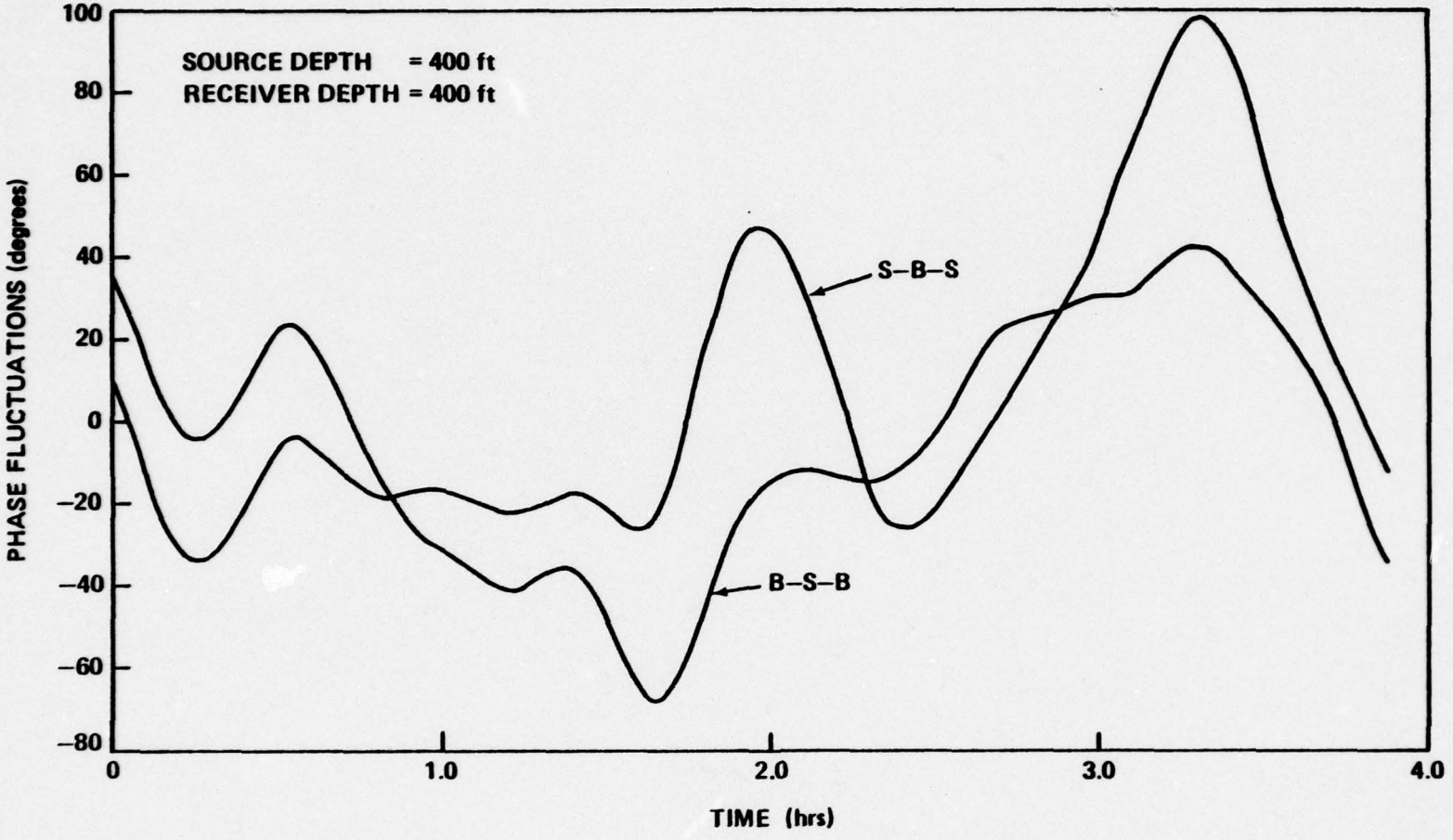

FIGURE 4.32 PHASE FLUCTUATIONS FOR DOMINANT EIGENRAYS AT A RANGE OF 100 NMI AND A FREQUENCY OF 50 HZ

However, direct examination of the time series permits some qualitative conclusions, which are not evident from Figure 4.4 In particular, we observe that

- As noted above, the trend from 50 Hz to 220 Hz suggests that the rate of fluctuations goes up (relaxation time goes down) as frequency increases
- At 50 Hz, as at 220 Hz, relaxation time decreases with increasing range.

4.3.2 North Atlantic (Summer) Environment

Table 4.3 summarizes results for the runs made in the North Atlantic (summer) environment. Figures 4.33 through 4.38 show the time series generated in these runs.

The purpose of these runs was to test whether predicted fluctuation characteristics might vary significantly from one environment to another. We observe that the 220 Hz parameters in Table 4.3 agree rather closely with their equivilents in Table 4.2, with the exception of the relaxation time at 35 nmi, which is considerably shorter in the Atlantic environments. Comparison of the corresponding two time series (Figure 4.8 and Figure 4.33) confirms that the Atlantic case exhibits more rapid fluctuations. The large uncertainties in these calculations make it impossible, however to determine whether this reflects a consistent environmental difference.

As with the Bermuda runs, there is some reason to question the statistical reliability of the 50 Hz results, but the tendency for lower frequency runs to fluctuate less rapidly is again discernable.

4.3.3 Experimental Comparisons

Model runs have been made for conditions which match those of two sets of experimental data. One of these, reported by Porter, Spindel, and Jaffee we refer to as "Eleuthera" data; the other is deep ocean data from Project Mimi reported by Clark and Kronengold, and referred to here as "Eleuthera-Bermuda" data. Both experiments were performed over deep ocean paths using a 406 Hz tonal generated by a bottom mounted projector at Eleuthera. The Eleuthera-Bermuda results were recorded by fixed hydrophones at Bermuda, and at an intermediate position between Eleuthera and Bermuda. The Eleuthera results were recorded by free drifting sonobuoys. (A doppler tracking system was used to follow the buoy motion so as to allow corrections for position changes to be made.)

The model run for the Eleuthera-Bermuda data was designed for comparison with the experimental results from the intermediate hydrophone at a range of 120 nmi; the time series generated for this case are shown in Figures 4.39 and 4.40. The Eleuthera model run assumed a range of 113 miles; the resulting time series for that set of conditions are shown in Figures 4.41 and 4.42.

TABLE 4.3

RESULTS OF PROPAGATION LOSS TIME SERIES FOR NORTH ATLANTIC (SUMMER) ENVIRONMENT

Range (nm)	Source Depth (Ft)	Receiver Depth (Ft)	Frequency = 220 Hz			Frequency = 50 Hz		
			Mean Loss (dB)	σ (dB)	τ (min)	Mean Loss (dB)	σ (dB)	τ (min)
35	100	4200	-93.4 $\pm$ 1.5	6.8	5.5	-94.1 $\pm$ 2.1	6.4	12.5
100	100	4200	-113.7 $\pm$ 1.3	6.2	5.3			

N. ATLANTIC (SUMMER)
RANGE = 35 NMI
FREQUENCY = 220 Hz

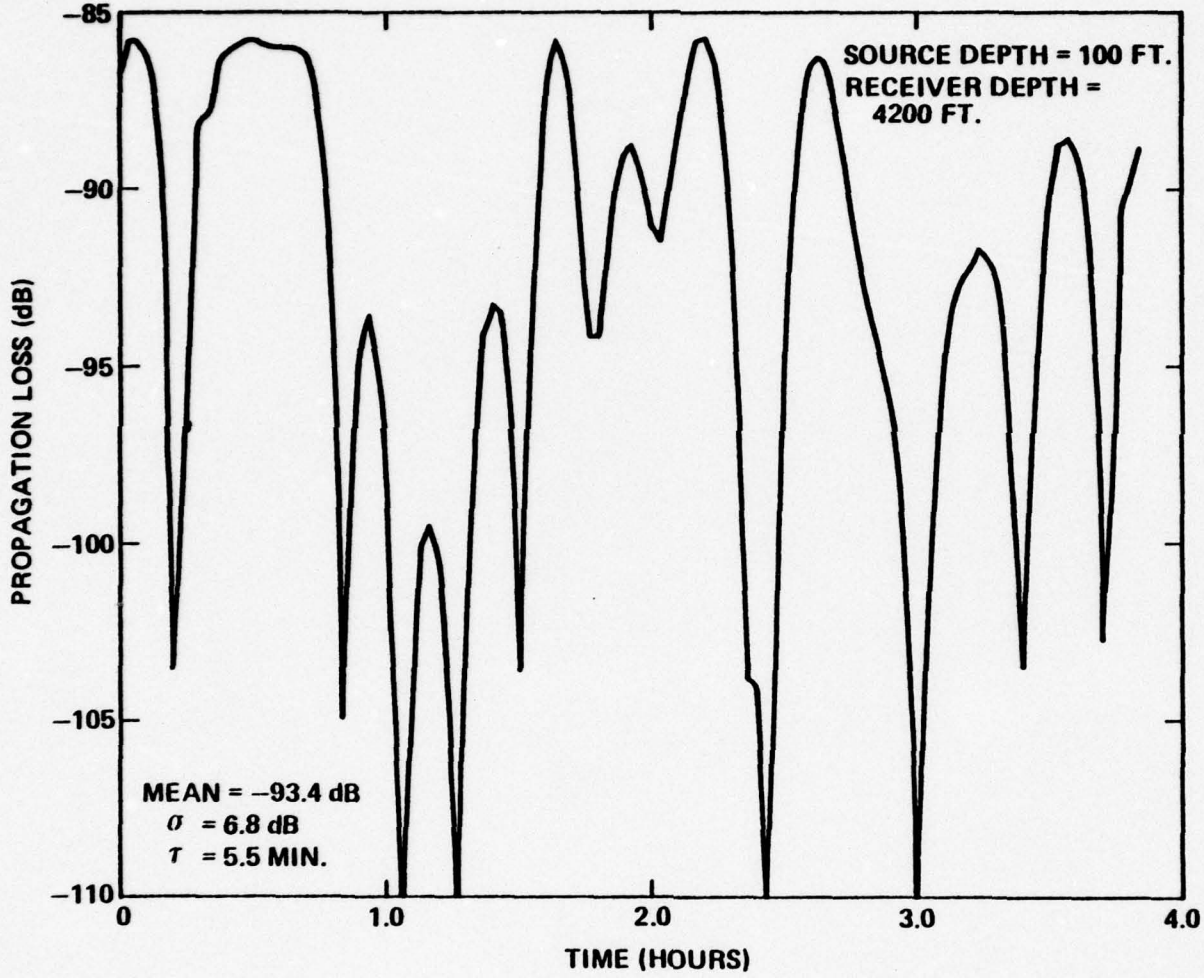

FIGURE 4.33 PROPAGATION LOSS TIME SERIES FOR A RANGE OF 35 NMI AND A FREQUENCY OF 220 HZ

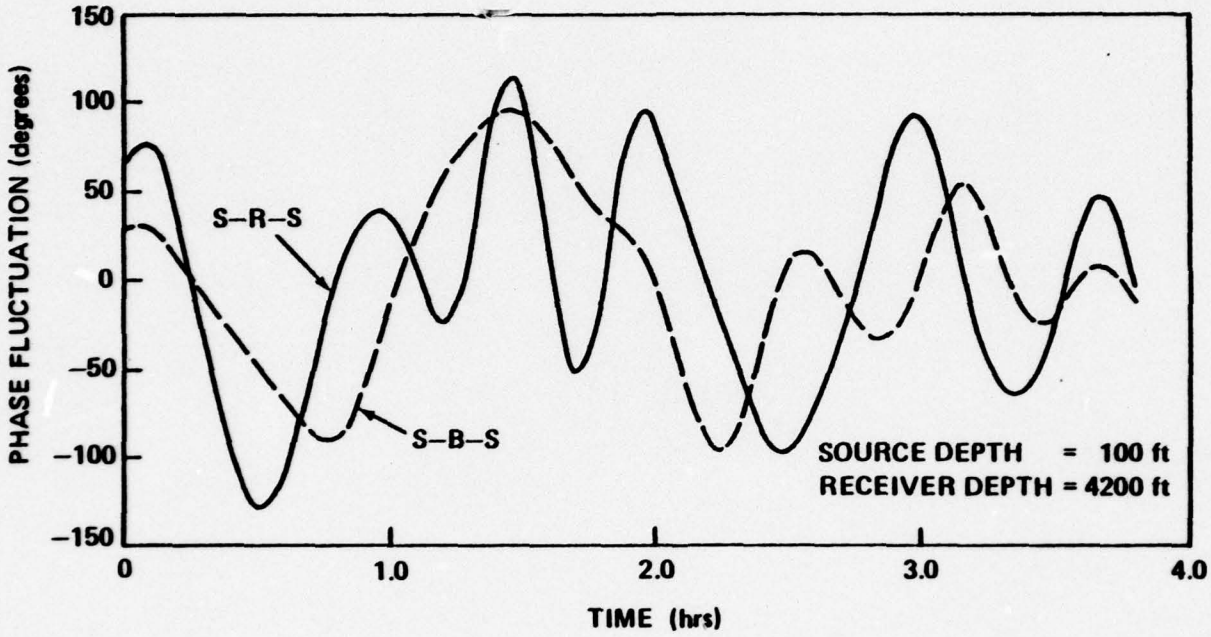

FIGURE 4.34 PHASE FLUCTUATIONS FOR DOMINANT EIGENRAYS AT A RANGE OF 35 NMI AND A FREQUENCY OF 220 HZ

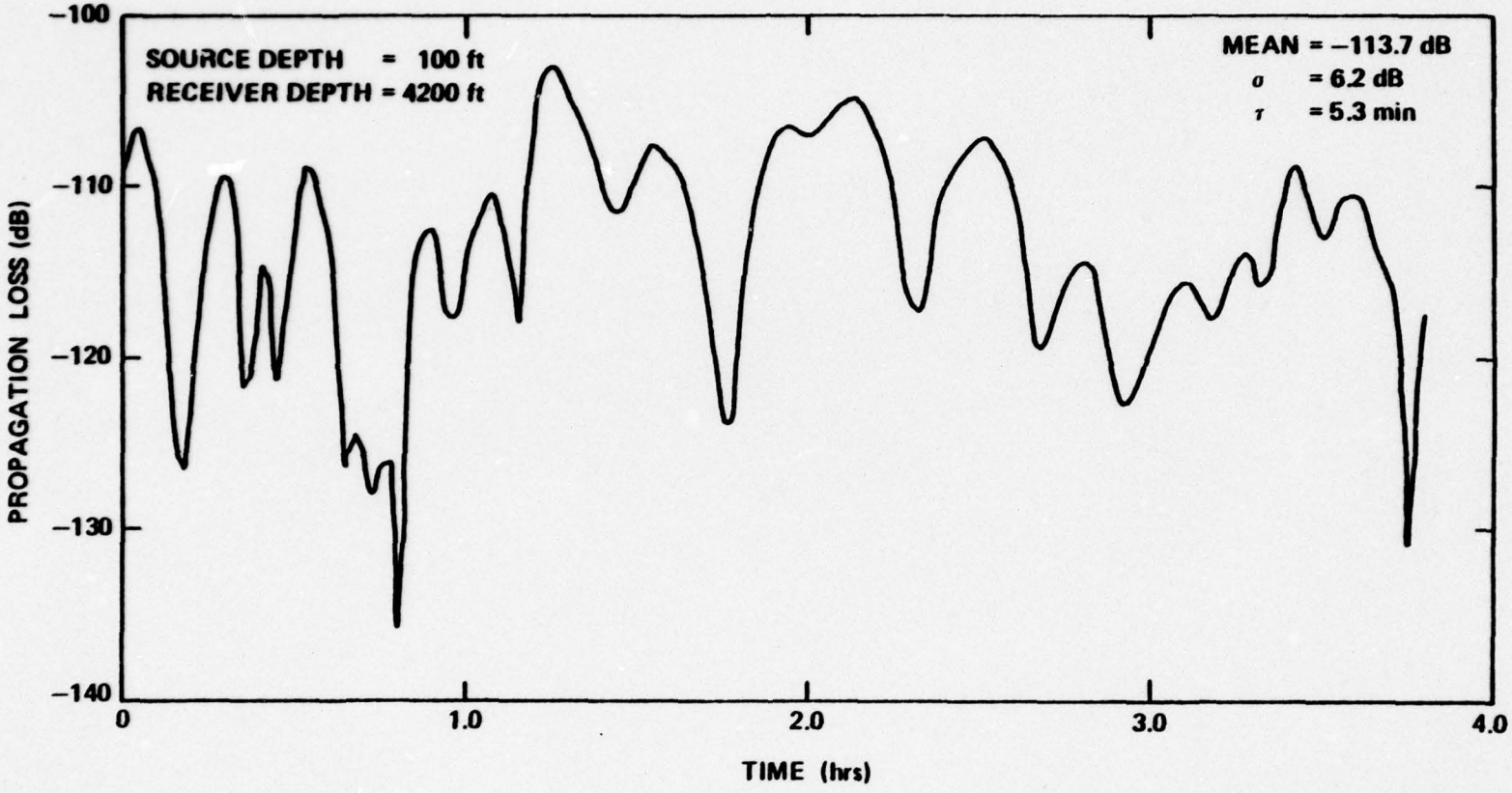

FIGURE 4.35 PROPAGATION LOSS TIME SERIES FOR A RANGE OF 100 NMI AND A FREQUENCY OF 220 HZ

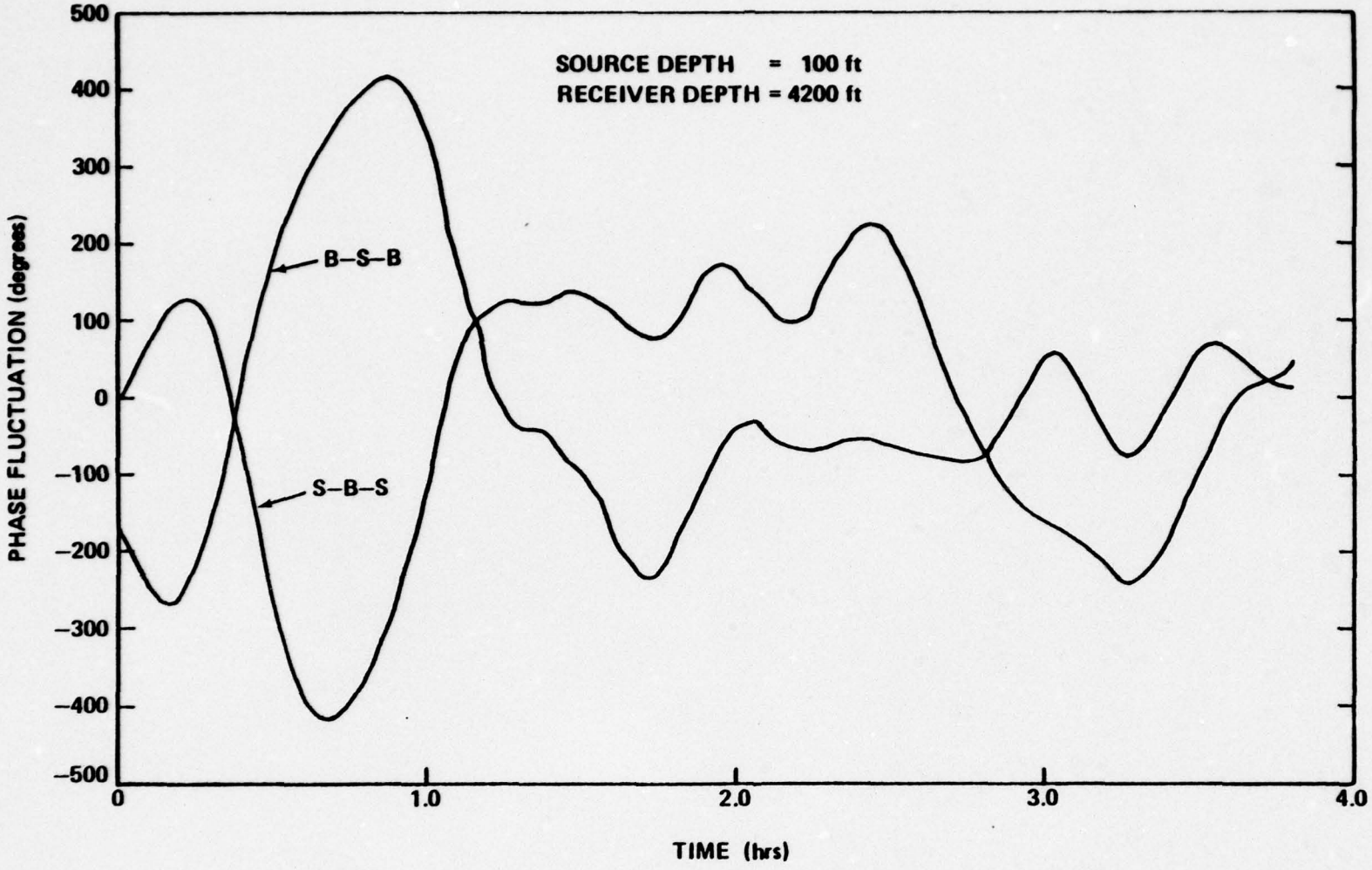

FIGURE 4.36 PHASE FLUCTUATIONS FOR DOMINANT EIGENRAYS AT A RANGE OF 100 NMI AND A FREQUENCY OF 220 HZ

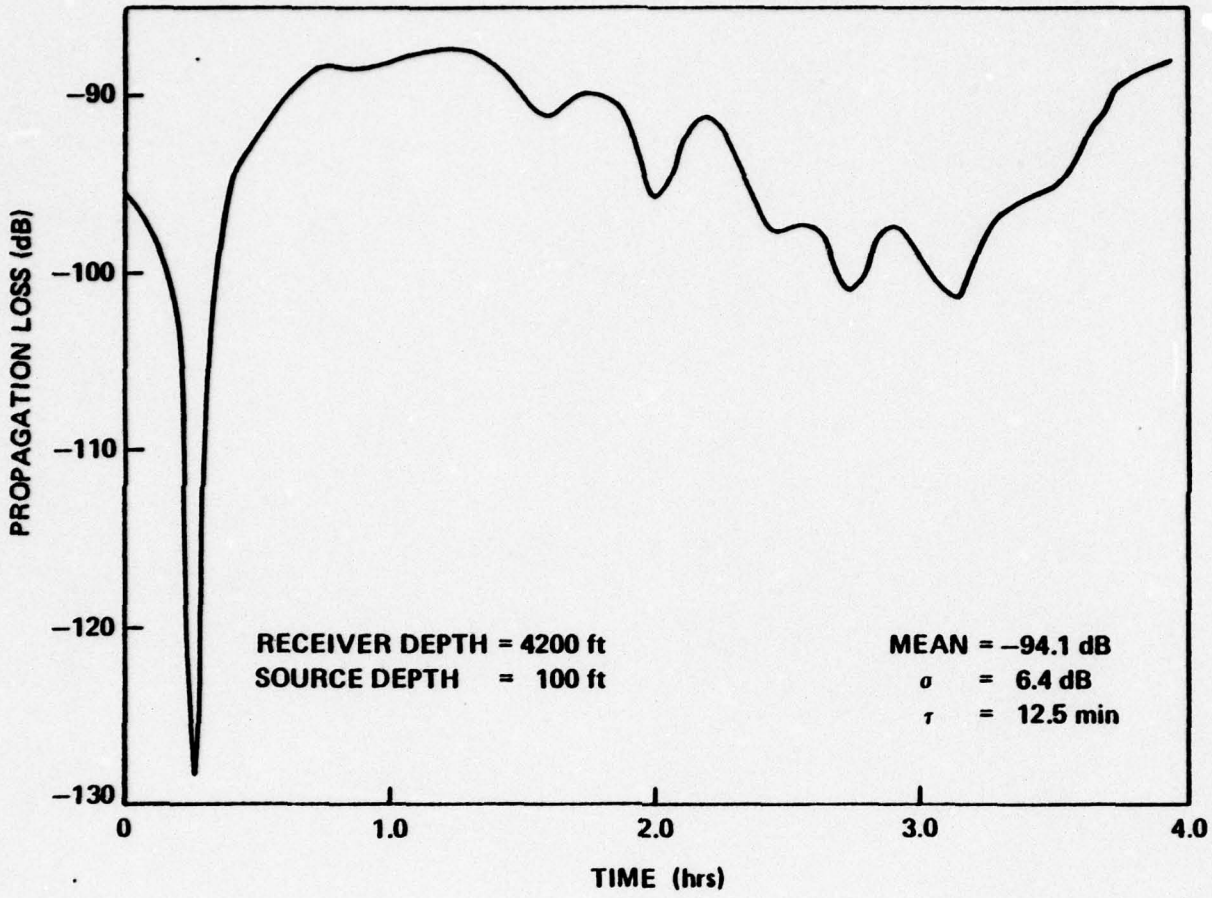

FIGURE 4.37 PROPAGATION LOSS TIME SERIES FOR A RANGE OF 35 NMI AND A FREQUENCY OF 50 HZ

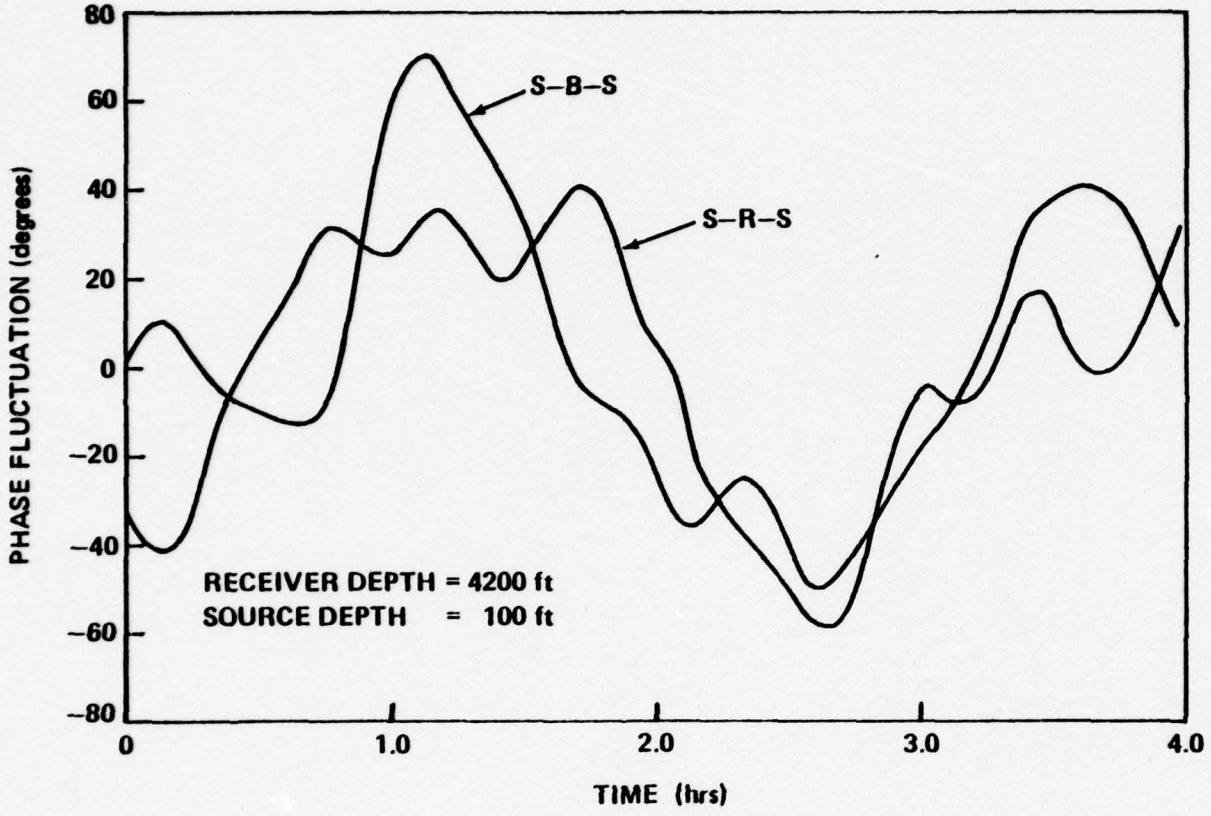

FIGURE 4.38 PHASE FLUCTUATIONS FOR DOMINANT EIGENRAYS AT A RANGE OF 35 NMI AND A FREQUENCY OF 50 HZ

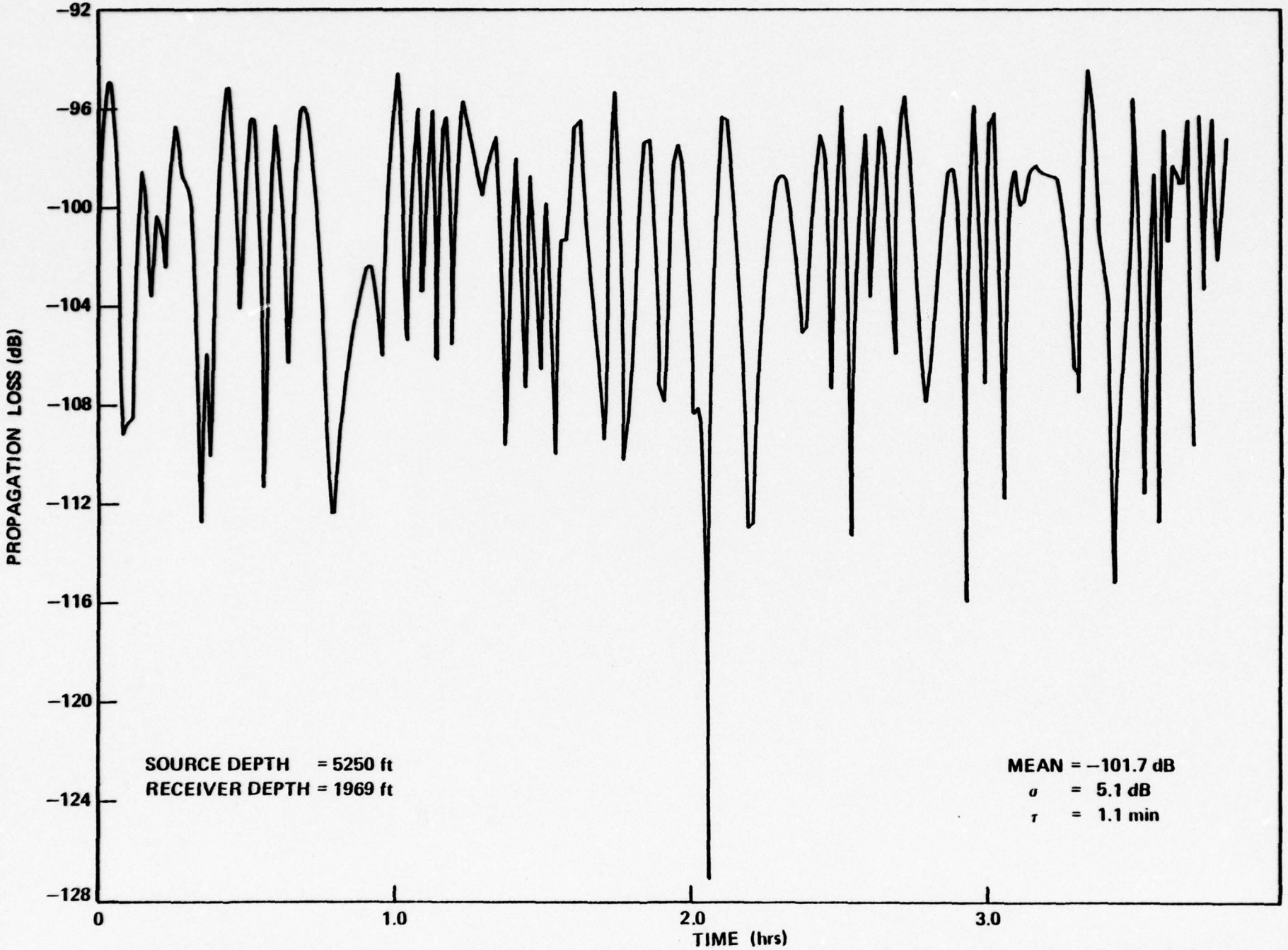

FIGURE 4.39 ELEUTHERA-BERMUDA PROPAGATION LOSS TIME SERIES FOR A RANGE OF 120 NMI AND A FREQUENCY OF 406 HZ

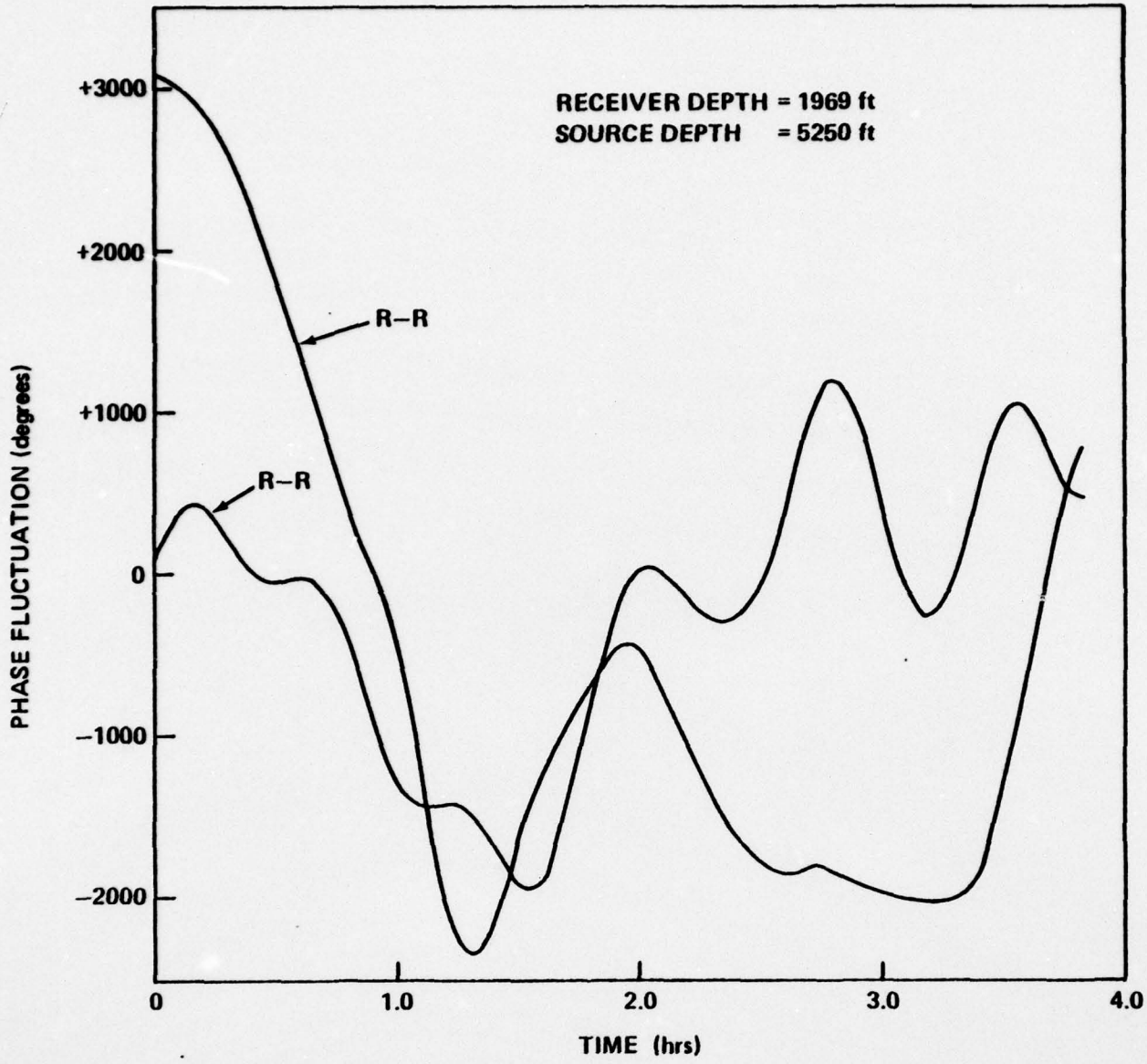

FIGURE 4.40 PHASE FLUCTUATIONS FOR DOMINANT EIGENRAYS AT A RANGE OF 120 NMI AND A FREQUENCY OF 406 HZ

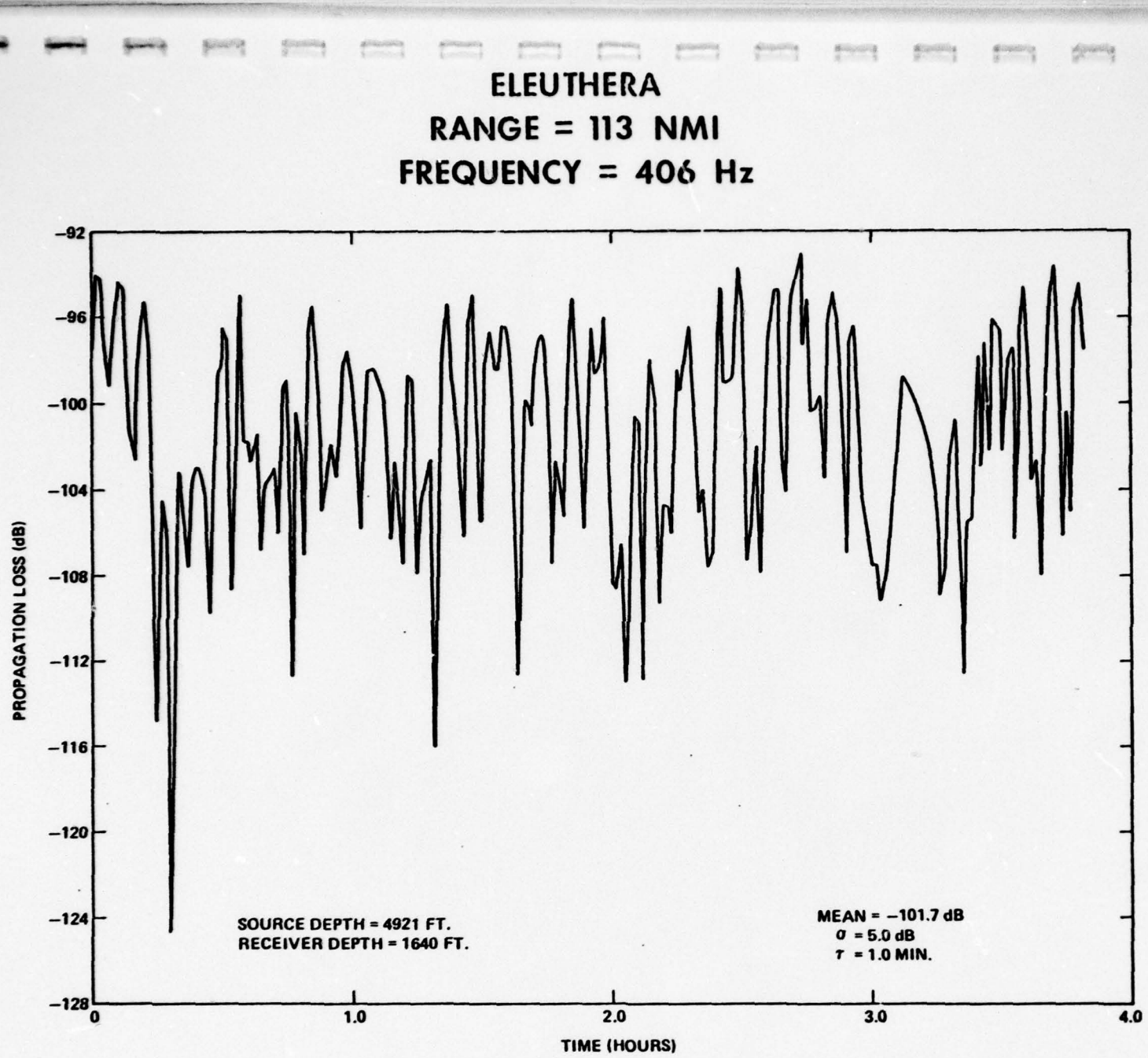

FIGURE 4.41 PROPAGATION LOSS TIME SERIES FOR A RANGE OF 113 NMI AND A FREQUENCY OF 406 HZ

Not surprisingly, the two time series are very similar in their properties, with essentially the same mean loss (101.7 dB) nearly the same σ (approximately 5 dB), and nearly the same relaxation time (approximately one minute). This reflects the very similar conditions (environment, range, frequency, source depth, receiver depth) prevailing in the two experiments.

Experimental results for the Eleuthera-Bermuda experiment were presented principally in the form of periodograms, precluding direct comparison with the time series generated by the model. Variance computations for these results, however, suggest a sigma of about six dB which is in reasonable agreement with model results. In addition, it is qualitatively obvious that the periodograms for the intermediate range hydrophone fall off more rapidly with frequency than does the long range periodogram, supporting the prior suggestion that propagation fluctuations oscillate more rapidly with increasing range.

Quantitatively, these periodograms show a strong semi-diurnal (12.48 hr) spectral component (hypothesized to arise from tidal effects) which is, of course, not present in the model. At the other extreme, they cut off at 10 cycles per hour, a limit imposed by the rate (once per three minutes) at which the original data was sampled. Most of the power in the spectrum appears to lie well below the 10 cph cut-off. This result appears to contradict model predictions; a one minute relaxation time corresponds to a frequency bandwidth of about 60 cph which is much larger than the less than 10 cph bandwidth suggested by the data. However, firm comparison of these time scales requires subjecting the model results to the same data reduction algorithms (filtering, sampling) as the data, and this has not been done here.

This point may be emphasized by turning to the Eleuthera experimental results where a somewhat more precise comparison with model results is possible. Here we have available a reasonably good sample time series, which is reproduced in Figure 4.43. To compare this time series with the model predictions, level crossing rates (number of crossings per hour) were estimated for levels in 5 dB steps, from 5 dB down from the time series maximum, to 30 dB down. The results are shown in Figure 4.44.

Such a plot compares both the rate of fluctuations observed (on the ordinate) and their magnitude (on the abscissa). We observe that the model generated level crossing rates are within 30 percent of those obtained experimentally (approximately 19 crossings per hour versus approximately 14 crossings per hour) while the widths of the two curves are substantially the same. We conclude that, in this case, the correspondence between model predictions and experimental results is rather good.

ACOUSTIC FLUCTUATIONS—ELEUTHERA EXPERIMENT

(Spindel, Porter and Jaffee)

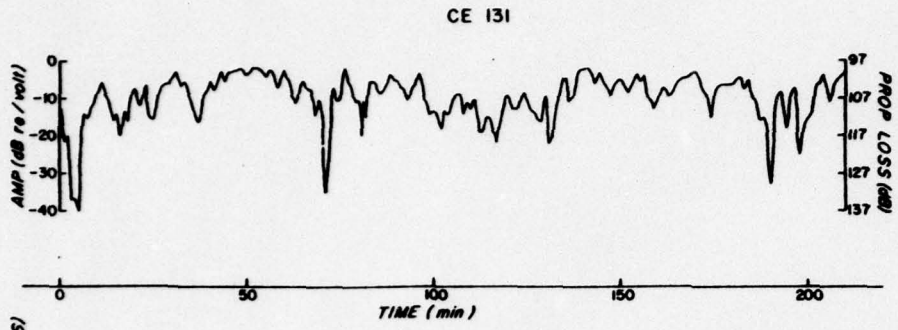

FIG. 8. Amplitude and phase time series of corrected 305-m hydrophone data. Transmission loss of 97 dB is signal amplitude of 1 V.

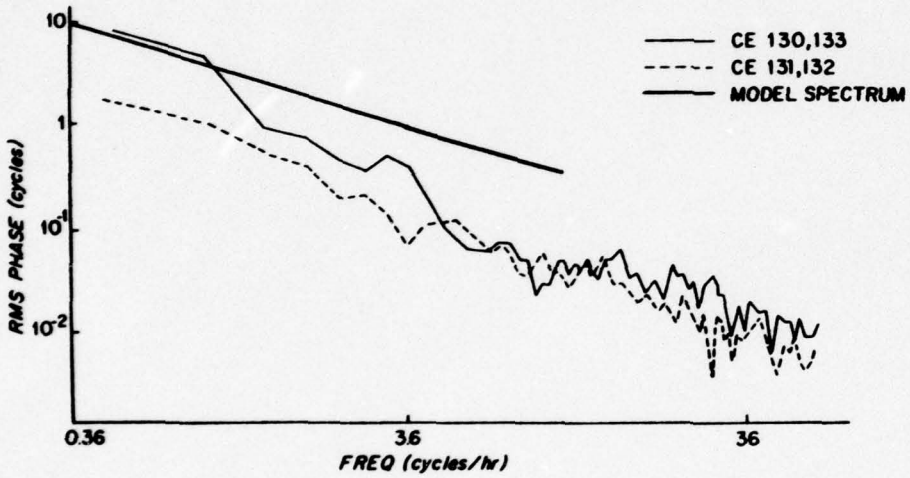

FIG. 10. Root-mean-square phase versus frequency for shallow (CE 131, 132 at 305 m) and deep (CE 130, 133 at 1500 m) hydrophones, together with predicted phase spectrum.

FIGURE 4.43 ACOUSTIC FLUCTUATIONS-ELEUTHERA EXPERIMENT

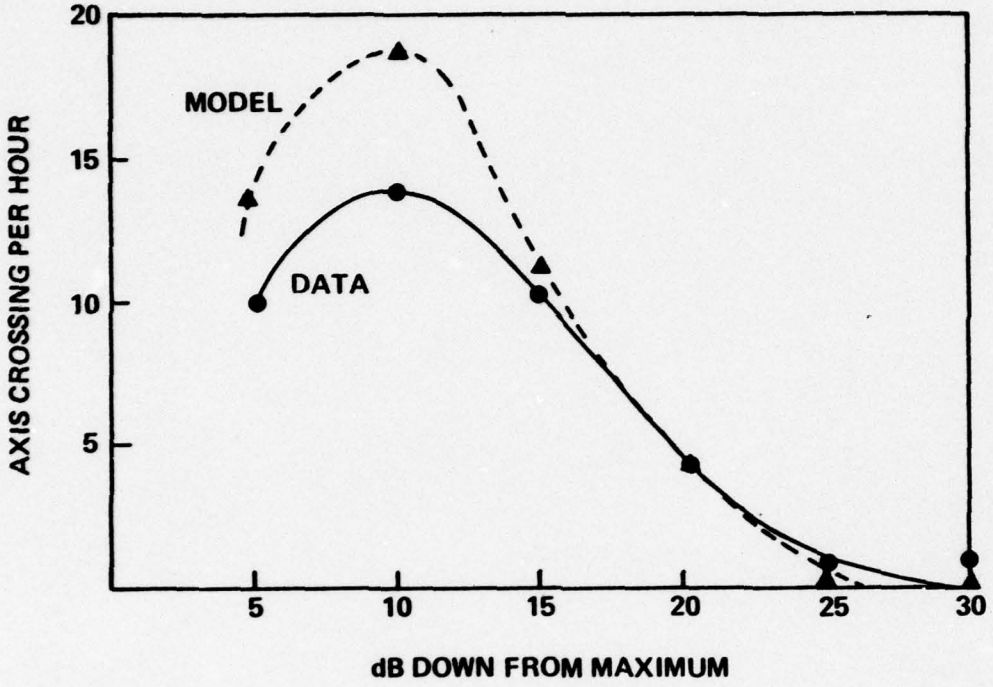

FIGURE 4.44 AXIS CROSSING RATE FOR ELEUTHERA DATA AND MODEL PREDICTIONS

4.4 SIGNIFICANCE AND CONCLUSION

Aside from specific details of the simulation results presented above, several general features are notable. We may summarize these as follows:

- The rate at which propagation fluctuations occur, for a fixed source and receiver, increases (the relaxation time decreases) as the acoustic frequency increases
- There is some evidence that fluctuation rates increase with increasing source-receiver separation
- Both predicted and observed fluctuations tend to a maximum value of about 5 to 6 dB, a value which is characteristic of phase random multi-path propagation. One set of runs shows evidence that this value decreases with range at short (less than 40 nmi) separations but the current runs are insufficient to determine whether this feature changes with source-receiver depth, frequency, or environment
- Computed relaxation times range from one to two minutes up to about 30 minutes. Values at 220 Hz, at ranges of 100 to 200 nmi, are about five minutes in both the Bermuda and Atlantic environments, and on the order of one to two minutes in the two 400 Hz cases examined.

All of these points are of potential significance to the performance of passive narrowband ASW sonars. The magnitude and rate of received signal and noise are critical factors in determining the performance of such systems. While propagation effects are certainly not the only contribution to these parameters, these effects can be important, under proper conditions, to the point of dominating system performance.

Conventionally, sonar fluctuation parameters are taken to be independent of range and essentially independent of frequency over the operating range of any particular sonar. Empirical fits to low frequency, long range, sonar performance suggest relaxation times, for the detection process, of hours rather than minutes. The possibility, suggested by the results above, that fluctuation parameters may vary with both frequency and range could be of considerable importance in optimizing sonar design and use. Crudely speaking, the cited propagation fluctuation characteristics imply relatively better performance with increasing range and frequency, than is predicted by conventional calculations. For example, to the extent that such effects dominate, sonars designed to reach a given range could have lower gains, and operate at higher frequencies, then would otherwise be necessary.

Of course, many phenomena besides those treated here can produce or modify observed fluctuations on any particular sonar. There are for example time fluctuations introduced when source or receiver move through spatial

propagation structure.* There are fluctuations in ambient noise which arise from an ensemble of sources (hence from a superposition of many spatial and, perhaps, frequency regimes) whose properties may differ significantly from the fluctuation characteristics of a single source. Additional fluctuations arise from variations in the properties of the sources themselves. Other mechanisms, not treated here, may also perturb acoustic propagation.

Finally, the sonar system itself modifies the properties of an incoming signal so that, ultimately, the observed fluctuations depend on the properties of the system. Long integration times will remove, or smooth, relatively rapid fluctuations. High resolution systems can introduce fluctuations by responding to changes in parameters which would not be resolvable on less powerful systems. This is not to suggest that the trends observed in this study are not of interest, but only that realistic assessment of sonar performance must integrate such results into a more comprehensive sonar model. As such models are developed, estimates of transmission statistics will play a central role.

---

* When the spatial structure arises from multipath interference, such fluctuations are closely related to those discussed above. That is, they also arise from varying phase relations among multipaths. However, in this case the time scale is set by platform speed rather than rate of change of medium properties.

V. SUMMARY AND CONCLUSIONS

Understanding and predicting the performance of low frequency passive sonars requires being able to describe not only mean values of parameters that determine system performance, but statistical variations as well. Of these parameters, propagation loss has a central role, since it helps determine the properties of both the observed signal field, and the observed noise field at a receiver. Of a number of phenomena which can generate propagation fluctuations, this report has concentrated, in particular, on how internal wave phenomena affect acoustic propagation between a stationary source and receiver.

A model has been developed which simulates multipath propagation through an internal wave field. The model depends on building up sample functions of an internal wave field from a specified spectral description, and propagating acoustic energy through this field using ray trace techniques. The internal wave calculation uses a power spectrum proposed by Garrett and Munk, and assumes an isotropic distribution of internal wave propagation directions. While the internal wave spectrum used is a single universal function, the acoustic propagation calculation is based on propagation parameters which are generic to particular environments of interest; hence the sensitivity of propagation loss under different environmental conditions to internal wave effects may be tested.

Qualitative features of model results match typical experimental observations of CW transmission. Of these the most striking are frequent deep fades in the propagation amplitude, and the character of related phase fluctuations which take place relatively slowly, but with large (many cycles) amplitude. In two detailed comparisions of model results with data,one shows very good agreement in both the magnitude and rate of fluctuations. An apparant anomoly in fluctuation rates observed in the other comparision may result from differences in processing and display between simulated results and experimental data; this case requires further examination.

Model results suggest a number of trends which may be significant from the standpoint of assesing sonar performance. These include:

- An apparant increase in fluctuation rates with increasing acoustic frequency
- A possible increase in fluctuation rates with increasing source-receiver seperation
- Standard deviations, for propagation fluctuations, of 5 to 6 dB under all conditions except short (approximately 40 miles) source-receiver seperations
- No obvious strong dependencies on environment, or on source-receiver depth, in the cases tested.

All these trends are potentially important in the assessment of sonar performance, but their significance is hard to assess, not least because the characteristics of any sonar system may themselves affect signal fluctuations in critical ways. Thus an important next step is to evaluate model predictions in the light of specific sonar processing concepts. Because the model uses simulation techniques this can be done in two ways: directly through additional simulations, or indirectly by using statistical parameters derived from model results in sonar system analyses.

A possible application of considerable interest would be to evaluate limits imposed, by internal wave activity, on Inter Array Processing (IAP). This technique depends on having coherent signal arrivals at two widely separated sensors. This coherence can be degraded or destroyed by perturbations introduced by internal waves. Adaptations of the model developed under this study could readily simulate this effect. Other possible applications include driving particular signal processing algorithms with signal time dependencies derived from the model, and assessing limitations on sonar array beamforming capabilities caused by coherence degredation across a wavefront. In each case the model, as developed in this study, offers substantial potential for investigating limits of sonar performance.

APPENDIX A
MATHEMATICAL FORMALISM

BASIC PROPERTIES

In this section we outline some of the mathematical formalism which underlies the description of internal wave activity given in Chapter IV. The treatment is based largely on the 1974 paper of Garrett and Munk. [5] In particular we use the Garrett-Munk estimate of the power spectrum of internal waves. We also adapt the Garret-Munk solutions for the normal modes of internal waves. These are based on the assumption that the internal wave bouyancy frequency (the "Brunt-Väisälä" frequency) varies exponentially with depth.* Estimates of the effect of internal wave activity on acoustic propagation are based on ray trace estimates of unperturbed propagation parameters, and an extension of an approximation introduced by Porter Spindel and Jaffee.[6]

We treat internal waves in the ocean as a superposition of traveling waves of the form:

$$\delta(\bar{\alpha}, \omega) = \frac{z_{\alpha\,\omega}(z)}{n_o} A(\bar{\alpha}, \omega)\ e^{i(\bar{\alpha} \cdot \bar{r} - \omega t)} \qquad (1)$$

---

* This is equivalent to assuming (see Appendix B, Equation 12) that the depth derivative of the logarithim of sound speed varies exponentially with depth. This characterization is meant only to capture general trends, and real sound speed profiles frequently depart from it radically. While we use the Garrett-Munk internal wave model functions derived from this approximation, acoustic ray trace and transmission parameters were based on estimates of actual sound speed profiles, at sites of interest.

where:

δ is vertical displacement due to internal waves

$\bar{\alpha}$ is a two dimensional (horizontal) wave vector

ω is internal wave frequency

z is the vertical wave function associated with mode $(\bar{\alpha},\omega)$

A is the complex amplitude (a random variable) of mode $(\bar{\alpha},\omega)$

n_o is the peak internal wave bouyancy frequency.

The total displacement at a given location r, at time t is, formally, just a sum over the constituent modes. That is:

$$\delta(\bar{r}, z, t) = \sum_{(\bar{\alpha},\omega)} \frac{z_{\alpha,\omega}(z)}{n_o} A(\bar{\alpha},\omega) \; e^{i(\bar{\alpha} \cdot \bar{r} - \omega t)} \qquad (2)$$

The mean square of A is the mean energy carried by mode $(\bar{\alpha},\omega)$. If $E(\bar{\alpha},\omega)$ is defined as the power spectrum (mean energy density) associated with internal waves then:

$$\{|A|^2\} = \frac{1}{2\pi|\bar{\alpha}|} E(\alpha,\omega) \, \delta^2\bar{\alpha} \, \delta\omega$$

where $\delta^2 \bar{\alpha} \, \delta\omega$ is the size of a cell containing one mode, in wave number frequency space. Garrett and Munk propose, for $E(\alpha,\omega)$, the form

$$E(\alpha,\omega) = \begin{cases} \frac{2}{\pi} n_o^3 b^3 E \frac{\omega_f}{\nu \omega \sqrt{\omega^2 - \omega_f^2}} & \alpha_{min} \leq \alpha \leq \alpha_{max} \\ 0 & \text{otherwise} \end{cases} \qquad (3)$$

where $\nu = 20 \pi \sqrt{\omega^2 - \omega_f^2}$

$E = 2\pi \times 10^{-5}$

b = mean bouyancy frequency depth

n_0 = peak bouyancy frequency

ω_f = inertial frequency = $(2 \frac{\text{cycles}}{\text{day}})$ sin (lat) = .000145 sin (lat)

$\alpha_{max} = \nu/(b\, n_0)$

(In this formula all frequencies are circular (e.g., radians/sec) and the scaling factors used by Garrett and Munk are displayed explicitly.)

Garrett and Munk found that the discrete modal structure of Equation (2) predicts spatial coherencies for internal wave fields which are larger than those observed experimentally. They suggest that this reflects a more complex modal distribution and propose approximating this by replacing the discrete structure in (2) with a continum in $(\bar{\alpha},\omega)$ space. In this case the summation in (2) is replaced by an integral over this continuous distribution. We can retain the discrete structure of (2) by partitioning the integral into bins within which $\bar{\alpha}$ and ω are nearly constant. In each bin the phase factor is nearly constant, so that the integral is essentially over the terms $\tilde{z}$ A. This integral is again a Gaussian random variable with mean square equal to the sum of the mean square values of $\tilde{z}$ and A separately. This leads to

$$\delta(\bar{r},z,t) = \sum_{\bar{\alpha},\omega} \frac{\{\tilde{z}^2\}^{1/2}}{n_0} A'(\bar{\alpha},\omega)\ e^{i(\bar{\alpha}\cdot\bar{r} - \omega t)} \qquad (4)$$

where $\{Z^2\}^{1/2}$ is the root mean square value of $\tilde{z}$ over an $(\bar{\alpha},\omega)$ group, and the sum now is over averaged groups rather than single modes. A' is again a Gaussian Random amplitude, with mean square energy

$$\{A'^2\} = \frac{1}{2\pi\,|\alpha|}\ E(\bar{\alpha},\omega)\ \delta^2\bar{\alpha}'\ \delta\omega' \qquad (5)$$

where $\delta^2\bar{\alpha}'\ \delta\omega'$ is the size of the cell over which averaging takes place.

The solutions for single modes, $\tilde{z}(\alpha,\omega)$ as developed by Garrett and Munk, exhibit a strongly oscillatory depth dependence which varies rapidly from mode to mode, and the solutions are sensitive to detailed features of the depth dependence of oceanographic variables. Garrett and Munk point out that the mean square average of $\tilde{z}$ is a much smoother and less sensitive function of the form

$$\{\tilde{z}^2(z)\} = \begin{cases} \dfrac{n_0\ (\omega^2 - \omega_f^{\,2})}{n(z)\ \omega^2} & \omega_f < \omega < n(z) \\ 0 & \text{otherwise} \end{cases} \qquad (6)$$

where

ω_i = inertial frequency = 2 sin (latitude)

$n(z)$ = Brunt - Väisälä frequency = $\{-\frac{g}{\rho_o}\frac{\partial \rho}{\partial z}\}^{\frac{1}{2}}$

g = acceleration of gravity

ρ = density of seawater

n_o = peak value of $n(z)$

To connect the vertical excursions, δ, to acoustic propagation, we observe that these oscillations are mixing up water of different temperatures. This in turn affects the speed of sound. In Appendix B it is shown that the resultant change in sound speed at depth z may be written as

$$\Delta c(z) = -\left(\frac{\mu c_o}{g}\right) n^2(z)\ \delta \qquad (7)$$

where g is the acceleration of gravity, μ is a proportionality constant, and c_o is the unperturbed local sound speed. The change in sound speed is equivilent to a change in the local index of refraction given by

$$N_a(\bar{r},z,t) = \frac{\Delta c}{c_o} = -\left(\frac{\mu}{g}\right) n^2(z)\ \delta \qquad (8)$$

While perturbations in the refractive index can occur throughout the water column, the Garret-Munk formulation suggests that the major contributions tend to lie in a well localized region at the base of the thermocline. Porter, et. al[6] take advantage of this by introducing an approximation which treats the sum of all the variations in index throughout the water column as taking place in a thin layer at the base of the thermocline. That is, they assume that at the base of the thermocline there is a thin slab whose total acoustic thickness differs from that of the unperturbed water column by

$$N_a(\bar{r},t) = \int_0^{\text{Bottom}} N_a(\bar{r},z,)\ dz \qquad (9)$$

In this context it is straightforward to treat the effect of internal waves on a ray trace model of acoustic propagation. Rays which do not cross this thin internal wave layer are unaffected. For those rays that do cross, reflections from the layer are ignored (because the change in index of refraction is small), any horizontal displacement of the ray is ignored (because the slab is thin) and any change in direction is ignored (because the boundaries of the slab are parallel). The remaining effect is a perturbation in phase as the ray crosses the perturbed region, and this is given by

$$\delta\phi = \frac{2\pi}{\lambda} N_a(r_j, t_j)/|\cos \theta_j| \tag{10}$$

where λ is the acoustic wavelength of the ray, θ_j is the angle (from the vertical) at which the ray crosses the slab, and $\bar{r}_j$ and t_j are the location and time of the crossing.

In an actual propagation situation there can be several rays connecting source and receiver, and each ray can cross the internal wave layer more than once. Each time a ray crosses it receives an additional phase perturbation. Let the positions where ray k crosses the internal wave layer depth be $\bar{r}_j^k$, and let the corresponding crossing times be $t - t_j^k$ (t the arrival time at the receiver). Then the total phase perturbation for ray k is:

$$\delta\phi_k = \frac{2\pi}{\lambda} \sum_j N_a(\bar{r}_j^k, t - t_j^k)/|\cos \theta_j^k| \tag{11}$$

To connect this to acoustic propagation, note that the total acoustic transmission from source to receiver is given by

$$I(\bar{R}, t) = \left|\sum_k E_k e^{i(\phi_k + \delta\phi_k)}\right|^2 \tag{12}$$

where E_k and ϕ_k are the underturbed amplitude and phase, respectively, of ray k, and $\delta\phi_k$ is given by (11). Note that the perturbing phase, as given by (11) is explicitly a function of time, and implicitly a function of source range (since this determines how many times each ray crosses the layer).

EXPLICIT REPRESENTATIONS

Equation 12 is the formal result required, but we are not yet in position to use it. In order to evaluate (11) we need an explicit expression for $N_a(\bar{r},t)$. This requires evaluating the integral in (9) (including the z dependence in δ), which, in turn, requires supplying an explicit representation for $n(z)$. The first step simply involves combining (8), (9) and (4), giving:

$$N_a(\bar{r},t) = -\int_0^{\text{Bottom}} \frac{\mu}{g} n^2(z)\ \delta(\bar{r},z,t)\ dz \tag{13}$$

$$= -\frac{\mu}{g n_o} \sum_{\bar{\alpha},\omega} F_{\alpha,\omega} A'(\bar{\alpha},\omega) e^{i(\bar{\alpha}\cdot\bar{r} - \omega t)} \tag{14}$$

where

$$F_{\alpha,\omega} = \int_0^{\text{Bottom}} dz\, n^2(z)\, \{\bar{z}^2(z)\}^{\frac{1}{2}} \tag{15}$$

As noted above the Garrett-Munk formalism assumes that n(z) is exponential in form, that is:

$$n(z) = n_o e^{-z/b} \tag{16}$$

Adapting this assumption, and using the expression for $\{\bar{z}^2(z)\}$ given by (6) we have

$$F_{\bar{\alpha},\omega} = \frac{(\omega^2 - \omega_i^2)^{\frac{1}{2}}}{\omega}\, n_o^2 \int_0^{b\ln(n_o/|\omega|)} dz e^{-3z/2b} \tag{17}$$

$$= \frac{2b}{3}\, n_o^2\, \frac{(\omega^2 - \omega_i^2)^{\frac{1}{2}}}{\omega} \left[1 - \left|\frac{\omega}{n_o}\right|^{3/2}\right] \tag{18}$$

where the upper limit of the integral in (15) is set by the range over which (6) is non-zero.

Combining (18) with (14), and using this result in (11), yields the following expression for the phase change along path k:

$$\delta\phi_k = \frac{4\pi}{3\lambda}\, \frac{\mu b n_o}{g|\cos\theta^k|} \sum_{\bar{\alpha},\omega} \left[1 - \left|\frac{\omega}{n_o}\right|^{3/2}\right] \sqrt{\frac{\omega^2 - \omega_i^2}{\omega^2}}\, A'(\bar{\alpha},\omega) \sum_j e_j^{\,i[\bar{\alpha}\cdot\bar{r}_j^k - \omega(t - t_j^k)]} \tag{19}$$

Part of the summations in (19) may be evaluated in closed form. The propagation vector $\bar{\alpha}$ is a two-dimensional vector in the horizontal plane. If we take the X-axis of our co-ordinate frame to be the propagation direction of interest then $\bar{\alpha}\cdot\bar{r} = \alpha_x x$ and (19) becomes

$$\delta\phi_k = \frac{4\pi}{3\lambda}\, \frac{\mu b n_o}{g|\cos\theta^k|} \sum_{\omega} e^{-i\omega t} \left[1 - \left|\frac{\omega}{n_o}\right|^{3/2}\right] \sqrt{\frac{\omega^2 - \omega_i^2}{\omega^2}} \times \sum_{\alpha_x} \sum_j e^{i(\alpha_x x_j^k + \omega t_j^k)}\, A''(\alpha_x, \omega) \tag{20}$$

where $A''(\alpha_x, \omega) = \sum_{\alpha_y} A'(\bar{\alpha}, \omega)$ (21)

A" is again a complex mean-zero Gaussian Random variable. In Appendix C we show that its variance is given by:

$$\{A''(\bar{\alpha},\omega)^2\} = \frac{E(\omega)\ \delta\alpha_x'\ \delta\omega}{\pi}\ \ln\left[\frac{\alpha_y^{max} + \alpha_{max}}{\alpha_y^{min} + \sqrt{\alpha_y^{min^2} + \alpha_x^2}}\right] \quad (22)$$

where

$$\alpha_y^{max} = \sqrt{\alpha_{max}^2 - \alpha_x^2}$$

$$\alpha_y^{min} = \begin{cases} \sqrt{\alpha_{min}^2 - \alpha_x^2} & \alpha_{min}^2 - \alpha_x^2 > 0 \\ 0 & \alpha_{min}^2 - \alpha_x^2 \leq 0 \end{cases}$$

The crux of using (12) to evaluate the acoustic intensity (I) is to find suitable ways of evaluating (20). Quantities such as E_k, ϕ_k, r_j^k, t_j^k, θ_j^k, can be obtained readily from a suitable ray trace program. The crucial problems are to select a suitable mesh size for the sum over $(\bar{\alpha},\omega)$, and to handle the random variables $A''(\bar{\alpha},\omega)$.

To take the second problem first, our technique is to implement a simulation approach in which values for the real and imaginary part of A" at each $(\bar{\alpha},\omega)$ mesh point, are selected randomly from a mean zero Gaussian distribution with variance given by (22). For each set of random numbers so selected, (20) and (12) can be evaluated at all values of $\bar{R}$ and t which are of interest. The result is one realization of the random function $I(\bar{r},t)$. Iterating this procedure can build up an ensemble of such functions from which relevant statistics (mean, variance, autocorrelation, distribution function, etc.) as functions of $\bar{R}$ and t, can be generated.

The question of selecting a mesh size for α_x and ω is somewhat more subtle. We approach the subject as follows: If a uniform mesh is chosen (e.g., $\delta\alpha_x$ and $\delta\omega$ constant) then for any given value of j, equation (20) is a double Fourier series. That is, ignoring the sum over j, we have a function which is periodic in range with period $2\pi/|\delta\alpha_x|$, and periodic in time with period $2\pi/\delta\omega$. This periodicity is quite clearly an artifact generated by the way the terms in equation (2) were grouped to form equation (4), rather than a real effect. To keep it from affecting the results it is necessary that the period be longer than all ranges and times of interest. That is, if we select some maximum range, R_{max}, and some maximum time T_{max}, of interest, we require

$$|\delta\alpha_x| < 2\pi/R_{max}$$

$$\delta_\omega < 2\pi/T_{max} \qquad (3)$$

The prescription for carrying out the calculation is then as follows:

a) Pick a mesh according to (3)

b) Randomly choose a value for the real and imaginary parts at A" at each mesh point

c) Carry out the sum in equation (20), and evaluate equation (12) for each $\bar{R}$ and t of interest

d) If desired repeat b) and c) to build up statistics.

APPENDIX B

SOUND SPEED - BOUYANCY FREQUENCY RELATIONSHIPS

BASIC RELATIONSHIPS

We wish to ascertain how vertical mixing of the water column affects the local speed of sound. The following treatment is based on a discussion given by Munk and Zachariasen[13] We observe that sound speed (c) depends on temperature (T), salinity (S), and pressure (P) so that

$$\frac{1}{c}\frac{\partial c}{\partial z} = \alpha\frac{\partial T}{\partial z} + \beta\frac{\partial S}{\partial z} + \gamma\frac{\partial P}{\partial z} \qquad (1)$$

where α, B, and ∂ are the fractional partial derivatives

$$\alpha = \frac{1}{c}\frac{\partial c}{\partial T}$$

$$\beta = \frac{1}{c}\frac{\partial c}{\partial s} \qquad (2)$$

$$\gamma = \frac{1}{c}\frac{\partial c}{\partial P}$$

The temperature gradient may be divided into two parts; an adiabatic component, representing the thermal gradient that would be present in an adiabatic ocean, and the remaining ("potential") gradiant. That is

$$\frac{\partial T}{\partial z} = \frac{\partial T_a}{\partial_z} + \frac{\partial T_p}{\partial_z} \qquad (3)$$

so we can write

$$\frac{1}{c}\frac{\partial c}{\partial z} = \left(\alpha \frac{\partial T_a}{\partial z} + \gamma \frac{\partial P}{\partial z}\right) + \left(\alpha \frac{\partial T_p}{\partial z} + \beta \frac{\partial T_s}{\partial z}\right)$$
$$= \frac{1}{c}\left(\frac{\partial C_a}{\partial z}\right) + \frac{1}{c}\frac{\partial C_p}{\partial z} \qquad (4)$$
$$= \gamma_a + \frac{1}{c}\frac{\partial C_p}{\partial z}$$

where

$$\gamma_a = \frac{1}{c}\frac{\partial C_a}{\partial z} = \alpha \frac{\partial T_a}{\partial z} + \gamma \frac{\partial P}{\partial z} = .0114\ \text{Km}^{-1} \qquad (5)$$

is the fractional sound gradient expected in an adiabatic isohaline ocean; it is approximately the gradient observed in the deep ocean.

When an element of the water column is displaced from its equilibrium depth by mixing, it carries with it its original value of salinity and T_p, but takes on the local values for P and T_a. Thus an element which has been displaced a distance δ has associated with it a sound speed which differs from the unperturbed speed at that depth by:

$$\frac{\delta c(z)}{c} \simeq \frac{1}{c}\left[C_p(z) - C_p(z-\delta)\right] \simeq \frac{1}{c}\frac{\partial C_p}{\partial z}\delta \qquad (6)$$

The gradient of C_p depends in an approximately linear fashion on the gradients of T_p and salinity. Similarly the internal wave bouyancy frequency depends on the same partial derivatives through a relationship of the form

$$n^2(z) = \frac{g}{\rho}\frac{\partial \rho_p}{\partial z} \simeq -g\left(a\frac{\partial T_p}{\partial z} - b\frac{\partial S}{\partial z}\right) = -ga\frac{\partial T_p}{\partial z}\left[1 - T_\mu\right] \qquad (7)$$

where T_μ, the "Turner Number" is defined as

$$T_\mu = \frac{b\,\partial S/\partial z}{a\,\partial T_p/\partial z} \qquad (8)$$

In terms of T_μ there is a relationship between $\frac{1}{c}\frac{\partial C_p}{\partial z}$ and $n^2(z)$ which may be expressed as

$$\frac{1}{c}\frac{\partial C_p}{\partial z} = -\frac{\mu}{g} n^2(z) \tag{9}$$

where

$$\mu = \frac{\alpha}{a}\frac{1 + (\alpha\beta/ab) T_\mu}{1 - T_\mu} \tag{10}$$

Thus, combining (6) and (9) we have

$$\frac{\delta c}{c} \approx -\frac{\mu}{g} n^2(z)\,\delta \tag{11}$$

which expresses the fractional change in sound velocity in terms of the bouyancy frequency $n(z)$.

Finally, we note that, from (4) and (9), we have

$$\frac{1}{c}\frac{\partial c}{\partial z} = \gamma_a - \frac{\mu}{g} n^2(z) \tag{12}$$

EVALUATION OF CONSTANTS

The proportionality factor μ, which appears above, is expected to vary with both depth and location. Typical values quoted in the literature vary from 11.6 to 24.5; for the calculations reported here, a value of 18 was used.

In equation A16 the approximation

$$n(z) = n_o e^{-z/b}$$

is introduced. From equation (2) we have, also, that

$$n(z) = \left[\frac{g}{\mu}\left(\gamma_a - \frac{1}{c}\frac{\partial c}{\partial z}\right)\right]^{1/2} \tag{13}$$

This relation may be used to fit for n_o and b, using the local velocity profile at any location of interest as an input. In the work reported here, this was done by fitting to the sound speed slope at the base of the thermocline ($\frac{\partial c}{\partial z}\big|_{z=0} = \frac{\partial c}{\partial z}\big|_0$), and the depth (h) of the sound channel axis

$\left(\frac{\partial c}{\partial z} \Big|_{z = h} = 0 \right)$. This yields

$$n_o = \left[\frac{g}{\mu} \left(\gamma_a - \frac{1}{c} \frac{\partial c}{\partial z} \Big|_0 \right) \right]^{\frac{1}{2}} \tag{14}$$

$$b = 2h / \ln \left[n_o^2 \frac{\mu}{g \gamma_a} \right] \tag{15}$$

Resulting values of b are on the order of 1 to 2 Km; of n_o, about .005 Rad/Sec. Specific values for the cases treated in Chapter IV are given in Table 4.1.

APPENDIX C
SUMMATION OVER TRANSVERSE WAVE NUMBER

Equation (21) reads

$$A''(\alpha,\omega) = \sum_{\alpha_y} A'(\bar{\alpha},\omega) \tag{1}$$

where $\bar{\alpha}$ is a two-dimensional wave number vector with cartesian components (α_x,α_y), $A'(\bar{\alpha},\omega)$ is a complex mean zero Gaussian random variate with variance given by (Equation A5).

$$\{A'^2\} = \frac{1}{2\pi|\bar{\alpha}|} E(\bar{\alpha},\omega)\, \delta^2\bar{\alpha}'\, \delta\omega' \tag{2}$$

and the sum is over a set of closely spaced grid points in $\bar{\alpha},\omega$ space. The values of A' at the various grid points are uncorrelated so that

$$\{A''(\alpha_x,\omega)^2\} = \sum_{\alpha_y} \{A'(\bar{\alpha},\omega)^2\}$$

$$= \sum_{\alpha_y} \frac{1}{2\pi|\bar{\alpha}|} E(\bar{\alpha},\omega)\, \delta\alpha_x'\, \delta\alpha_y'\, \delta\omega' \tag{3}$$

From Equation (A3), $E(\bar{\alpha},\omega)$ has the form

$$E(\bar{\alpha},\omega) = \begin{cases} E(\omega) & \alpha_{min}(\omega) \leq |\bar{\alpha}| \leq \alpha_{max}(\omega) \\ 0 & \text{otherwise} \end{cases} \tag{4}$$

Thus, $E(\bar{\alpha},\omega)$ does not depend explicitly on $\bar{\alpha}$ and we may write

$$\{A''(\alpha_x,\omega)^2\} = \frac{E(\omega)\,\delta\alpha_x'\,\delta\omega}{2\pi} \sum_{\alpha_y} \frac{\delta\alpha_y'}{|\bar{\alpha}'|} \tag{5}$$

where the limits on the sum in (5) are determined by the range of $|\bar{\alpha}|$ as given in (4). Using

$$|\bar{\alpha}| = \sqrt{\alpha_x^2 + \alpha_y^2}$$ we have

$$\alpha_y^{min} \leq |\alpha_y| \leq \alpha_y^{max} \tag{6}$$

where $$\alpha_y^{max} = \sqrt{\alpha_{max}^2 - \alpha_x^2} \tag{7a}$$

and $$\alpha_y^{min} = \begin{cases} \sqrt{\alpha_{min}^2 - \alpha_x^2} & \alpha_{min}^2 - \alpha_x^2 > 0 \\ 0 & \alpha_{min}^2 - \alpha_x^2 < 0 \end{cases} \tag{7b}$$

The range of α_y covers both positive and negative values. However the sum in (5) is symmetric so that we may write

$$\{A''(\alpha_x,\omega)^2\} = \frac{E(\omega)\,\delta\alpha_x'\,\delta\omega}{2\pi} \sum_{\alpha_x' = \alpha_y^{min}}^{\alpha_y^{max}} \frac{2\,\delta\alpha_y'}{\sqrt{\alpha_x^2 + \alpha_y^2}}$$

Finally we take advantage of the smallness of the mesh spacing ($\delta\alpha_y'$) to replace the sum in (6) with the equivilent integral, so that

$$\{A''(\bar{\alpha},\omega)^2\} = \frac{E(\omega)\,\delta\alpha_x'\,\delta\omega}{\pi} \int_{\alpha_y^{min}}^{\alpha_y^{max}} d\alpha_y / \sqrt{\alpha_y^2 + \alpha_x^2} \qquad (7)$$

which yields

$$\{A''(\bar{\alpha},\omega)^2\} = \frac{E(\omega)\,\delta\alpha_x'\,\delta\omega}{\pi} \ln\left[\frac{\alpha_y^{max} + \sqrt{\alpha_y^{max^2} + \alpha_x^2}}{\alpha_y^{min} + \sqrt{\alpha_y^{min^2} + \alpha_x^2}}\right] \qquad (8)$$

$$= \frac{E(\omega)\,\delta\alpha_x'\,\delta\omega}{\pi} \ln\left[\frac{\alpha_y^{max} + \alpha_{max}}{\alpha_y^{min} + \sqrt{\alpha_y^{min^2} + \alpha_x^2}}\right]$$

REFERENCES

1. "Proceedings of the First Workshop on Operations Research Models of Fluctuations Affecting Passive Sonar Detection" (U), NSRDC Report 76-0063, Volume I-CONFIDENTIAL, Volume II-SECRET

2. A.N. Kolmogorov, Doklady Akad. Nauk SSSR, 30, 301 (1941), A.N. Kolmogorov, Doklady Akad. Nauk SSR, 32, 16 (1941), German Translations in "Sammelband zur Statistischen Theorie Der Turbulenz" Akadamie-Verlag, Berlin (1958), pp. 71 and 77

3. W.B. Mosely and D.R. Del Balzo, "Oceanic Horizontal Random Temperture Structure", NRL Report 7673, Naval Research Laboratory, Washington, D.C., 1974

4. V.J. Tatarski, "Wave Propagation in a Turbulent Medium", translated by R.A. Silverman, McGraw-Hill, New York (1960), V.J. Tatarski, "The Effects of the Turbulent Atmosphere on Wave Propagation", U.S. Department of Commerce, National Technical Information Service, Springfield, VA., 1970

5. Cristopher Garrett and Walter Munk, "Space Time-Scales of Internal Waves", Geophysical Fluid Dynamics 2, 225 (1972)

6. R.P. Porter, R.C. Spindel, and R.J. Jaffee, "Acoustic Internal Wave Interaction at Long Ranges in the Ocean", J. Acoust. Soc. Am. 56, 1426-1436 (1974)

7. H.A. DeFarrari, "The Effects of Horizontally Varying Internal Wave Fields of Multipath Interference for Propagation Through the Deep Sound Channel", International Workshop on Low Frequency Propagation and Noise, ONR, 1975

REFERENCES CONT.

8. S.M. Flatte and F.D. Tappert, "Calculation of the Effect of Internal Waves on Oceanic Sound Transmission" J. Acoust. Soc. Am., 58, No. 6, 1975

9. R.C. Spindel, R.P. Porter, and R.J. Jaffee, "Long-Range Sound Fluctuations with Drifting Hydrophones", J. Acoust. Soc. Am., 56, 440-458 1974

10. J.G. Clark and M. Kronengold, "Long-Period Fluctuations of CW Signals in Deep and Shallow Water,", J. Acoust. Soc. Am., 56, 1071-1083, 1974

11. "Oceanographic Atlas of the North Atlantic Ocean, Section VI, Sound Velocity" U.S. Naval Oceanographic Office, Pub. #700, 1967

12. I. Dyer, "Statistics of Sound Propagation in the Ocean" J. Acoust. Soc. Am., 48, 337-345, 1970

13. W.H. Munk and F. Zachariasen, "Sound Propagation Through a Fluctuating Stratified Ocean Theory and Observation" J. Acoust. Soc. Am., 59, 818-838, 1976.

DISTRIBUTION LIST

ADDRESS	# of Copies
Naval Underwater Systems Center Newport, RI 02840	1
Naval Underwater Systems Center New London, CT 06320	1
Naval Research Laboratory Washington, DC 20390	
Code 2029	2
Technical Information Division	1
Naval Air Development Center Warminster, PA 18974	
M. Metersky	1
A. Greco	1
David W. Taylor Naval Ship Research and Development Center Bethesda, MD 20034	
Dr. J. Pulos, Code 1864	1
Office of Naval Research 800 N. Quincy Street Arlington, VA 22217	

Code 222	1
Code 486	1
Code 431	3
Naval Electronic Systems Command Washington, DC 20360	
Code 320	2
Institute For Defense Analyses 400 Army-Navy Drive Arlington, VA 22202	1
S.R.I. International 333 Ravenswood Avenue Menlo Park, CA 94025	1
Science Applications, Inc. 1651 Old Meadow Road McLean, VA 22101	
Dr. R. Cavanaugh	1
Naval Postgraduate School Monterey, CA 93940	
Technical Livrary	1
Operations Research Department	1
Center for Naval Analysis 1400 Wilson Boulevard Arlington, VA 22209	
Library	1
Dr. A. Kaufman	1
Bell Telephone Laboratories Whippany Road Whipany, NJ 07981	
Dr. I. Fretwell	1
Dr. H. Deferrari R.S.MA.S. 4600 Rickenbacker Causeway Miami, FL 33149	1

Dr. O. Diachok
Naval Research Laboratory
Washington, DC 20375
Code 8160 — 1

Defense Documentation Center
Cameron Station
Alexandria, VA 22314 — 12

Naval Oceanographic Research
Development Activity
Bay St. Louis, MS 39520
Code 320 — 1

END
9-78
DDC